Dual-Doppler Derived Vorticity as a Predictor of Hail Size in Severe Thunderstorms

Trevor White

Thesis submitted to the faculty of the Virginia Polytechnic Institute and State University
in partial fulfillment of the requirements for the degree of

Master of Science
In
Geography

Laurence W. Carstensen, Committee Chair
David F. Carroll
J. Michael Ruohoniemi

December 2, 2016

Keywords: hail size, severe thunderstorm, supercell, dual Doppler

Dual-Doppler Derived Vorticity as a Predictor of Hail Size in Severe Thunderstorms

Trevor White

Academic Abstract

One of the primary missions of the National Weather Service (NWS) is to use a network of more than 150 NEXRAD radar installations to monitor weather for threats to life and property. Large hail produced by severe thunderstorms is a major focus of this mission. An algorithm known as the Maximum Estimated Size of Hail (MESH) algorithm is in operational use to diagnose the presence and size of hail. This study aims to use dual-Doppler observations as well as the MESH algorithm to test the idea that storms that rotate produce larger hail. Previous studies have used polarimetric radar products to detect the presence of large hail and dual-Doppler methods have been used to study embryonic hail, but no research has tested the theory of hail and rotating storms with observational evidence. A set of 59 case studies was gathered; each included a hail report submitted by a trained weather spotter or NWS employee and complete radar observations through the depth of a storm from two radars. The radar observations were resampled to a three-dimensional Cartesian grid and a dual-Doppler analysis was run on each case study. A strong correlation – stronger even than the MESH algorithm – was found between measured vorticity and hail size, lending credence to the idea that rotating storms do indeed have a higher ceiling for hail production. However, no correlation was found between MESH error and rotation. Further research will be required to evaluate whether or not this relationship can be used to augment the MESH algorithm so as to improve its skill.

Dual-Doppler Derived Vorticity as a Predictor of Hail Size in Severe Thunderstorms

Trevor White

Public Abstract

The National Weather Service (NWS) uses a nationwide network of long-range weather radars to monitor the atmosphere over the United States. One of the primary applications of that network is to protect life and property by identifying and monitoring storms capable of producing large hail. The probable size of hail is estimated using an algorithm on raw radar data. This study uses multi-radar analysis methods to establish a metric for storm rotation, which is used in conjunction with the operational hail size algorithm to test the theory that rotating storms produce larger hail. A set of 59 case studies, each composed of data from a pair of radars as well as a measured hail size from a storm spotter, was gathered and analyzed. Analysis resulted in three values per case study: actual hail size, predicted hail size, and storm rotation intensity. Storm rotation and actual hail size were found to be strongly correlated, lending credence to the idea that rotation increases a storm's hail production ceiling. However, no strong correlation was found between the operational algorithm's error and storm rotation. Additional research will be required to determine if the relationship between rotation and actual hail size can be used to improve the skill of current operational algorithms.

Acknowledgements

I would like to thank my advisor, Dr. Bill Carstensen, for his insight and encouragement during this research and my time with Virginia Tech Geography as a whole. His expertise with geospatial systems and datasets made this work possible. I would also like to thank my committee members, Dr. Mike Ruohoniemi and Dave Carroll. Dr. Ruohoniemi's knowledge of radar systems and willingness to cross interdisciplinary boundaries proved indispensable in the completion of this study. Dave's years of mentorship both in the classroom and in the field, culminating in his contributions as a committee member, made possible my dream of a career in severe weather research.

I also wish to thank Dr. Pam Heinselman at the National Severe Storms Laboratory as well as Dr. Josh Wurman, Dr. Karen Kosiba, and Paul Robinson at the Center for Severe Weather Research for providing data that was used verify methods for this study.

Lastly, I want to express my gratitude to all of the faculty, staff, and students in the Department of Geography. I'm happy to be a part of the Virginia Tech Geography family and look forward to continuing collaboration.

Table of Contents

Table of Figures

Appendix: Case Studies

Chapter 1: Introduction

The idea that rotating storms produce larger hail is commonly believed in the severe weather community. It is backed up by literature in objective studies such as Nelson and Young (1979) as well as by more qualitative evidence from storm spotters in the form of hail reports and tornado reports often being collocated (Figure 1). The assumption makes logical sense, as a helical trajectory allows for more collisions with liquid water in a storm than a linear trajectory. The National Weather Service uses several derivative radar products to help forecast hail and issue warnings on severe thunderstorms in the interest of protecting life and property. The algorithms used, such as MESH (discussed later in the chapter) have been shown to have good skill at estimating hail size (Witt et al. 1998). However, algorithms in operational use do not take storm organization and rotation into account. This study intends to quantify the relationship between actual measured vorticity and the size of hail produced by storms and to explore the possibility of augmenting the MESH algorithm if vorticity proves to be a feasible predictor.

NEXRAD Radar

A network of more than 150 NEXRAD WSR-88D radars (Figure 2) has monitored weather in the United States since the mid-1990's, providing the National Weather Service with radar intelligence to support day-to-day operations (Crum and Alberty 1993). Each radar in the network can detect the presence and measure the intensity of precipitation (reflectivity). Additionally, the radars use the Doppler effect to measure the radial component of raindrop velocity within storms. The WSR-88D operates in the S-band

(10cm), allowing reflectivity products to be measured accurately out to 460km, while Doppler velocity products can be measured reliably out to 230km (Radar Operations Center 2009).

The 88D is a traditional pencil-beam radar, wherein a single beam is emitted while the emitter is rotated. The radar collects data at multiple elevations by tilting the emitter upward after each successive sweep. The pattern and quantity of different elevation angles is known as the Volume Coverage Pattern (VCP); WSR-88D radars are configured to operate in a number of different VCP's, including several specific to diagnosing convection (Warning Decision Training Branch 2008). Due to this study's focus on hail, most data used was collected using VCP 11 and 12 (Figure 3), which are designed to rapidly sample tall thunderstorms with many elevation angles.

Data is made available to end-users in well-documented files. Data files consist of individual rays of data grouped into sweeps, which are in turn grouped into volumes (Radar Operations Center 2016). The data are in polar coordinates in the [Elevation Angle, Azimuth, Range] domain centered on the geographic location of the radar.

Dual-Doppler Analysis

This study relies on dual-Doppler analysis to compute the speed and direction of wind within a storm. This method requires observations of a storm from two radars located at azimuthally separated positions such that the measured radial component of velocity from both radars includes sufficiently different proportions of the U (east/west) and V (north/south) components of wind (Dowell and Shapiro 2003). Given horizontal wind components, objective analysis of the wind field is based on the simple idea that mass has to go somewhere. Thus, analysis begins at one of two boundary layers: at the surface,

where air cannot move downward, or at the very top of a storm where air cannot move upward. Kosiba et al. (2013) use the ground as the boundary condition, thereby establishing that convergent winds must be forcing mass upward and divergent winds must be caused by mass moving downward. The analysis can then proceed upward (or downward, should an upper boundary condition be used), adjusting vertical velocity in successive layers such that the mass budget is balanced. This analysis method results in a complete three-dimensional wind field for the sampled volume.

Study Area

Due to the sparse nature of the radar network, radars had to be carefully selected for the study. The dual-Doppler coverage area for a given pair of radars is a two-lobed structure, much like a Venn diagram with missing overlap (Figure 4). Due to beam divergence over distance, the radars have to be close enough to have good resolution for analysis, but not so close that the coverage area shrinks away to nothing. The coverage area is also restricted due to the basic operation of Doppler radar. In order to adequately measure velocity, a higher pulse rate must be used, thereby limiting range due to what is known as the "Doppler Dilemma" (National Severe Storms Laboratory 2007). This significantly restricts the dual-Doppler geometry of radars as the distance between them increases, as illustrated in Figure 5. Eventually, with increasing range, the coverage area becomes a successively smaller rounded triangle. Thus, radars were selected that were no more distant than 130km from one another. This range was selected because the maximum range at which high quality velocity data can be collected tends to be in that vicinity during convective hail-producing events. The selected study areas are shown in Figure 6.

The MESH Algorithm

The **M**aximum **E**stimated **S**ize of **H**ail (MESH) algorithm is part of the Multi-Radar Multi-Sensor (MRMS) suite of products developed by the National Severe Storms laboratory. It was developed by Witt et al. (1998) and uses vertically integrated radar reflectivity weighted by temperature data to infer the maximum size hail stone that one might reasonably expect from a given storm. For this study, the MRMS version of the algorithm was replicated and verified against output from Gibson Ridge GR2Analyst software.

Chapter 2: Literature Review

Single-Radar Hail Analysis

Experimentation using dual-polarization (polarimetric) radar has shown promising results for predicting and diagnosing the presence and size of hail in convective storms. Multiple polarization axes in radar allow the detection of hydrometeor shape and size distribution. Aydin et al. (1986) proposed a parameter based on reflectivity (Z) and differential reflectivity (Z_{DR}), named H_{DR}. It provides a way of classifying radar returns as either containing hail or not containing hail, providing an additional product for near-term forecasting of severe weather events. Heinselman and Ryzhkov (2006) examined the hydrometeor classification algorithm (HCA), an algorithm that incorporates both polarimetric and non-polarimetric radar returns to make a determination on the type of precipitation falling at a particular geographical location. Their results showed that the introduction of polarimetric data greatly enhanced the skill of the HCA, elevating the probability of detection (POD) of hail to nearly 100% while keeping the false alarm rate (FAR) near zero (Heinselman and Ryzhkov 2006).

Other approaches to single-radar hail prediction make use of radial velocity and single-polarization radar products. Witt and Nelson (1991) examined 49 case studies of severe hail producing thunderstorms. Using divergence of radial velocity at upper levels of the storms – indicative of the presence of a strong updraft – as well as delta-velocity within divergence signatures, they were able to predict maximum hailstone size within a confidence interval of +/- 1.4cm (Witt and Nelson 1991). A modified form of the Vertically Integrated Liquid (VIL) Algorithm was proposed by Amburn and Wolf (1997). Using the

depth of a storm, they proposed the normalization of VIL by dividing by storm top height to compute VIL density. For the study, 221 different thunderstorms were studied during all seasons at varying ranges from the radar. As VIL density increased in the case studies, so did hail size. Once VIL density increased to over 4.9g * m^{-3} hail sizes ranged from 25-45mm. No hailstone tennis ball sized (63mm) or greater was associated with a VIL density less than 4.75 (Amburn and Wolf 1997).

A similar algorithm, also using vertical integration of radar reflectivity, was proposed by Witt et al. (1998). Their approach weights radar reflectivity values from the 0°C altitude through the -20°C altitude to place emphasis on the level in a storm that would be responsible for hail growth. The algorithm output is a value known as the Severe Hail Index (SHI). To compute the Maximum Expected Hail Size (MEHS), the square root of SHI is taken to arrive at MEHS in tenths of an inch. While not necessarily a perfect predictor of hail size, MEHS can serve as an effective predictor of hail damage potential and was shown to, in most cases, return a value that was larger than the 75^{th} percentile hailstone that fell from a given cell (Witt et al. 1998).

Marzban and Witt (2001) go an altogether different direction, incorporating many different parameters into a Bayesian Neural Network to predict hail size. Selected parameters input to the machine learning network were vertically integrated liquid (VIL), severe hail index (SHI), storm top divergence, mid-level rotation velocity, wet-bulb zero altitude, melting level altitude, vertically integrated wet bulb temperature, equilibrium level wind speed, and storm relative wind flow at -20C (Marzban and Witt 2001). Compared with the MEHS parameter proposed by Witt et al. (1998), the neural network had a lower error and more accurately predicted hail.

Dual-Doppler Methods

Multi-Doppler techniques have been used for more than a half-century to infer wind flow in storms. Kropfli and Miller (1976) used a pair of synchronized radars to sample a storm that developed in an environment with a weak wind field. From the data collected, the horizontal wind field as well as vertical velocities could be computed, showing kinematic structures such as divergence coincident with heavy precipitation at the surface and vortices adjacent to the precipitation core indicating that the storm may have impeded upper level wind flow (Kropfli and Miller 1976). Similarly, Smull and Houze Jr (1987) analyzed an advancing squall line in Oklahoma using synchronized radars in Norman and Cimarron to retrieve u, v, and w velocities. Both techniques use the tried and true method of deriving vertical velocity from horizontal wind components; w is assumed to be zero at a boundary condition (the ground, in both cases) and u, v, and w are iteratively solved upward in the storm. Due to the nature of the iterative calculation, there can be cases in which the algorithm does not converge to a solution. Dowell and Shapiro (2003) further refine the technique through the addition of a measure of stability of the computed wind field at each step. The stability condition incorporates the parameters of the observations (azimuth and elevation angle) as well as the grid spacing of the Cartesian coordinate domain of the analysis.

Kosiba et al. (2013) used the method to analyze the low-level wind field of a tornadic supercell in Goshen County, WY on 5 June 2009. Data was collected by a pair of mobile Doppler radars in close proximity to a tornadic supercell. They sample the data to a Cartesian grid using the Gaussian method laid out by Barnes (1964) and refined by Koch et al. (1983). Parameters specific to analysis of fine scale radar data described by Majcen et al.

(2008) were used prior to executing the dual-Doppler wind synthesis. The analysis resulted in a very high-resolution (100m) three-dimensional grid and is one of the highest resolution dual-Doppler datasets to date (Kosiba et al. 2013). The results of the analysis form the basis for verification of the dual-Doppler code used in this study. The dual-Doppler analysis methods in WSR Toolkit were run on the data used in Kosiba et al. (2013) and shown to produce the same results. With performance under optimal conditions proven to be suitable, the analysis methods could be used on NEXRAD data for this study.

Dual-Doppler Hail Size Estimation

Several dual-Doppler oriented studies have focused on hail. Nelson (1983) explores two case studies of hailstorms that affected Oklahoma City, OK. The internal wind field of the storm was synthesized using multi-Doppler techniques and hail growth was modeled. The study found that updraft intensity only matters to a point; the horizontal size of an updraft as well as the wind field around it supplying embryos for hail growth have a significant effect on the size and quantity of hail produced. The results suggest that, in addition to a need for more case studies, quantification of the upper level wind flow as well as suspended material (due to an intense updraft) may help predict hail potential (Nelson 1983). Ziegler et al. (1983) also focuses on analysis of a hailstone's path through a storm; trajectory analysis of simulated hail as it grew showed that the advection of hail embryos into a storm's updraft from outside sources was an important factor in the hail production potential of a storm. The findings brought forth by Foote (1984) agree with the previous two studies; the origin and transport of embryos into a hailstorm is extremely important to the ultimate hail production potential. Additionally, their findings agreed with the conceptual model that hail growth occurs during only a single pass through an updraft.

Conway and Zrnic (1993) extend dual-Doppler hail research with the addition of polarimetric data. Through study of embryo trajectories coupled with polarimetric radar observations, they found that melted hydrometeors above the freezing level as well as hydrometeors that encounter the updraft above the freezing level are two major sources of embryos to support hail growth (Conway and Zrnic 1993).

Chapter 3: Exploring the Relationship of Vorticity and Hail Size

Introduction

Despite the sparse nature of the weather radar network in the United States, there are still some areas with NEXRAD radars close enough to one another so as to allow dual-Doppler analysis of storms producing severe hail. It is a generally accepted truth in meteorology – and corroborated in literature – that storms with significant vertical vorticity have a higher ceiling for hail production (Nelson and Young 1979). Using the areas of the country in which multiple radars have overlapping coverage with a suitable beam-crossing angle, the relationship between hail size and vorticity present in a storm may be explored.

Data

Several sources of data have been employed in this study. The sole source of radar data is the National Center for Environmental Information (NCEI) archive of NEXRAD WSR-88D data, accessed for each storm report via Amazon Web Services. Reflectivity and velocity moments from Level II radar volumes were used in analysis. Availability of data proved a significant problem for this study. The most favorable pairs of radars involved at least one radar operated by the Department of Defense (see Figure 6) that did not have any archival data available until March 2013. Only two radar pairs selected for the study were solely operated by the National Weather Service during their entire operational lives (KVNX-KICT and KGRK-KEWX). These had data available dating back to the 1990's (see Figure 6). The extra data availability made little difference in terms of final case studies as very little data for KVNX was available with 0.5 degree by 250-meter resolution prior to

2011. Due to the kilometer-scale sampling resolution used in this study (discussed in the next section), legacy 1.0 degree by 1.0 kilometer data would not have been suitable. Each case study is composed of a pair of volumes – one from each radar.

Ground truth data for hail size was drawn from the National Center for Environmental Information (NCEI) database of severe weather reports in which on-the-ground observers report hail stone sizes found in the field. The reports were filtered to use only data from National Weather Service employees and trained SKYWARN spotters. By filtering data to only the most reliable sources, error was kept to a minimum. There were several instances that a hail report came from the extreme north side of a storm and were significantly smaller than one might expect. Therefore, instances in which the observed hail size and MESH output for a cell differed by more than 50mm were eliminated.

Thermodynamic data was required to feed into the MESH algorithm. The North American Regional Reanalysis (NARR) was used via a web API exposed by NOAA to acquire vertical thermodynamic profiles of the atmosphere at the time and location of chosen case studies. Geopotential height, temperature, and relative humidity was retrieved and used in analysis.

Case Studies

Case studies selected by examining the 80,316 severe hail reports from January 2011 through June 2016 and overlaying them onto the dual-Doppler coverage map shown in Figure 6. Because the actual coverage area for each radar changes based on the PRF used at the time a storm was ongoing (National Severe Storms Laboratory 2007), no assumptions were made regarding the viability of any case study until data was downloaded and examined in detail. The vast majority of hail reports falling within dual-

radar coverage were eliminated due to issues with range folding (RF) obscuring necessary velocity data or incomprehensibly aliased velocities due to high wind speeds in the upper levels of the storm. After filtering, 59 hail reports were left and selected to be case studies. A graphic of each case study, the date and time, and size of reported hail are listed in Case Studies.

Methods

Radar Sampling

In this study, radar data analysis was done in a Cartesian grid. Therefore, raw radar data in polar coordinates had to be resampled to (X, Y) prior to analysis. WSR Toolkit, a custom radar data analysis software package written specifically for this research and named for the **W**eather **S**urveillance **R**adar data it designed to use, was implemented both to sample and interrogate input radar data. Once a case study was isolated, an analysis domain was defined such that the entire cell of interest was included in the bounds. Additionally, a minimum and maximum altitude in meters above mean sea level was defined for each case study.

With the bounds of an analysis set, the X, Y, and Z subdivision steps could be defined. For the sake of consistency, a sampling resolution of 1km was selected for X, Y, and Z resolution. The horizontal domain varied based on the size of the storm analyzed, but the vertical domain was always set to 0-20km above ground level. To compute sampled values at each 3D grid cell (henceforth referred to as a 'voxel'), the radar sweeps above and below a voxel were analyzed. To avoid a noisy gridding output (Figure 7), the voxel is broken into a sub-grid of 3x3 cells (Figure 8). The gate value for each data moment is sampled into the

sub-grid by taking the azimuth and distance of the center of each sub-cell and determining what gate that cell falls into. By this method, the data is oversampled, effectively allowing the resulting value to be a weighted average of the gates intersecting the voxel of interest. The sweeps above and below the voxel of interest are sampled at the location of the voxel, as illustrated in Figure 9. The resulting values are then interpolated using inverse distance-weighted (IDW) interpolation in accordance with the vertical distance between the voxel and each of the sampled sweeps. Second-power IDW interpolation was used as a compromise between linear interpolation, which rarely captured actual radar data values, and nearest neighbor, which caused sharp changes between successive grid points. In cases in which a voxel falls below the beam center of the lowest tilt, cells below the half-power beam horizon are not processed. Similarly, a cell that is above the half-power beam horizon at the highest tilt is also culled from the analysis.

A significant problem for sampling that had to be dealt with was storm advection during a radar volume. Because all sweeps in a radar volume are not taken simultaneously, a storm can move a significant distance over the course of a volume scan, illustrated in Figure 10. To correct for this effect and restore the vertical relationship of data, the location of the radar for the purpose of sampling can be relocated for each sweep in accordance with sweep time and storm motion. For instance, if a storm is moving northeast at 25m/s during a volume scan, the radar location for a sweep occurring one minute after the first sweep would be moved southwest by 1.5km. This method (illustrated in Figure 11), while spatiotemporally imperfect, corrects this effect as well as possible to improve the accuracy of algorithms that rely on vertical storm structure.

Earth curvature posed a unique problem for this study. Due to the large distances associated with NEXRAD-derived dual-Doppler analyses, curvature of the Earth had to be taken into account when using radar beam elevation angle in the dual-Doppler formula. It is typically assumed that beam elevation relative to gravity is constant over a dual-Doppler domain; in the vast majority, this is true because the analyses are completed at fairly close range (such as Kosiba et al. (2013)). However, effective elevation of the beam relative to gravity occurs with distance as the Earth falls away from the beam. To correct this, a spherical Earth was assumed and the distance of an observation in decimal degrees was computed. The distance in decimal degrees, when added to the beam angle, is the effective sampled elevation. Taken to the extreme, this means that the effective sampling elevation approaches 90° as distance from the radar approaches infinity. In practice, this value rarely exceeds 1.5° due to the need for radars to be within approximately 130km of one another. This is illustrated in Figure 12. If a volume equidistant from a pair of radars is simultaneously sampled at a beam elevation angle of 0 degrees, the axis of gravity is perpendicular to the radar beam at the location of the radar, but as distance increases the effective beam elevation increases. In analyses that accept input from two radars, the effect is doubled. It is especially important when working with radial velocities; a velocity sample close to the radar in this example is entirely horizontal but a sample at long range has lost some of its horizontal component and gained a non-zero vertical component.

Dual-Doppler Analysis

To verify accuracy of the dual-Doppler analysis methods herein, fine scale data from mobile radar was used. The Center for Severe Weather Research (CSWR) provided two volume scans from the Goshen County, WY storm intercept during the VORTEX2 field study

on June 5, 2009. The provided data was one of the dual-Doppler volumes collected by DOW6 and DOW7 used in Kosiba et al. (2013).To prepare data for sampling, a voxelized volume was calculated in sinusoidal coordinates, with the central meridian running through the center of the analysis domain and false northing computed to place (0, 0) at the intersection of the central meridian with the southern boundary of the analysis region. The sampling methodology was based on the Barnes (1964) scheme as modified by Koch et al. (1983). Kosiba et al. (2013) implements a two-pass implementation on a 100m grid with a second pass convergence parameter, in accordance with the findings of Majcen et al. (2008).The sampling results were then placed in a three-dimensional array and handed off to the dual-Doppler routine.

The Dual-doppler algorithm as laid out in Dowell and Shapiro (2003) was implemented and tested on the sampled data. In the verification phase, integration of vertical velocity was done from the bottom of the dataset upward. An initial boundary condition of w=0 was used, and the wind field was successively calculated by moving upward and iterating computation of u, v, w, and convergence (Dowell and Shapiro 2003).Once results of the analysis were verified against the findings of Kosiba et al. (2013), the method was tested on voxelized results from WSR Toolkit's sampling algorithm (Figure 13). Because the method of sampling was non-Gaussian, retrieved vertical velocity values were much noisier. However, because this study focuses primarily on vorticity and the elevation angles from which data are sampled are relatively shallow, this was not shown to have a significant impact on retrieved vorticity values.

Gridded Data Analysis

Implemented in WSR Toolkit is a rudimentary system that allows user-defined analyses to be run on gridded radar data. Currently implemented analyses include VIL, VIL Density, Echo Tops, Composite Reflectivity, Severe Hail Index (SHI), Probability of Severe Hail (POSH), and Maximum Estimated Size of Hail (MESH). Where possible, the methodology used by NSSL's Multi-Radar Multi-Sensor (MRMS) system to calculate a given derived radar product was replicated. To confirm that WSR Toolkit gridding worked properly, MRMS values for the aforementioned derivative radar products were compared with WSR Toolkit values. When resampling of a radar volume is complete, the resulting three-dimensional grid of voxels is passed to each analysis routine and a derived product is calculated and added to each voxel. This method was chosen so that algorithms designed to run on gridded radar products (such as those that make up the MRMS product suite) can be built and run in the same way they operate in everyday National Weather Service use..

Hail-Growth Zone Vorticity Analysis

After data was advection corrected and gridded and a dual-Doppler analysis was complete, a modified version of the MESH algorithm (in the form of a WSR Toolkit plugin) was executed on the analysis results. MESH is the square root of the Severe Hail Index (SHI), which is defined as follows, defined by the Warning Decision Training Branch (2014):

$$\dot{E} = 5 \times 10^{-6} \times 10^{0.084Z} W(z)$$

Where $\dot{E}$ is hail kinetic energy, Z is radar reflectivity, and W(Z) is a weight based on reflectivity, as illustrated by the Warning Decision Training Branch (2014):

$$W(Z) = \begin{cases} 0 & \text{for } Z \leq Z_{\mathrm{L}} \\ \dfrac{Z - Z_{\mathrm{L}}}{Z_{\mathrm{U}} - Z_{\mathrm{L}}} & \text{for } Z_{\mathrm{L}} < Z < Z_{\mathrm{U}} \\ 1 & \text{for } Z \geq Z_{\mathrm{U}}. \end{cases}$$

Where Z_L and Z_U are lower and upper reflectivity thresholds, respectively. Values of 40dBZ and 50dBZ were used, in accordance with Warning Decision Training Branch (2014). A temperature weight is also applied, using 0C and -20C as thresholds:

$$W_{\mathrm{T}}(H) = \begin{cases} 0 & \text{for } H \leq H_0 \\ \dfrac{H - H_0}{H_{\mathrm{m20}} - H_0} & \text{for } H_0 < H < H_{\mathrm{m20}} \\ 1 & \text{for } H \geq H_{\mathrm{m20}}, \end{cases}$$

Once each level of the analysis is complete, the values are vertically integrated to compute SHI:

$$SHI = 0.1 \int_{H_o}^{H_t} W_T(H_T) \dot{\mathrm{E}}\, \mathrm{dH},$$

Where H_0 is ground level, H_t is the maximum altitude of the analysis, W_T and H_T are weights, Ė is hail kinetic energy, and dH is the change in height between analysis layers.

The maximum value from the analysis region was accepted as the final maximum hail size value (for later comparison for case study quality determination) and dual-Doppler derived vorticity was weighted in all voxels in accordance with W_T and H_T for each voxel then averaged across all areas producing a non-zero SHI value to produce a weighted average vorticity for areas of the storm assumed to be involved in hail growth.

Results

With the case studies isolated and methodology established, radar data associated with each case was gridded and analyzed using a WSR Toolkit plugin designed to simultaneously calculate MESH and average vorticity in areas where hail growth is probable. Figure 14 depicts the distribution of computed MESH values for all case studies. The chief difference between it and the actual reported hail size values (Figure 15) is the presence of reports under 0.75 inches, which are not archived by the National Center for Environmental Information and do not exist in records. In this case, those results are instances in which the MESH algorithm underestimated hail size. In a direct comparison of MESH results versus reported hail size, shown in Figure 16, MESH does well at predicting the size of actual hailstones produced by a given storm. It tends to overestimate, which is expected behavior as it is designed to predict the *maximum* size one might expect and was verified using the largest hailstones spotters reported – quite likely not the largest produced.

Next, we examine the relationship between measured vorticity and size of reported hail. In Figure 17, actual reported hail size is plotted against vorticity as measured in the hail growth region of the storm, established by the MESH algorithm. There is limited data available for storms with negative measured vorticity, although one might reasonably expect hail production potential to increase as negative vorticity becomes stronger. Instead of introducing further complexity into the model by trying to handle positive and negative vorticity, we will use the absolute value of measured vorticity (Figure 18). Plotting the results of the MESH algorithm in the same fashion show a similar though much noisier trend (Figure 19). A trend line placed on the plot of reported hail and measured vorticity

yields an impressive R^2 value of 0.514 (Figure 18). This correlation will be explored later in this chapter. The plot of MESH results against vorticity also shows that a linear regression can explain a large amount of variance in hail size, though the plot is noisier and has a lower R^2 value of 0.1 (Figure 19). This is not unexpected, as MESH is by design unaware of anything but radar reflectivity and temperature; as discussed earlier no velocity data is assimilated into the algorithm.

A linear regression was run using the absolute value of measured vorticity as a predictor of hail size. The result of that regression is shown in Figure 20. It shows that vorticity is correlated with the size of hail produced by storms at a significance of $P<0.0001$ – much stronger than the commonly employed significance level of $P<0.05$. This, however, does not tell the entire story. Figure 21 shows MESH error, expressed in inches difference from a reported size, plotted against the absolute value of measured vorticity. At first glance, it does not appear that the absolute value of measured vorticity is necessarily a good predictor of MESH error. Though a regression (results shown in Figure 22) showed that vorticity itself had acceptable ($P<0.05$) significance, the intercept was unsuitable. A multiple regression run using Max MESH and vorticity to predict hail size (Figure 23) does show improvement versus using either variable alone; all regression coefficients return with high significance and the R^2 for the model rises to 0.53 from 0.51. Based on this data, it seems that vorticity can be used as an input to adjust returned MESH values to improve forecast skill, however it should be employed only on storms known to be producing severe hail, as the regression equation uses vorticity as the primary predictor.

Conclusion

The strong correlation between measured vorticity and reported hail size, on the face of it, seems very interesting but poses a difficult chicken-and-egg problem. There are two ideas in play. First, it is possible that rotating storms tend to produce larger hailstones because a longer, helical trajectory of a hail embryo allows a hailstone to grow larger. However, that is difficult to separate from the second idea that a storm existing in a shear environment conducive to long life and hail production will naturally begin to rotate as a consequence of wind dynamics in the northern hemisphere (Smith et al. 2012). Thus, rotation occurring in a favorable shear environment may enhance the size of hail or the same favorable shear environment may cause large hail and the tendency to rotate as two parallel effects. The inseparability of these concepts based on data available for this study leads to the conclusion that a vorticity input to the MESH algorithm will not significantly improve its skill at estimating hail size. It is, however, patently clear from Figure 18 that while the floor for hail production remains similar through much of the spectrum of vorticity, the ceiling does markedly increase. Overall, this result confirms what we already knew: better-organized storms that, in the northern hemisphere, tend to exhibit positive vorticity will also tend to produce larger hail.

Several key limitations affected this study. First and foremost, there was no ground truth hail data available for sizes below 0.75" due to 1.00" being the threshold for severe hail. This limited evaluation of the hail size floor of storms with increasing vorticity and most certainly had a negative impact on the relationship shown through the linear regression. Although the policy for recording hail events is unlikely to change, access to hail datasets collected for other research may help to fill in this hole. Second, case study

availability was a big limiting factor. The geographical extent of dual-Doppler coverage near radar pairs was not as favorable as in traditional dual-Doppler studies such as that of Kosiba et al. (2013) in which portable radar units were added to the arsenal at appropriate locations to create dual dopler conditions in desirable locations.. If the study area were extended to other less favorable radar pairs, additional case studies could be found. Further case studies would hopefully provide additional data points for significant severe hail of 2.00" or higher diameter. Development of a GIS method to calculate and report constrained dual-Doppler coverage (such as in Figure 5) would greatly enhance this process. The third and final significant barrier in this study was the inability to analyze storms without any sort of ground truth for hail production. During the process of searching for case studies, there were many instances in which a storm produced a verified hailstone outside appropriate radar coverage but passed through the study area without a report. This, in addition to the lack of reports on storms producing less than severe hail, greatly limited available data.

For future research, it may prove necessary to relax the restriction of only using dual-Doppler vorticity and back off to a single-radar approach. The restriction for this study was born of the idea that all rotation will exhibit azimuthal shear on radar, but not all azimuthal shear is guaranteed to be rotation. This resulted in relatively high quality but also relatively sparse data. Newman et al. (2013) proposed a way of diagnosing circulations in storms out to well over 100km from a radar station. This approach has the potential to increase available case studies by at least an order of magnitude because it does not rely on favorable geometry of a second available radar station. Future work may also benefit from attempting to control for additional radar variables; storm height is an obvious candidate

for expansion of this research, although controlling for more variables will necessitate a larger sample size. Environmental variables might also be considered, including wind and thermodynamic data.

Additionally, a brief field study should take place to collect additional verification case studies. To ensure collection of hailstones with minimal loss of mass due to melting, hail-producing thunderstorms should be intercepted just upwind on the west side of the precipitation. Cross sections should be driven through the hail track of the storm, with 30-40 hailstones collected per cross section to ensure the largest hailstones are found. Assuming a rough West to East storm motion, collection of data should occur on North-South routes that cross the path of the thunderstorm. The storm should be closely followed and the synchronization of the two radars scanning it should be monitored, so as to ensure an acceptable dual-Doppler case study on the collected hail. The aforementioned theoretical GIS model would give guidance as to where to pursue storms to maximize potential for dual-Doppler data.

Figures

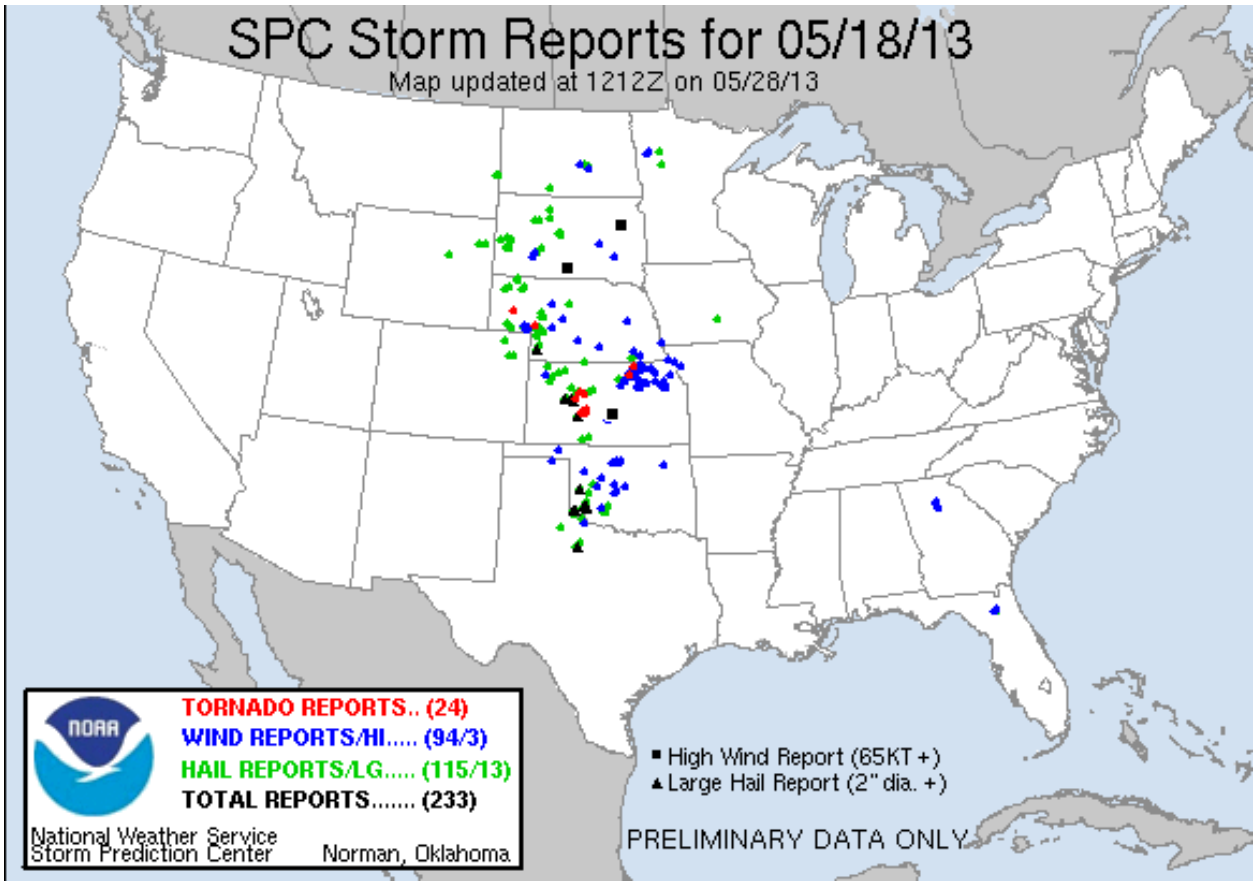

Figure 1: NOAA Storm Prediction Center storm reports for May 18, 2013. The tornadoes (red dots) generally occur near green dots (large hail), qualitatively indicating some level of correlation of rotating storms and large hail.

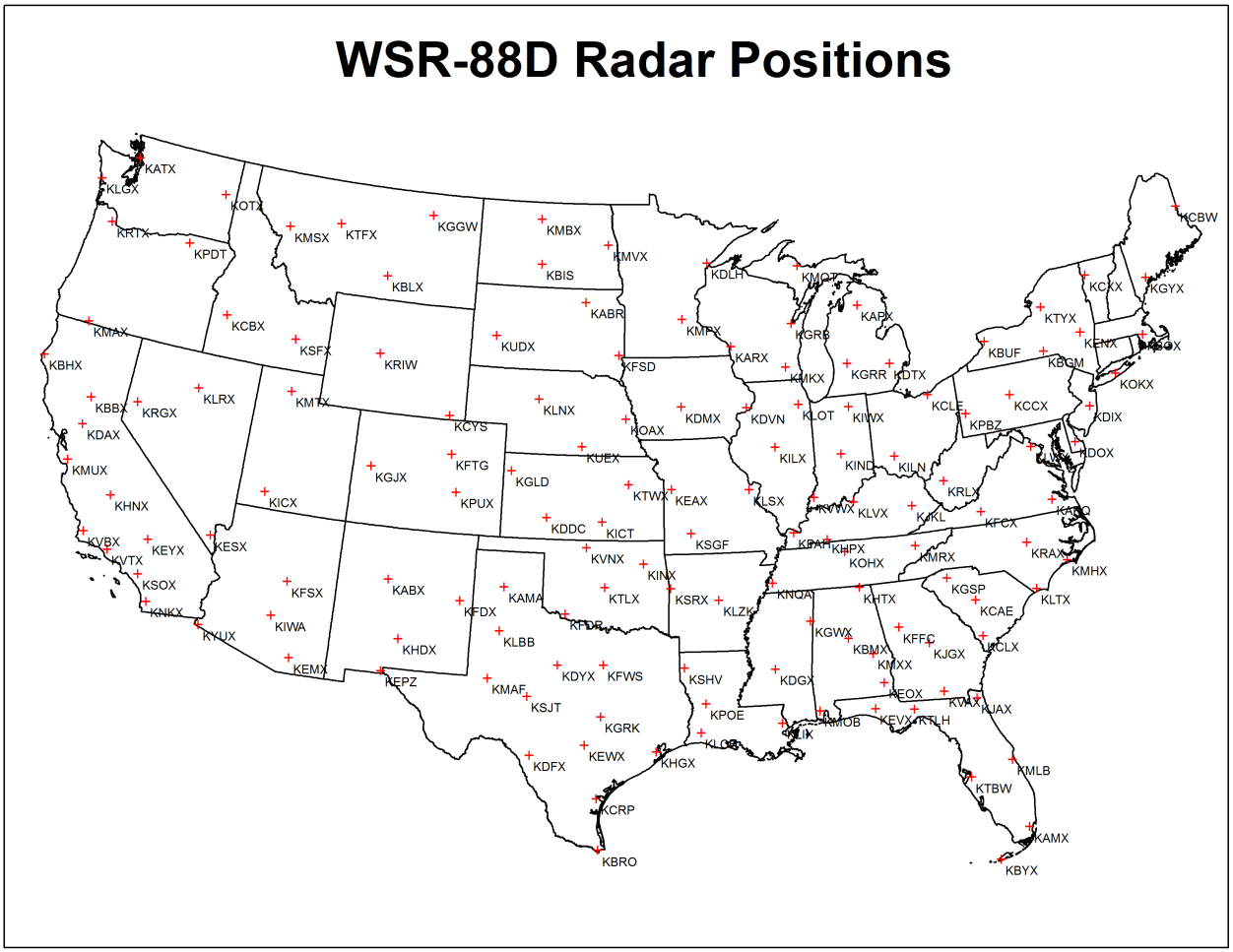

Figure 2: Positions of NEXRAD WSR-88D Radars

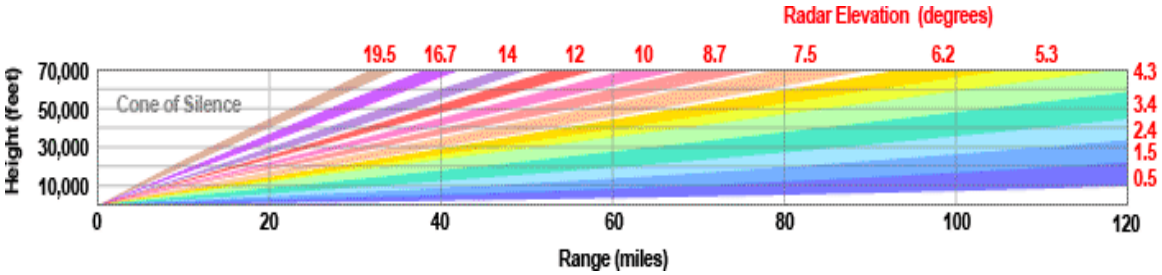

Figure 3: Illustration of beam elevation angles used in Volume Coverage Pattern 11.

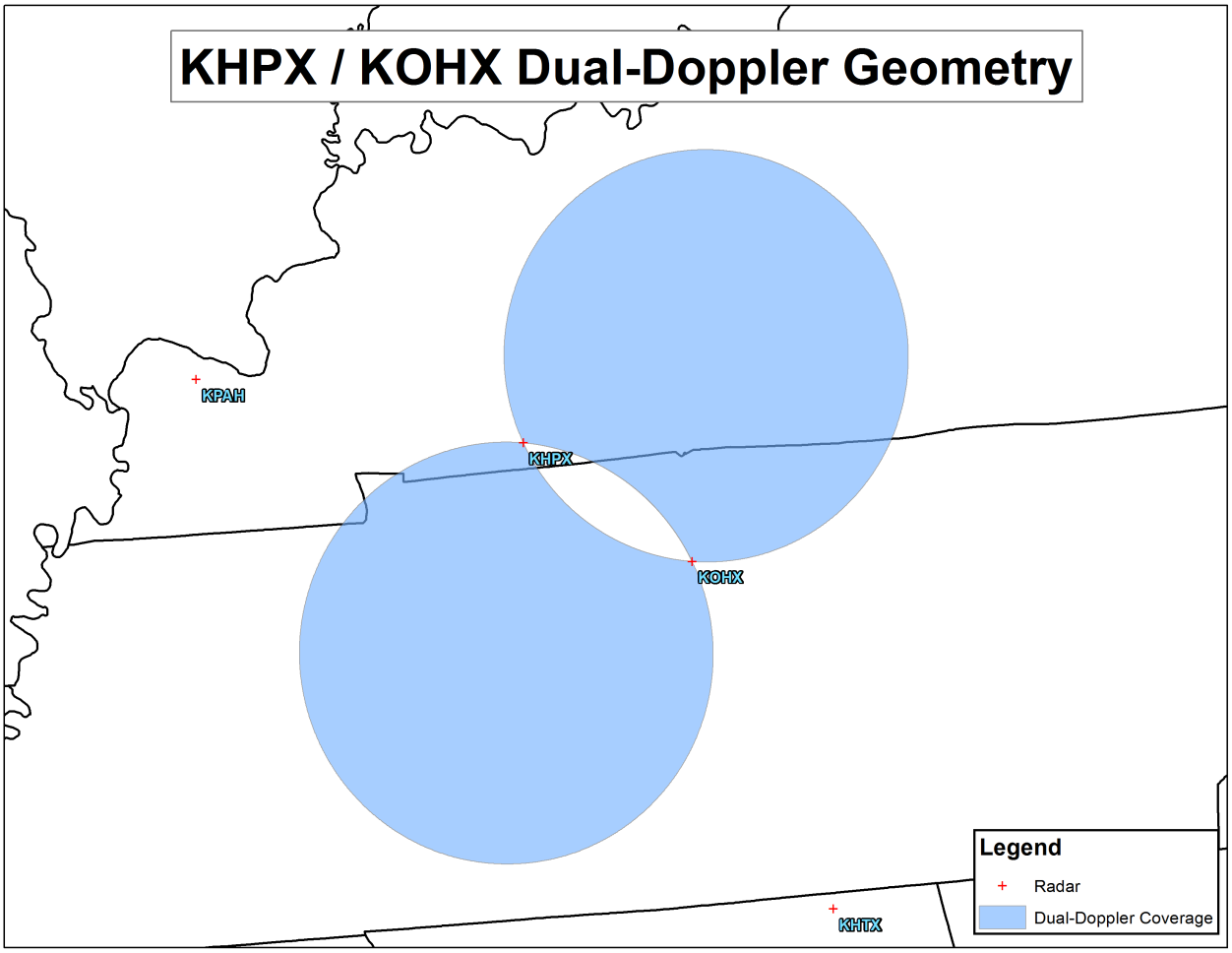

Figure 4: Dual-Doppler geometry for KHPX and KOHX in Kentucky and Tennessee.

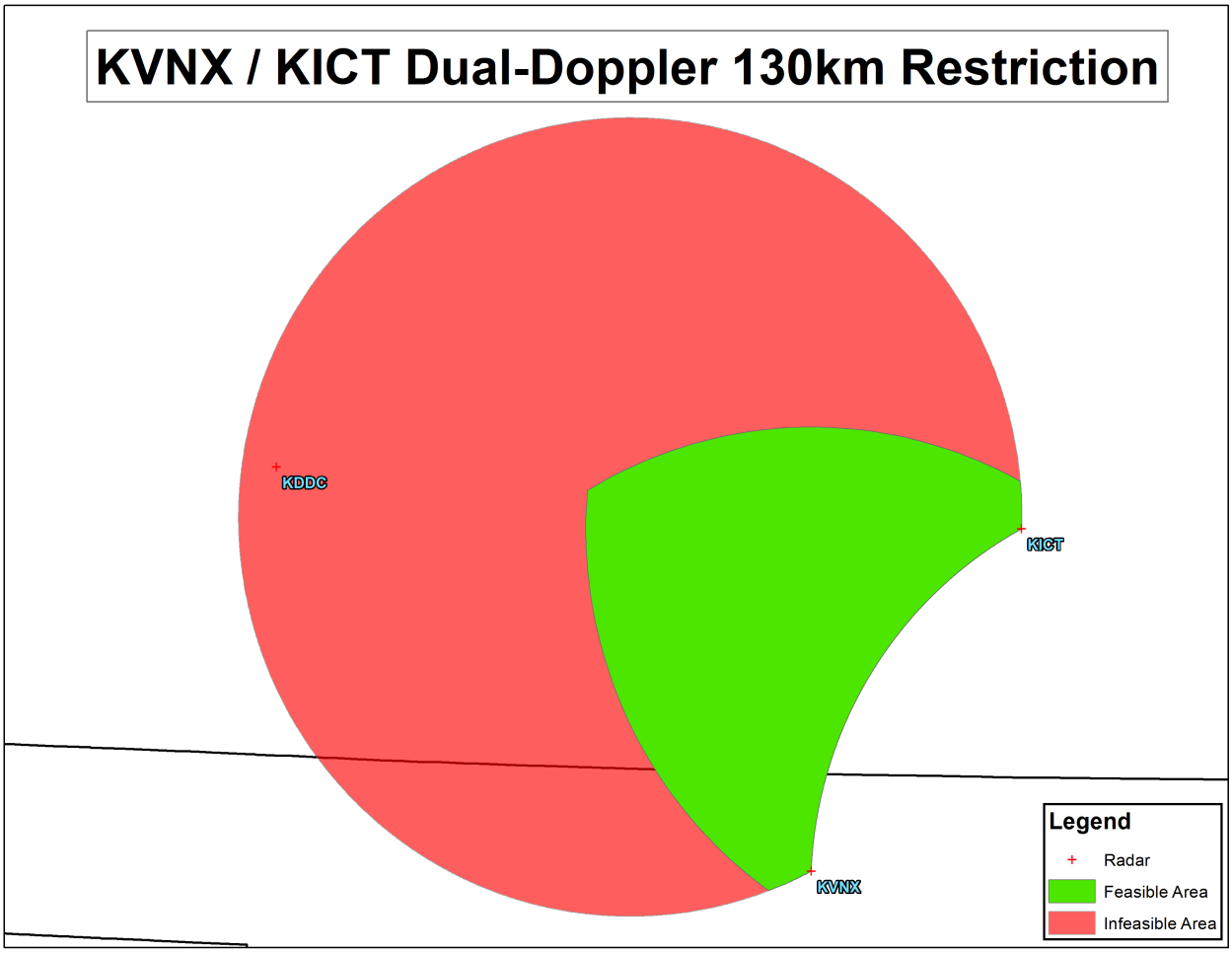

Figure 5: One side of a dual-Doppler lobe formed by KICT and KVNX in KS/OK. The green area denotes the usable portion of the coverage area, given a 130km maximum range for the radar.

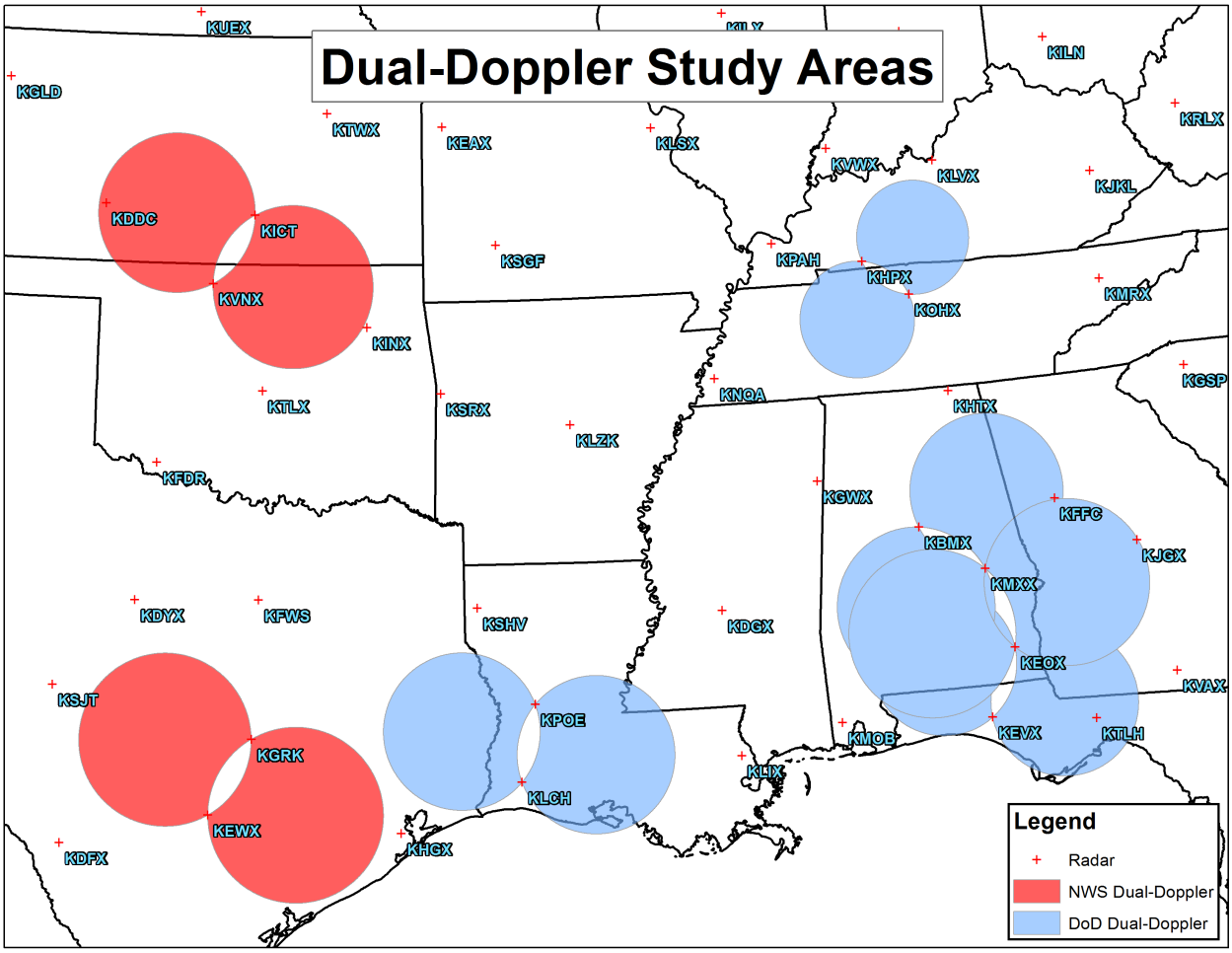

Figure 6: Dual-Doppler study areas used. Red areas use only National Weather Service radars. Blue dual-Doppler lobes involve at least one radar owned by the Department of Defense.

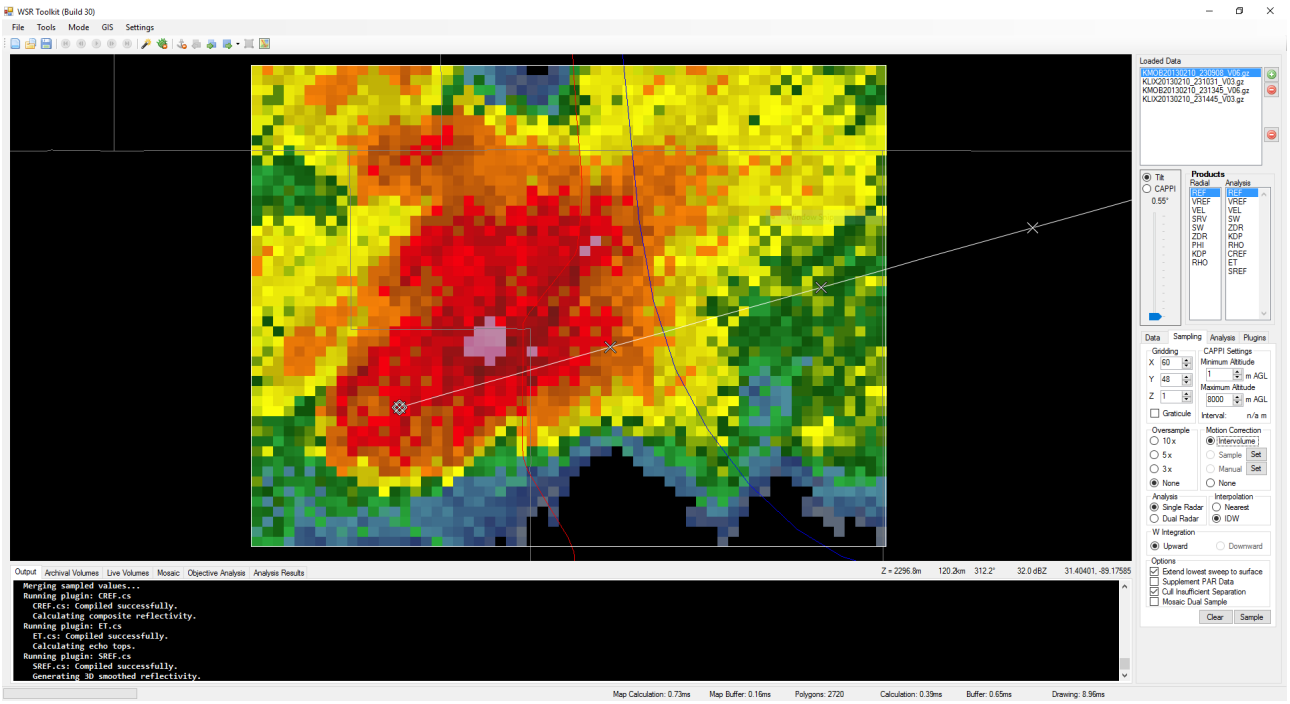

Figure 7: Gridded reflectivity from the 10 February 2013 supercell that produced an EF4 tornado in Hattiesburg, MS.

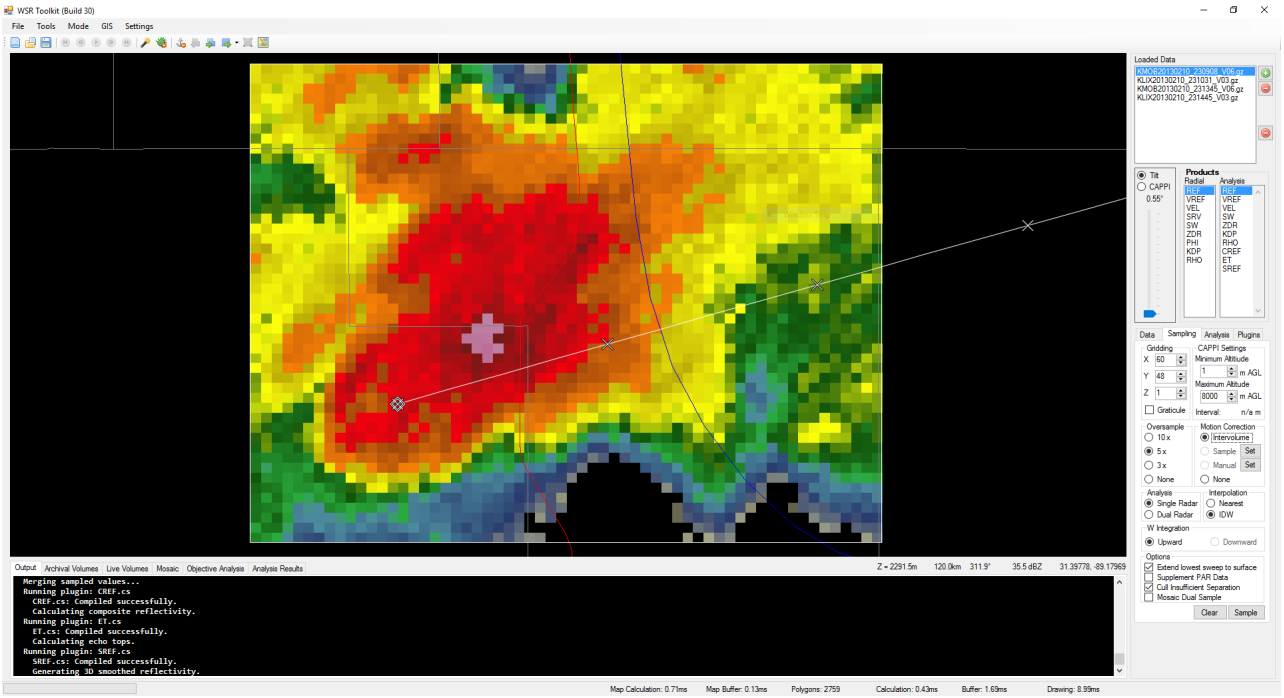

Figure 8: 5x5 subsampled gridded reflectivity from the 10 February 2013 supercell that produced an EF4 tornado in Hattiesburg, MS.

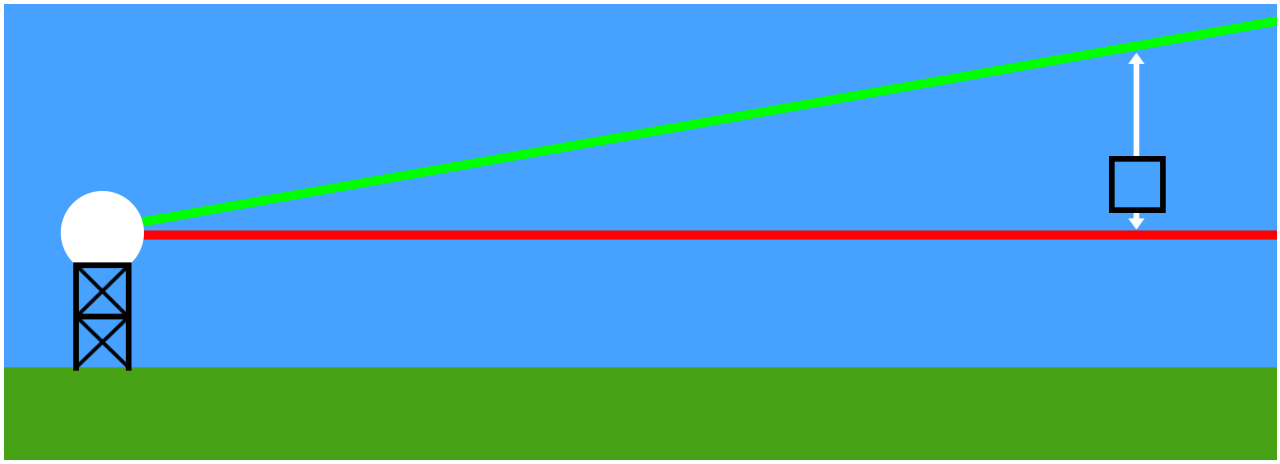

Figure 9: An illustration of a voxel between two radar beam elevations. The lower sweep would be sampled at the location of the voxel, then the upper beam would be sampled and the two values would be combined.

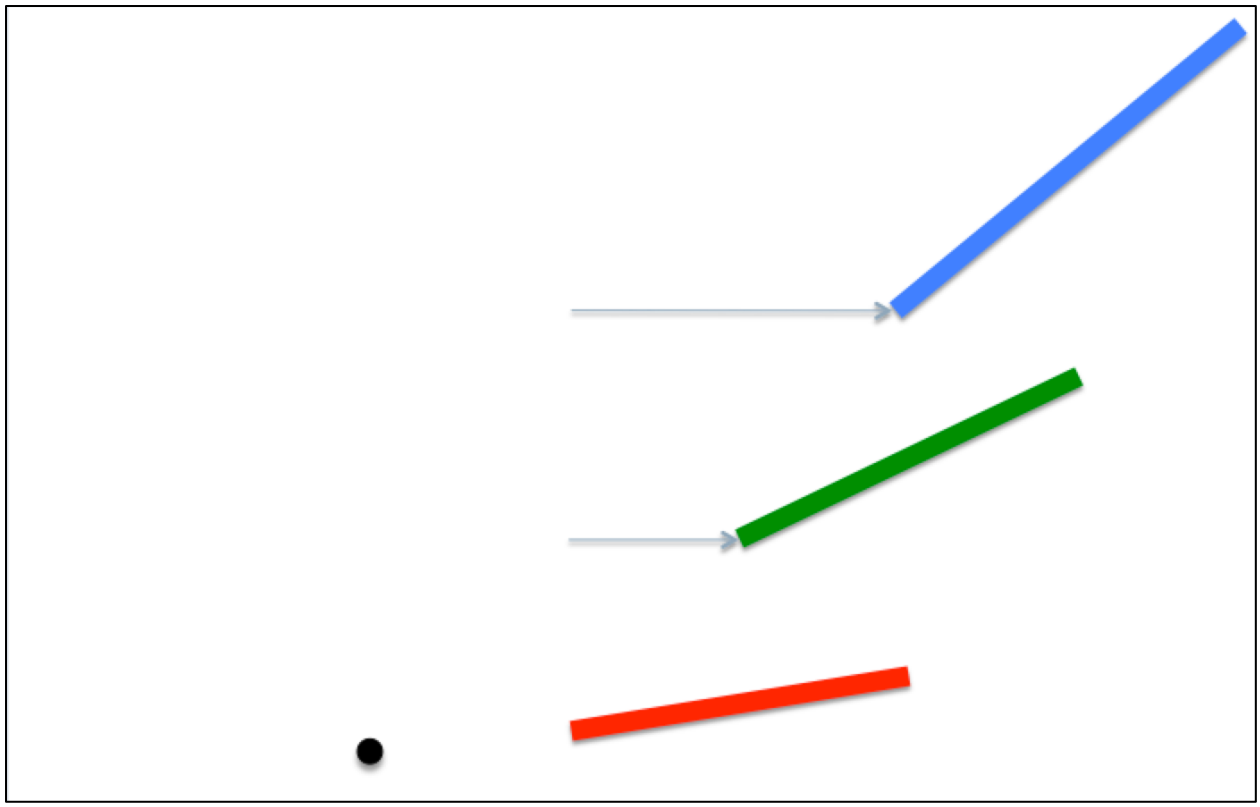

Figure 10: Illustration of storm motion on successive radar sweeps. The location of the radar is marked as the black dot. After the first sweep (red), the storm moves downwind. By the time the second (green) sweep is taken, the storm has moved and the region previously located directly above the region sampled in the first sweep does not appear so in the data. The same is true of the third (blue) sweep, except that it is further offset from the first.

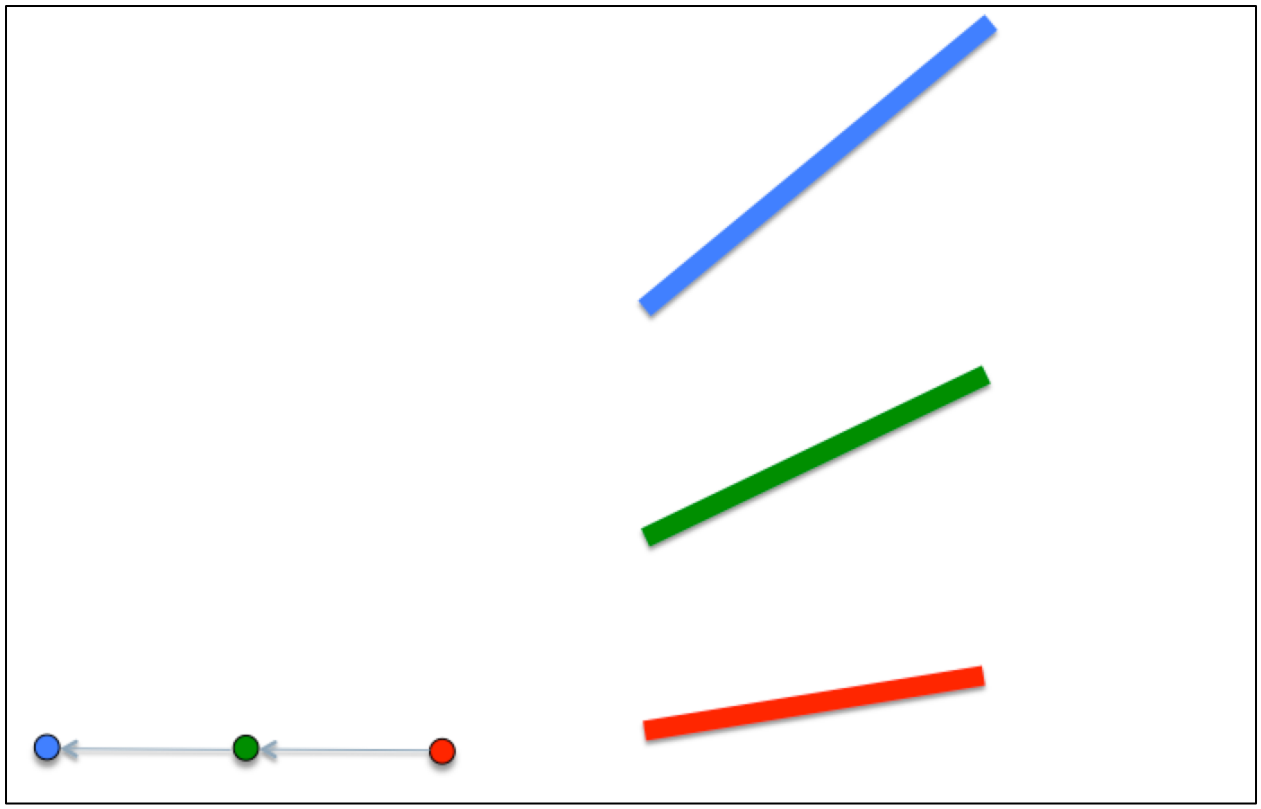

Figure 11: Illustration of virtually moving the radar location for sampling to restore vertical storm structure. As shown in Figure 10, storms move between sweeps. Therefore, if storm motion is known the radar can be moved backward against storm motion to correct for the effect. For the purpose of sampling, the radar in this case is moved backward for the second (green) and third (blue) sweeps to bring back the vertically stacked orientation of the sampled volumes.

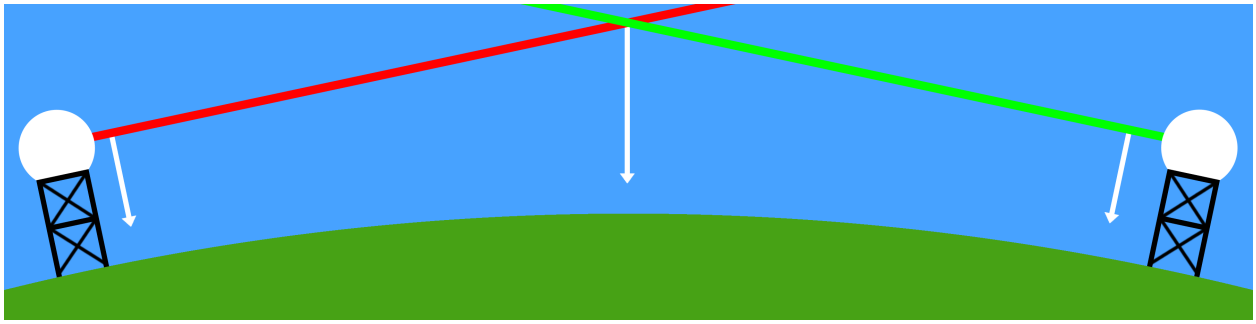

Figure 12: Illustrates two radars sampling a distant volume at beam elevation of 0 degrees. Close to the radar, the beam is perpendicular to gravity. At range, the beam's elevation relative to gravity has increased.

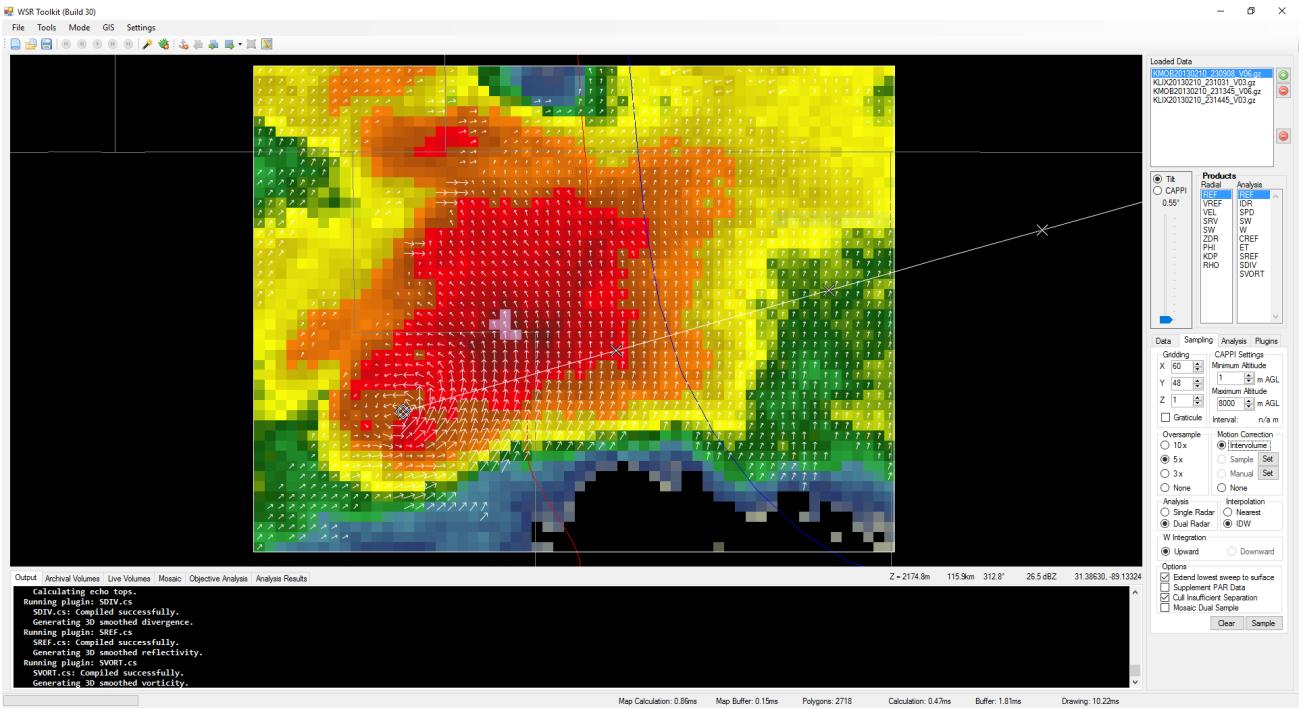

Figure 13: Dual-Doppler analysis of the 10 February 2013 supercell that produced an EF4 tornado in Hattiesburg, MS.

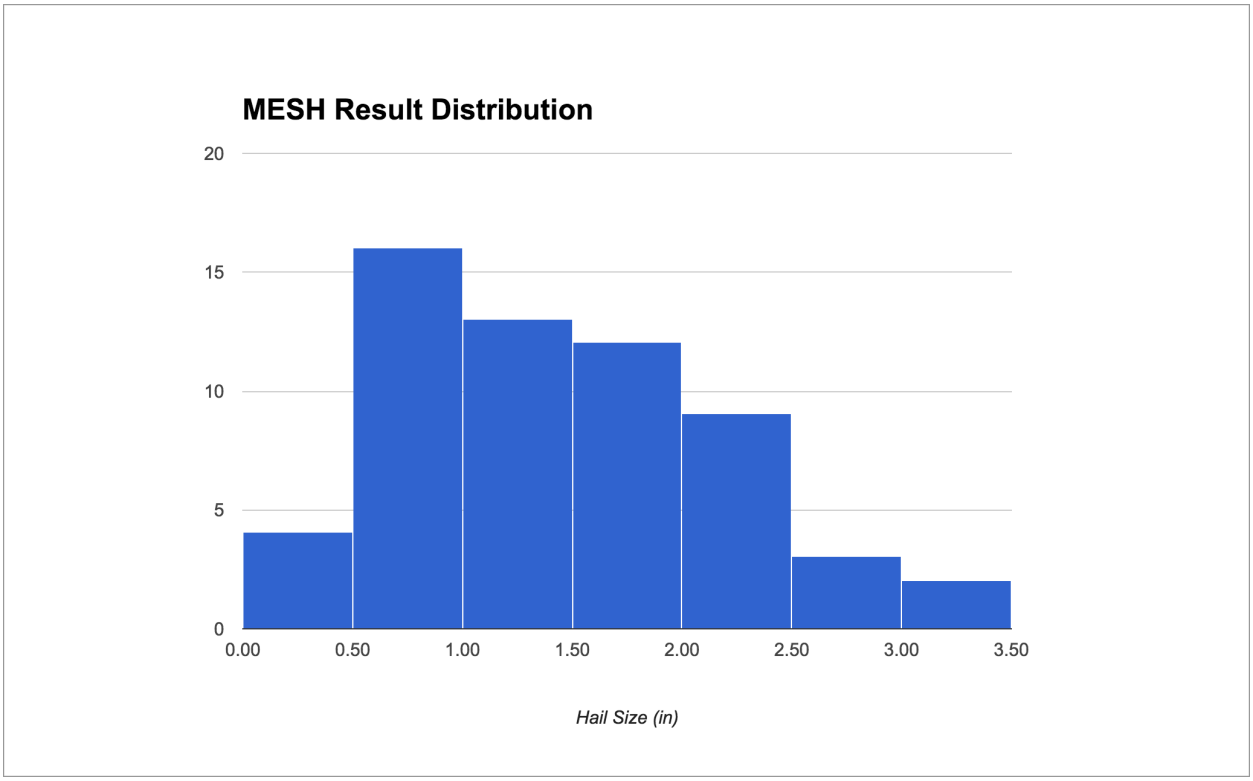

Figure 14: Distribution of MESH results over 59 case studies.

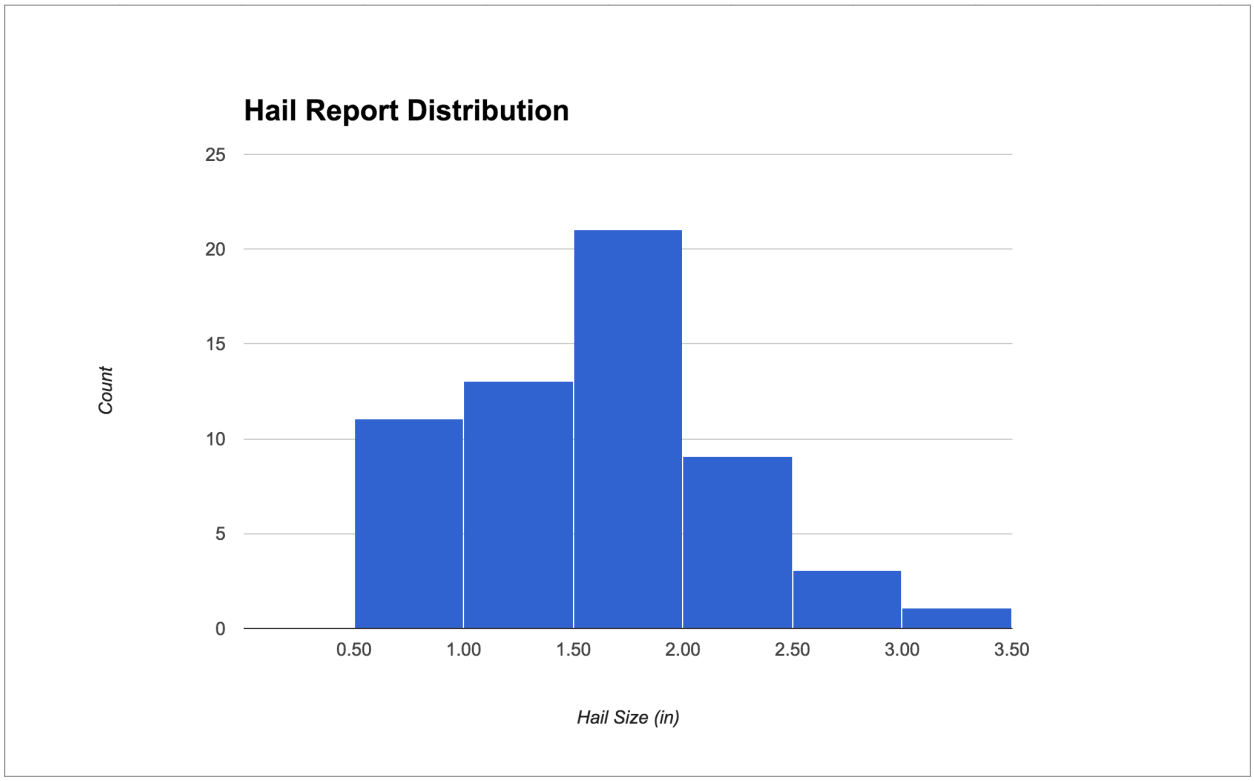

Figure 15: Distribution of hail size in reported hail for 58 case studies. 4.25" outlier omitted in this plot.

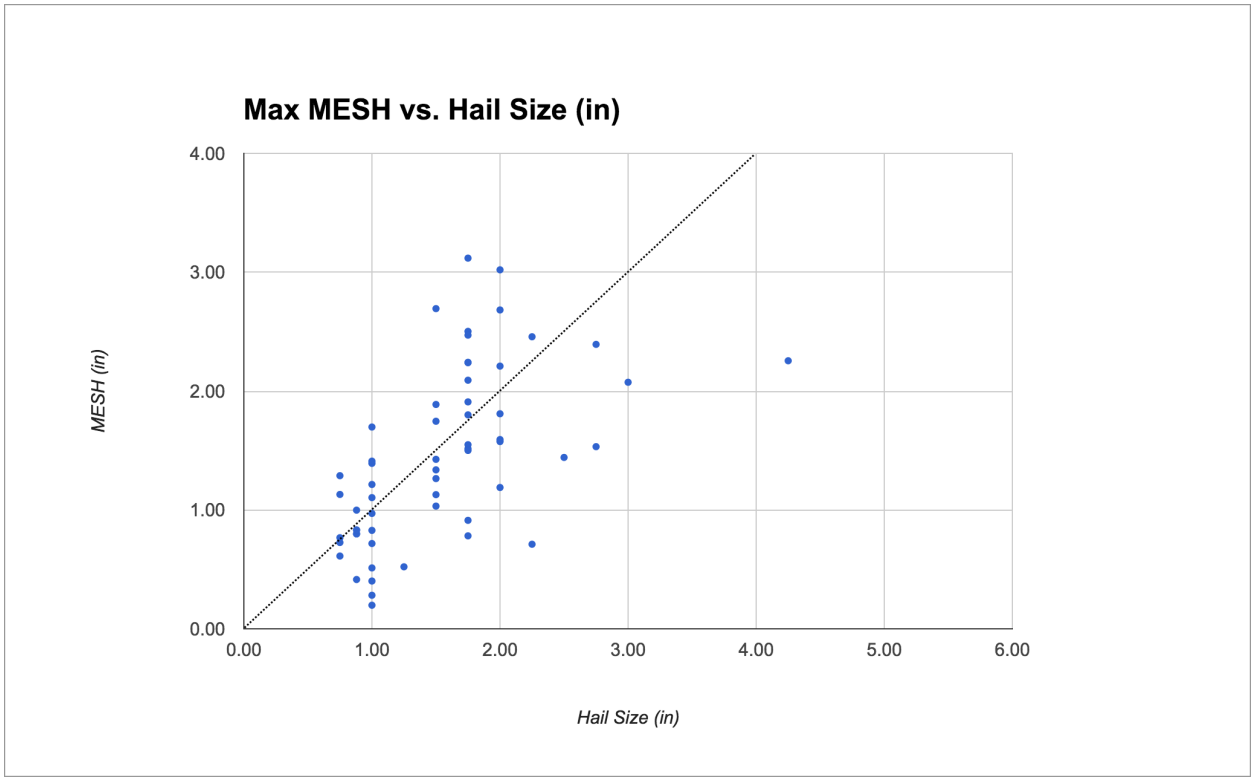

Figure 16: MESH values plotted as a response to reported hail size. Line shown at Y = X.

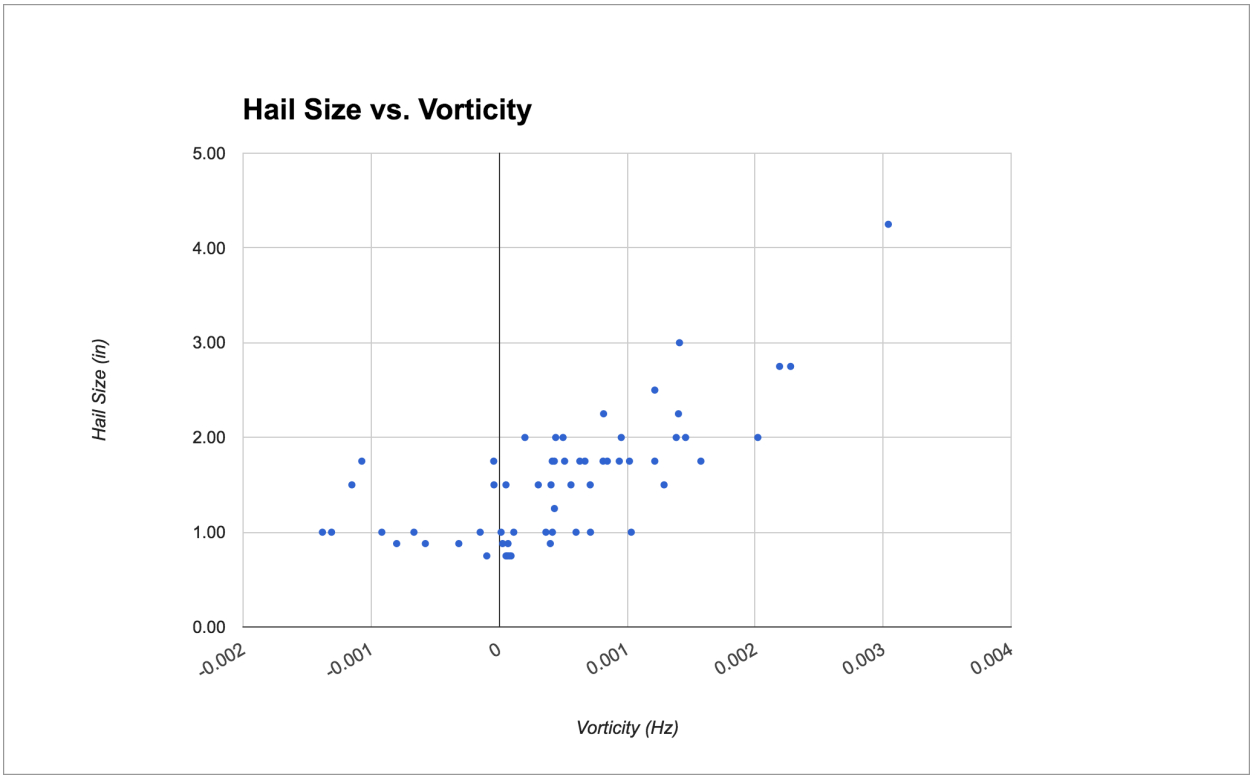

Figure 17: Reported hail size plotted against measured vorticity in the upper levels of the storm.

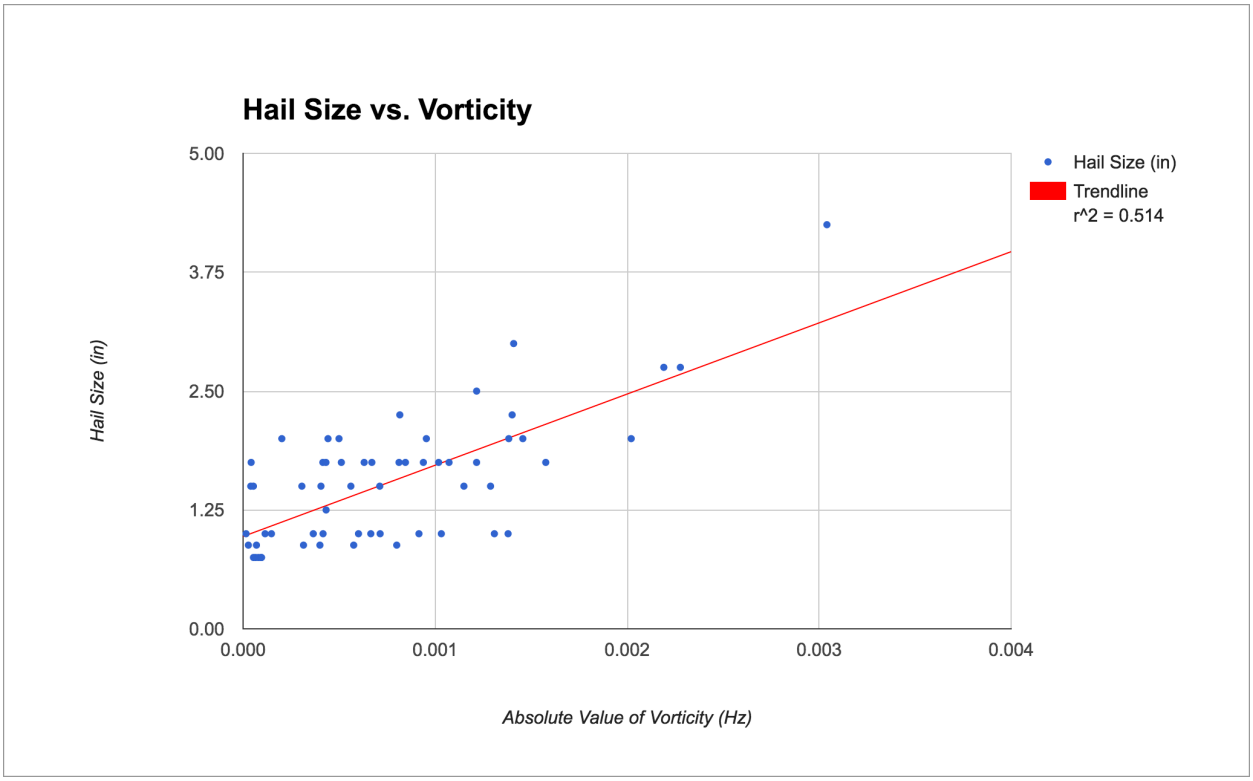

Figure 18: Reported hail size plotted against vorticity with a trend line overlaid.

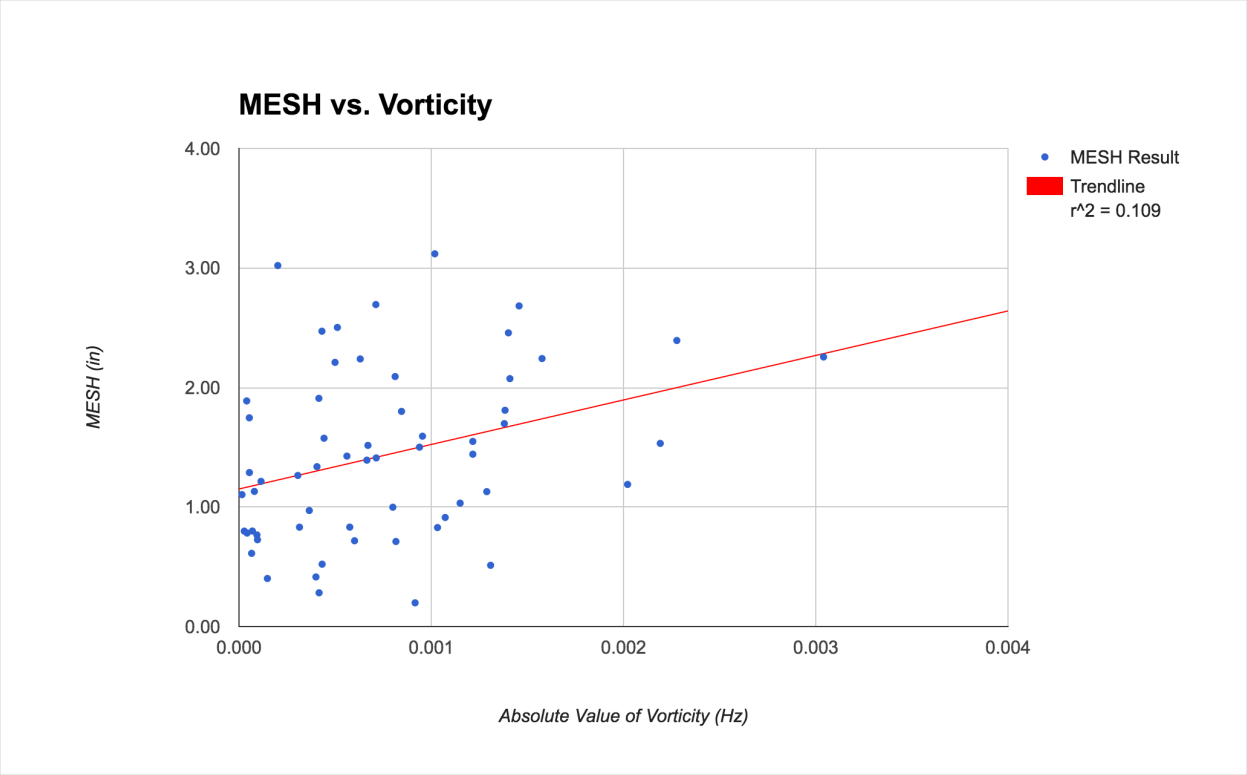

Figure 19: MESH plotted against the absolute value of measured vorticity with a trend line overlaid.

Overall Fit

R-square	0.514
Adj R-square	0.505
Residual SD	0.468
Sample SD	0.666
N observed	59
N missing	

Coefficients

	Estimate	Std. Error	t value	Pr(>|t|)
(Intercept)	0.971	0.095	10.203	< 0.0001
Vorticity	748.758	96.499	7.759	< 0.0001

ANOVA Table

	Df	Sum Sq	Mean Sq	F value	Pr(>F)
Model	1	13.211	13.211	60.206	< 0.0001
Residual	57	12.507	0.219		
Total	58	25.718	0.443		

Figure 20: A linear regression using absolute value of measured vorticity as a predictor of hail size.

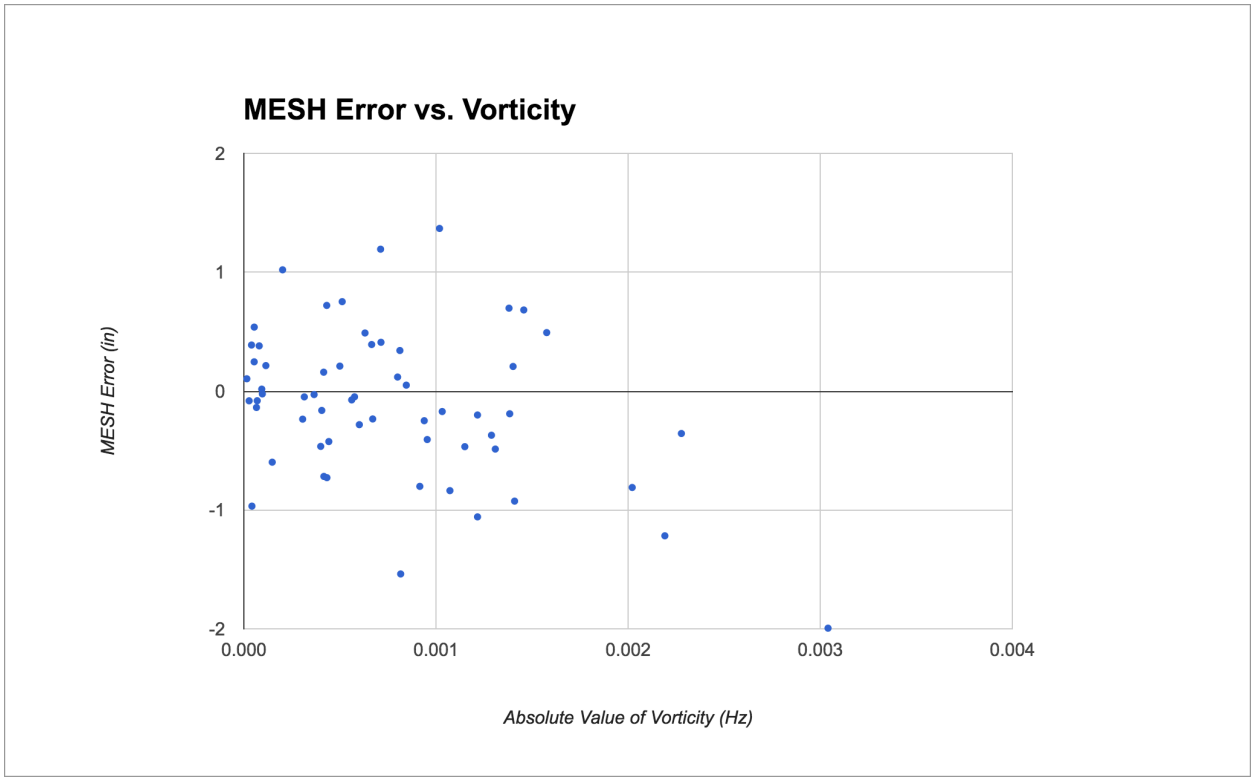

Figure 21: Error of the MESH algorithm in inches as a function of the absolute value of measured vorticity.

Overall Fit

R-square	0.143
Adj R-square	0.128
Residual SD	0.592
Sample SD	0.634
N observed	59
N missing	

Coefficients

	Estimate	Std. Error	t value	Pr(>|t|)
(Intercept)	0.179	0.120	1.490	0.1416
Vorticity	-376.304	122.009	-3.084	0.0031

ANOVA Table

	Df	Sum Sq	Mean Sq	F value	Pr(>F)
Model	1	3.337	3.337	9.512	0.0031
Residual	57	19.995	0.351		
Total	58	23.331	0.402		

Figure 22: Linear regression using the absolute value of measured vorticity as a predictor of error in the MESH algorithm.

Regression Analysis: Hail Size (in) versus Max MESH, Vorticity

Method

Rows unused 939

Analysis of Variance

Source	DF	Adj SS	Adj MS	F-Value	P-Value
Regression	2	14.059	7.0295	33.76	0.000
Max MESH	1	4.279	4.2790	20.55	0.000
Vorticity	1	5.323	5.3231	25.57	0.000
Error	56	11.659	0.2082		
Total	58	25.718			

Model Summary

S	R-sq	R-sq(adj)	R-sq(pred)
0.456290	54.67%	53.05%	46.69%

Coefficients

Term	Coef	SE Coef	T-Value	P-Value	VIF
Constant	0.649	0.135	4.80	0.000	
Max MESH	0.01569	0.00346	4.53	0.000	1.11
Vorticity	469.4	92.8	5.06	0.000	1.11

Regression Equation

Hail Size (in) = 0.649 + 0.01569 Max MESH + 469.4 Vorticity

Fits and Diagnostics for Unusual Observations

Obs	Hail Size (in)	Fit	Resid	Std Resid		
2	4.250	2.956	1.294	3.21	R	X
20	3.000	1.945	1.055	2.35	R	
22	2.000	1.853	0.147	0.35		X

R Large residual
X Unusual X

Figure 23: Report for a multiple regression using Max MESH and vorticity to predict hail size.

References

Amburn, S. A., and P. L. Wolf, 1997: VIL density as a hail indicator. *Weather and forecasting*, **12,** 473-478.

Aydin, K., T. Seliga, and V. Balaji, 1986: Remote sensing of hail with a dual linear polarization radar. *Journal of Climate and Applied Meteorology*, **25,** 1475-1484.

Barnes, S. L., 1964: A technique for maximizing details in numerical weather map analysis. *Journal of Applied Meteorology*, **3,** 396-409.

Branch, W. D. T., cited 2016: Quick Reference VCP Comparison Table for RPG Operators. [Available online at http://www.wdtb.noaa.gov/tools/RPS/VCPCompTable.pdf.]

——, cited 2016: Severe Hail Index. [Available online at http://www.wdtb.noaa.gov/courses/MRMS/ProductGuide/SevereWeather/severe-hail-index.php.]

Center, N. R. O.: NEXRAD Technical Information. [Available online at https://www.roc.noaa.gov/wsr88d/Engineering/NEXRADTechInfo.aspx.]

——, 2016: Interface Control Document for the RDA/RPG.

Conway, J. W., and D. S. Zrnic, 1993: A study of embryo production and hail growth using dual-Doppler and multiparameter radars. *Monthly weather review*, **121,** 2511-2528.

Crum, T. D., and R. L. Alberty, 1993: The WSR-88D and the WSR-88D Operational Support Facility. *Bulletin of the American Meteorological Society*, **74,** 1669-1687.

Dowell, D. C., and A. Shapiro, 2003: Stability of an iterative dual-Doppler wind synthesis in Cartesian coordinates. *Journal of Atmospheric and Oceanic Technology*, **20,** 1552-1559.

Foote, G. B., 1984: A study of hail growth utilizing observed storm conditions. *Journal of climate and applied meteorology*, **23,** 84-101.

Heinselman, P. L., and A. V. Ryzhkov, 2006: Validation of polarimetric hail detection. *Weather and forecasting*, **21,** 839-850.

Koch, S. E., M. Desjardins, and P. J. Kocin, 1983: An interactive Barnes objective map analysis scheme for use with satellite and conventional data. *Journal of Climate and Applied Meteorology*, **22,** 1487-1503.

Kosiba, K., J. Wurman, Y. Richardson, P. Markowski, P. Robinson, and J. Marquis, 2013: Genesis of the Goshen County, Wyoming, tornado on 5 June 2009 during VORTEX2. *Monthly Weather Review*, **141,** 1157-1181.

Kropfli, R., and L. Miller, 1976: Kinematic structure and flux quantities in a convective storm from dual-Doppler radar observations. *Journal of the Atmospheric Sciences*, **33,** 520-529.

Laboratory, N. S. S., 2007: A Guide for Interpreting Doppler Velocity Patterns: Northern Hemisphere Edition. Second ed.

Majcen, M., P. Markowski, Y. Richardson, D. Dowell, and J. Wurman, 2008: Multipass objective analyses of Doppler radar data. *Journal of Atmospheric and Oceanic Technology*, **25,** 1845-1858.

Marzban, C., and A. Witt, 2001: A Bayesian neural network for severe-hail size prediction. *Weather and Forecasting*, **16,** 600-610.

Nelson, S. P., 1983: The influence of storm flow structure on hail growth. *Journal of the Atmospheric Sciences*, **40,** 1965-1983.

Nelson, S. P., and S. K. Young, 1979: Characteristics of Oklahoma hailfalls and hailstorms. *Journal of Applied Meteorology*, **18,** 339-347.

Newman, J. F., V. Lakshmanan, P. L. Heinselman, M. B. Richman, and T. M. Smith, 2013: Range-correcting azimuthal shear in Doppler radar data. *Weather and Forecasting*, **28,** 194-211.

Smith, B. T., R. L. Thompson, J. S. Grams, C. Broyles, and H. E. Brooks, 2012: Convective modes for significant severe thunderstorms in the contiguous United States. Part I: Storm classification and climatology. *Weather and Forecasting*, **27,** 1114-1135.

Smull, B. F., and R. A. Houze Jr, 1987: Dual-Doppler radar analysis of a midlatitude squall line with a trailing region of stratiform rain. *Journal of the atmospheric sciences*, **44,** 2128-2149.

Witt, A., and S. P. Nelson, 1991: The use of single-Doppler radar for estimating maximum hailstone size. *Journal of Applied Meteorology*, **30,** 425-431.

Witt, A., M. D. Eilts, G. J. Stumpf, J. Johnson, E. D. W. Mitchell, and K. W. Thomas, 1998: An enhanced hail detection algorithm for the WSR-88D. *Weather and Forecasting*, **13,** 286-303.

Ziegler, C. L., P. S. Ray, and N. C. Knight, 1983: Hail growth in an Oklahoma multicell storm. *Journal of the Atmospheric Sciences*, **40,** 1768-1791.

Appendix

Case Studies

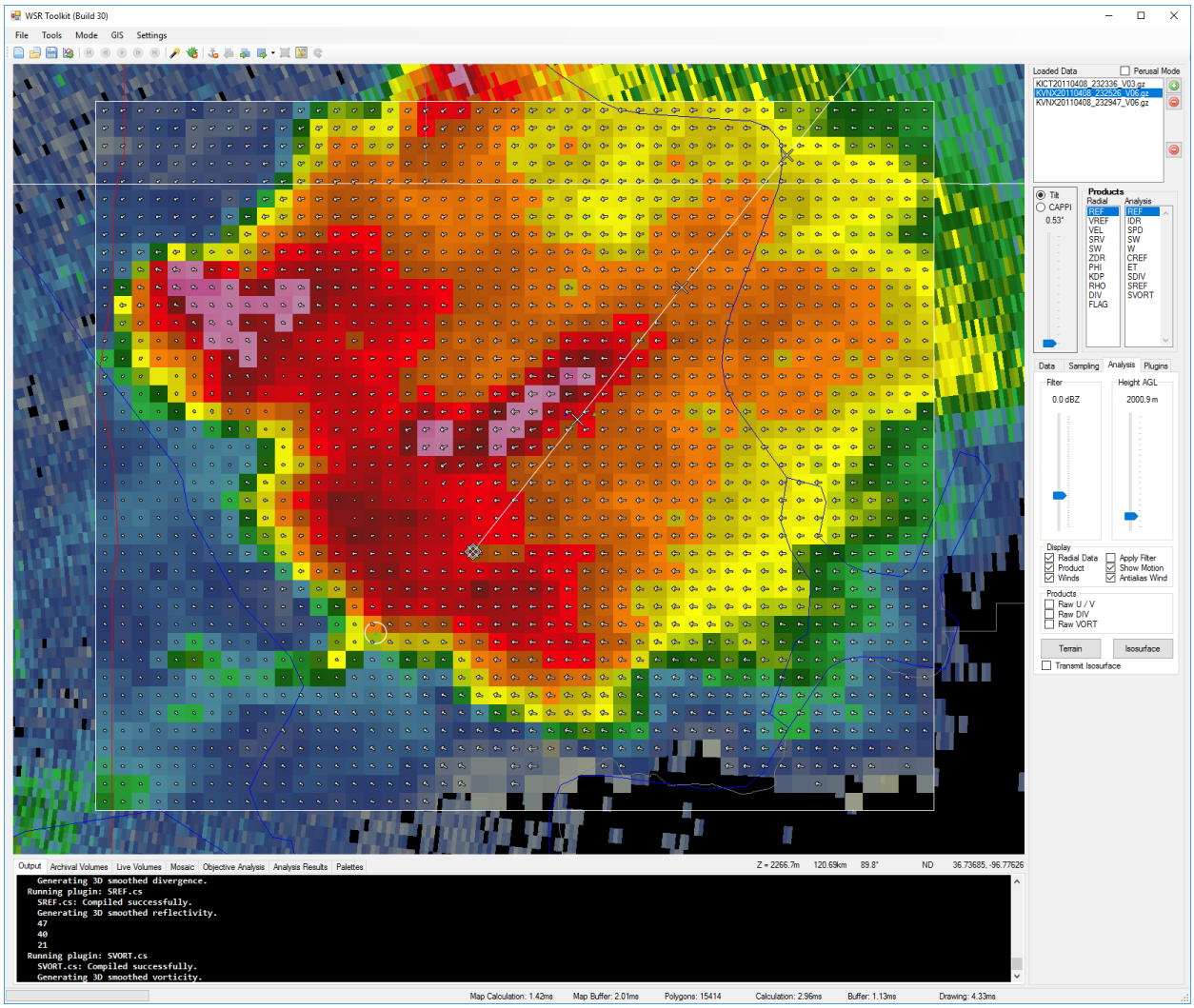

Case 1: Single cell storm in Kansas on April 8, 2011 at 2323Z. 1.50" hail report.

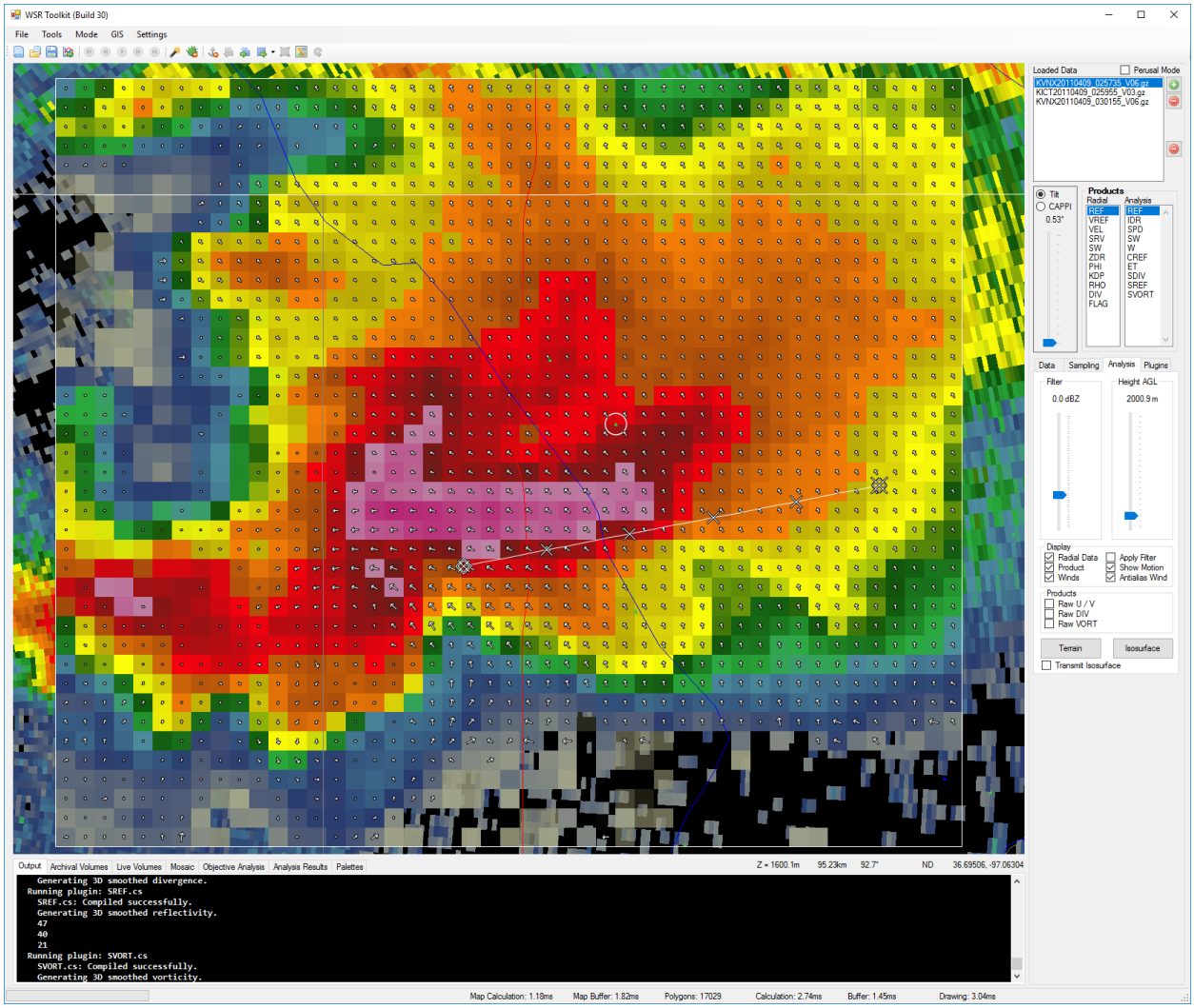

Case 2: Supercell in Kansas on April 9, 2011 at 0257Z. 4.25" hail report.

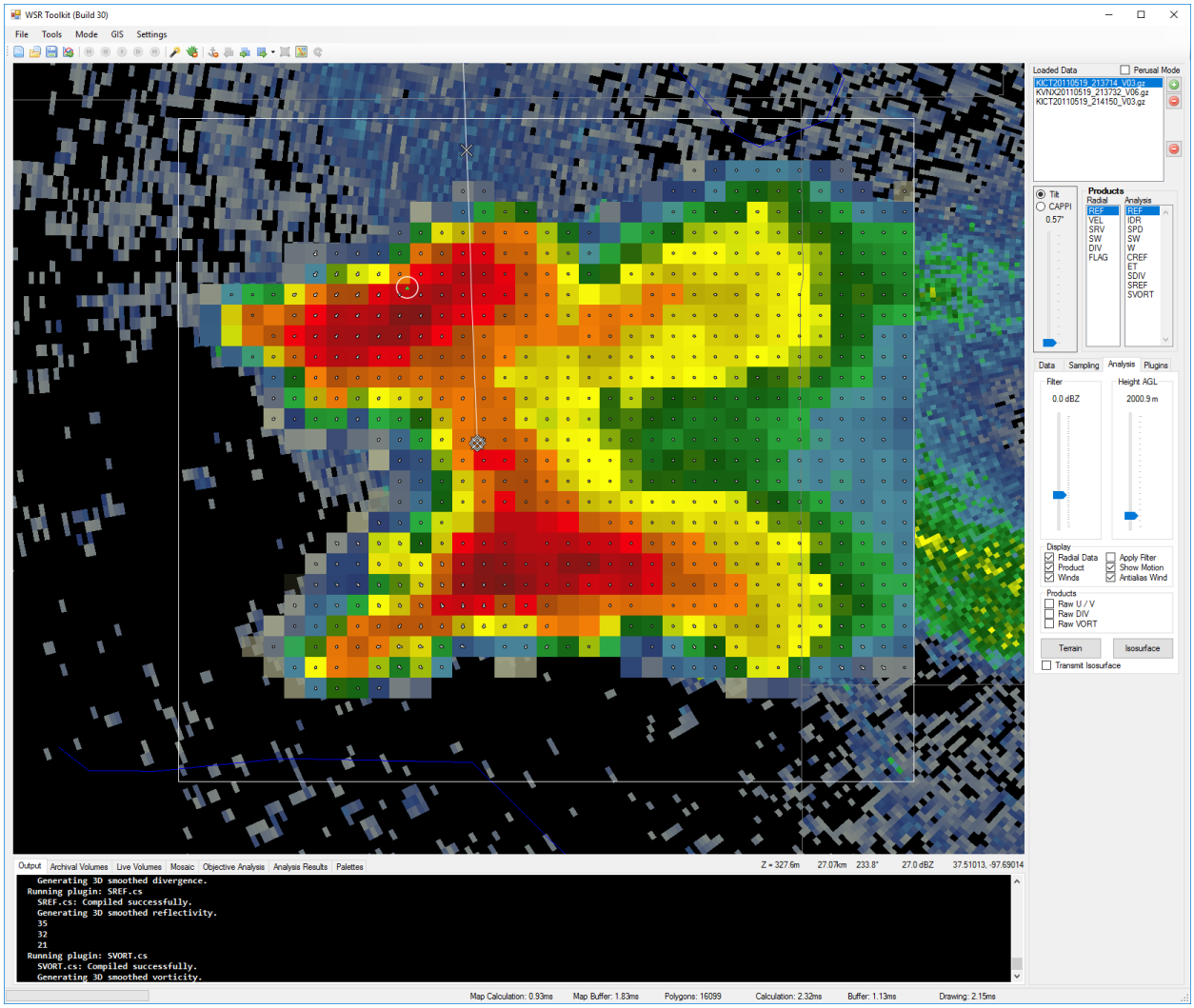

Case 3: Multicell in Kansas on May 19, 2011 at 2137Z. 1.00" hail report.

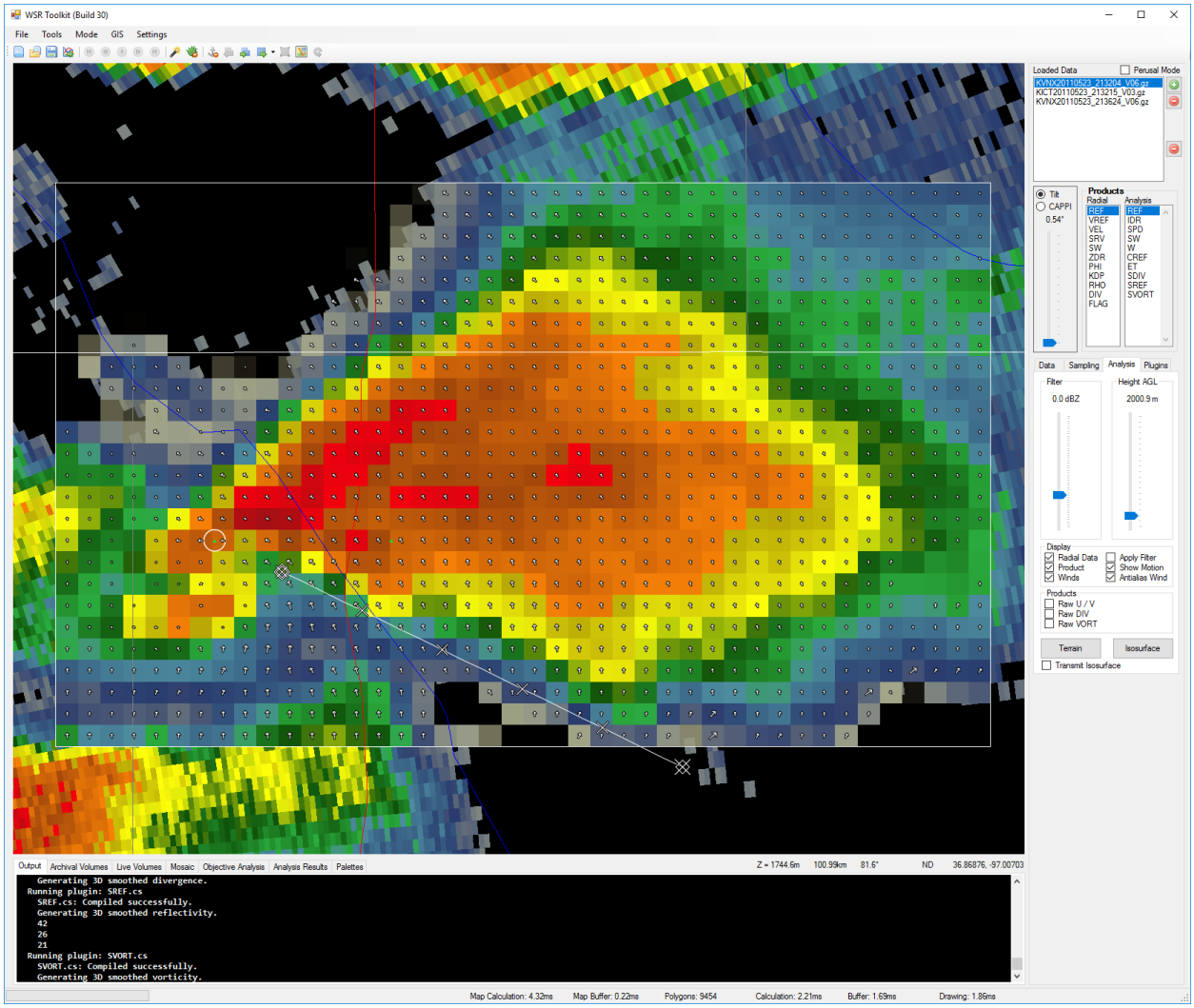

Case 4: Supercell in Kansas on May 23, 2011 at 2132Z. 2.00" hail report.

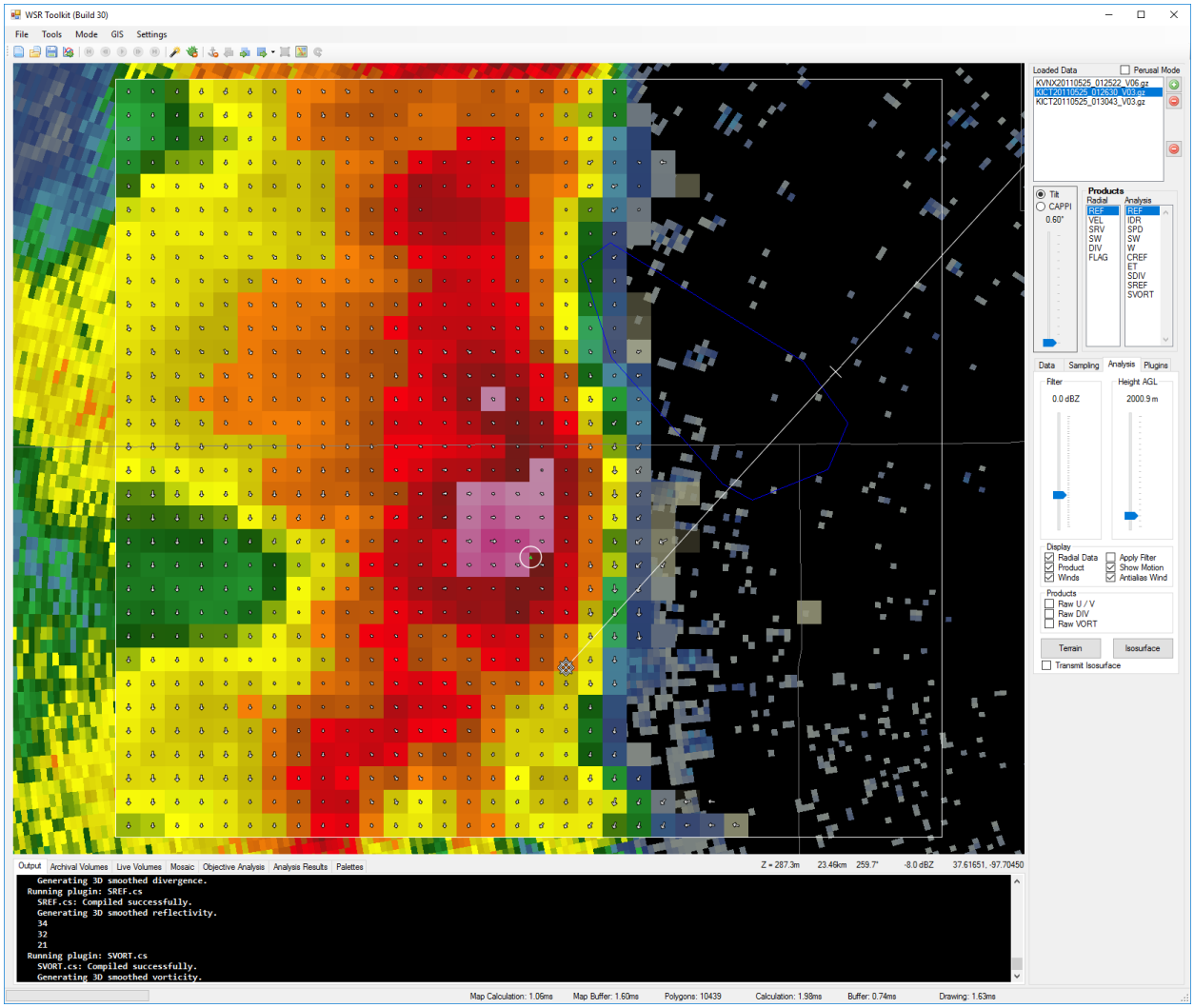

Case 5: Line segment in Kansas on May 25, 2011 at 0125Z. 0.88" hail report.

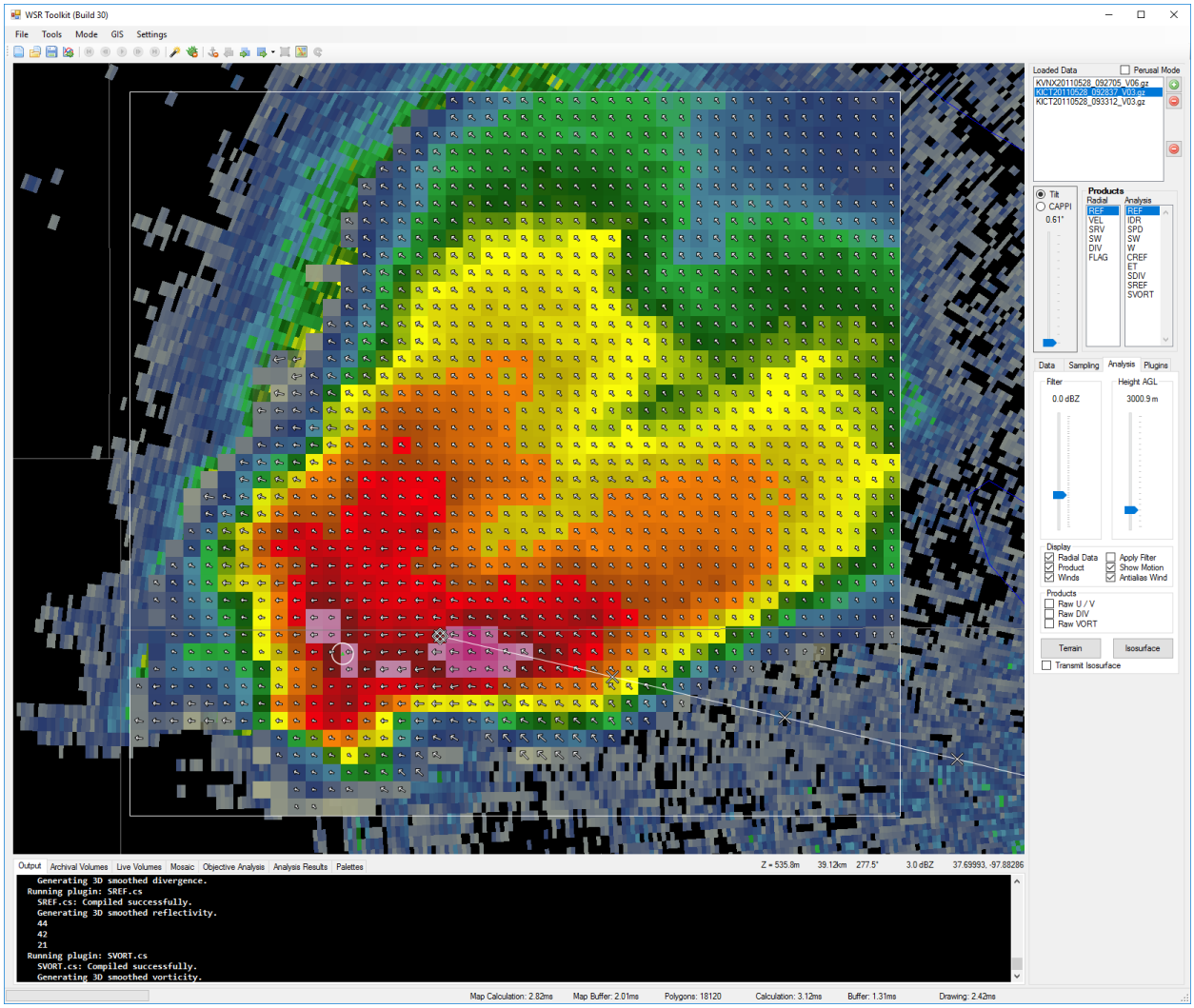

Case 6: Supercell in Kansas on May 28, 2011 at 0927Z. 1.75" hail report.

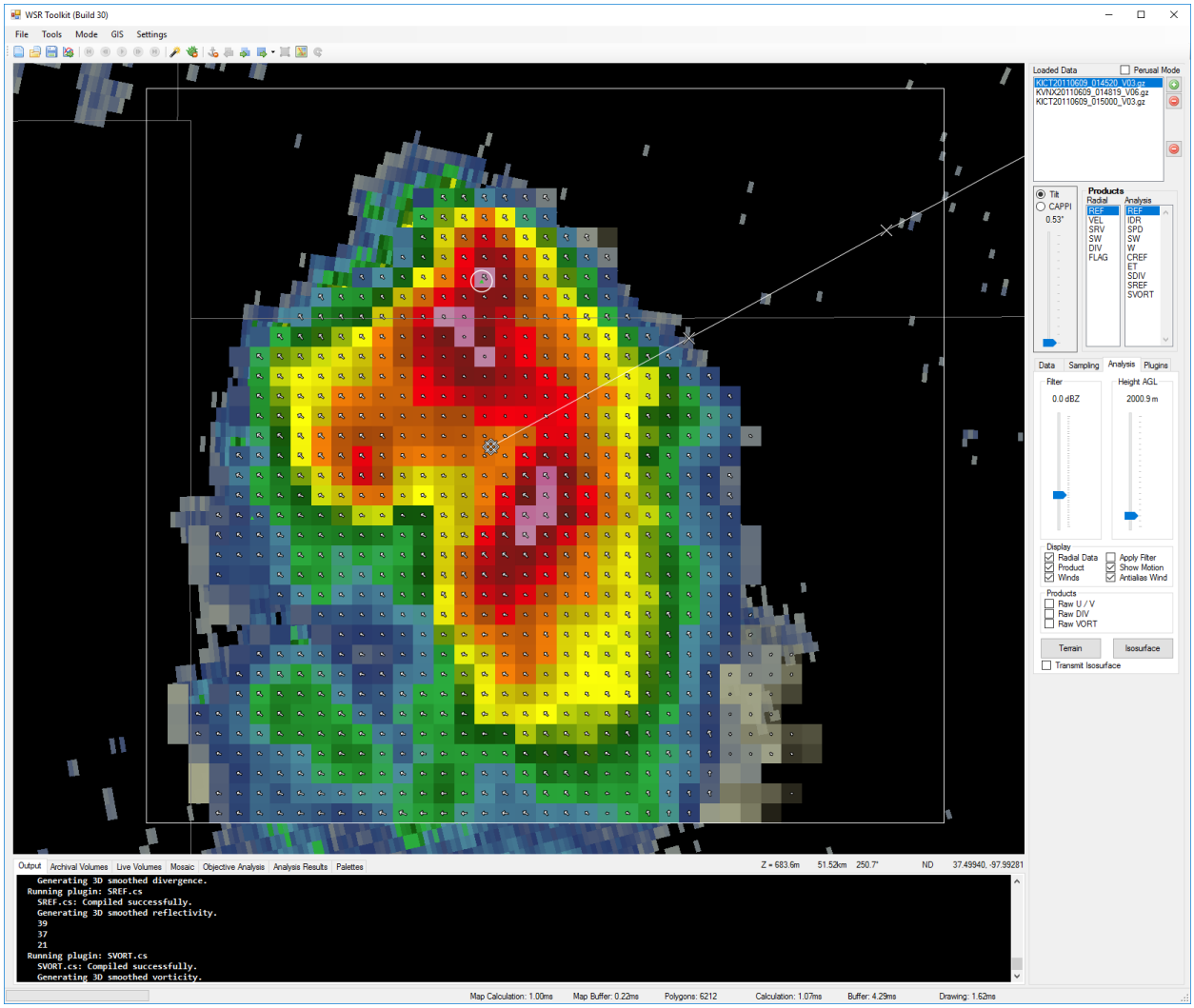

Case 7: Multicell in Kansas on June 9, 2011 at 0145Z. 1.50" hail report.

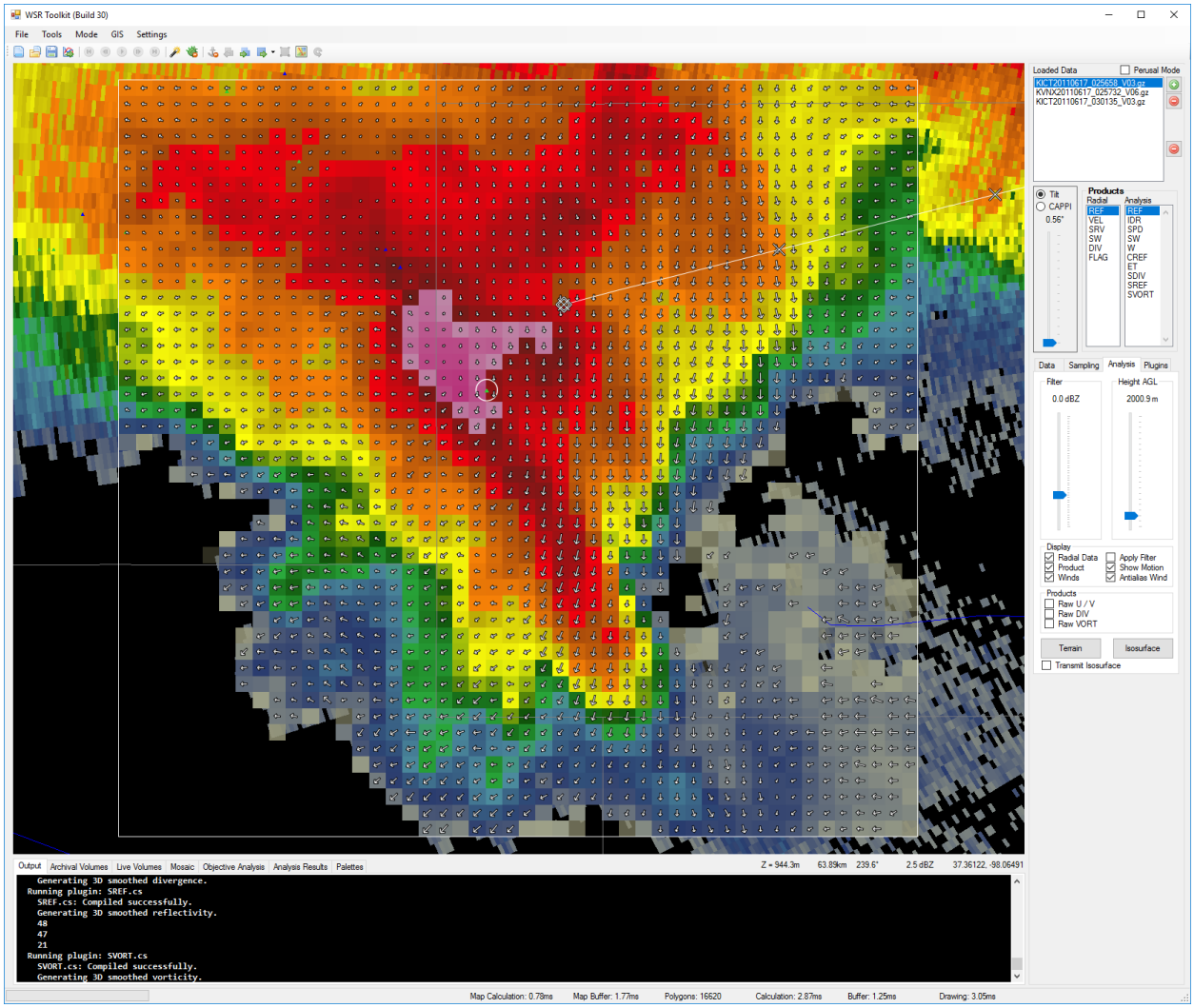

Case 8: Multicell in Kansas on June 17, 2011 at 0256Z. 1.75" hail report.

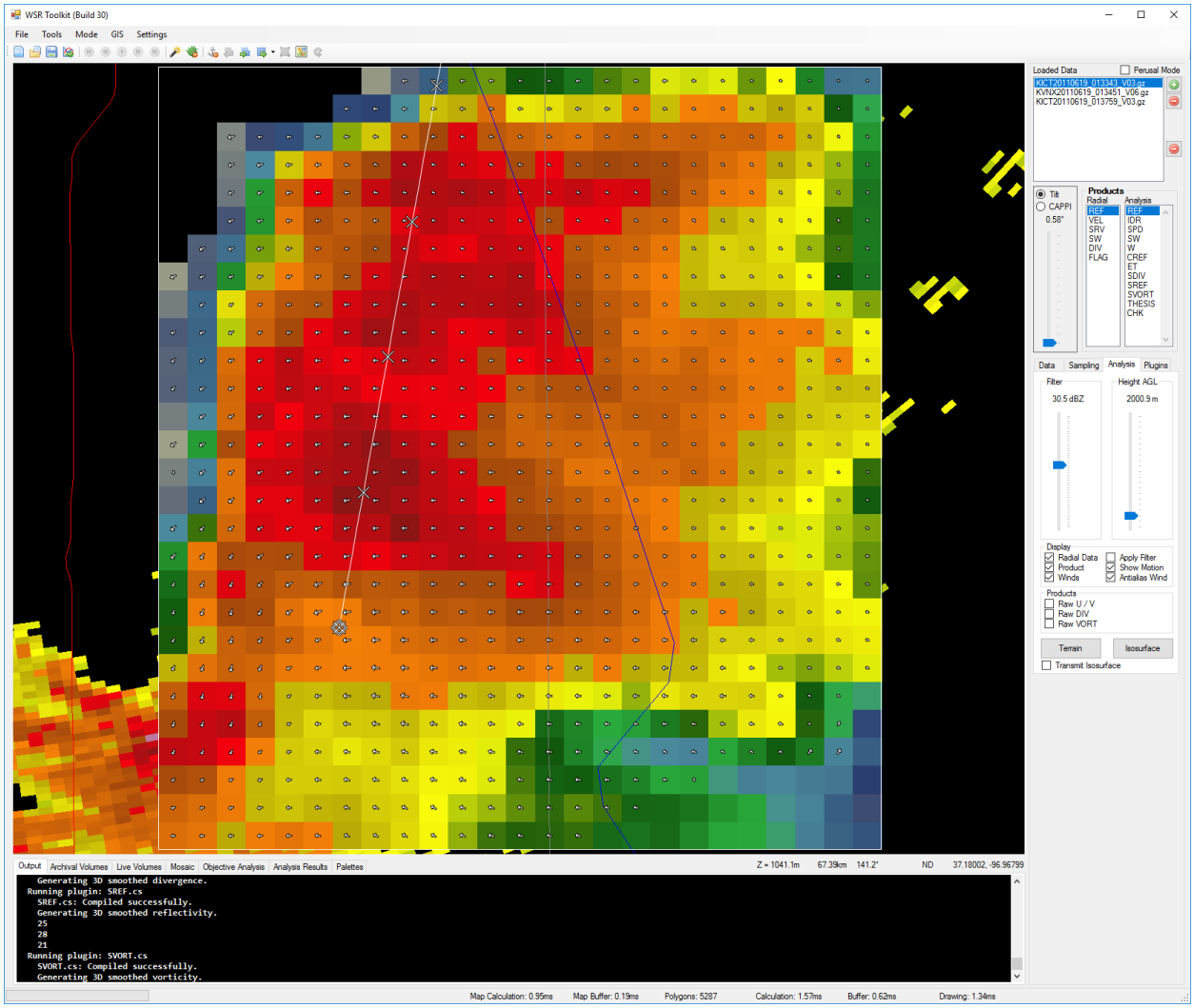

Case 9: Multicell in Kansas on June 19, 2011 at 0133Z. 2.50" hail report.

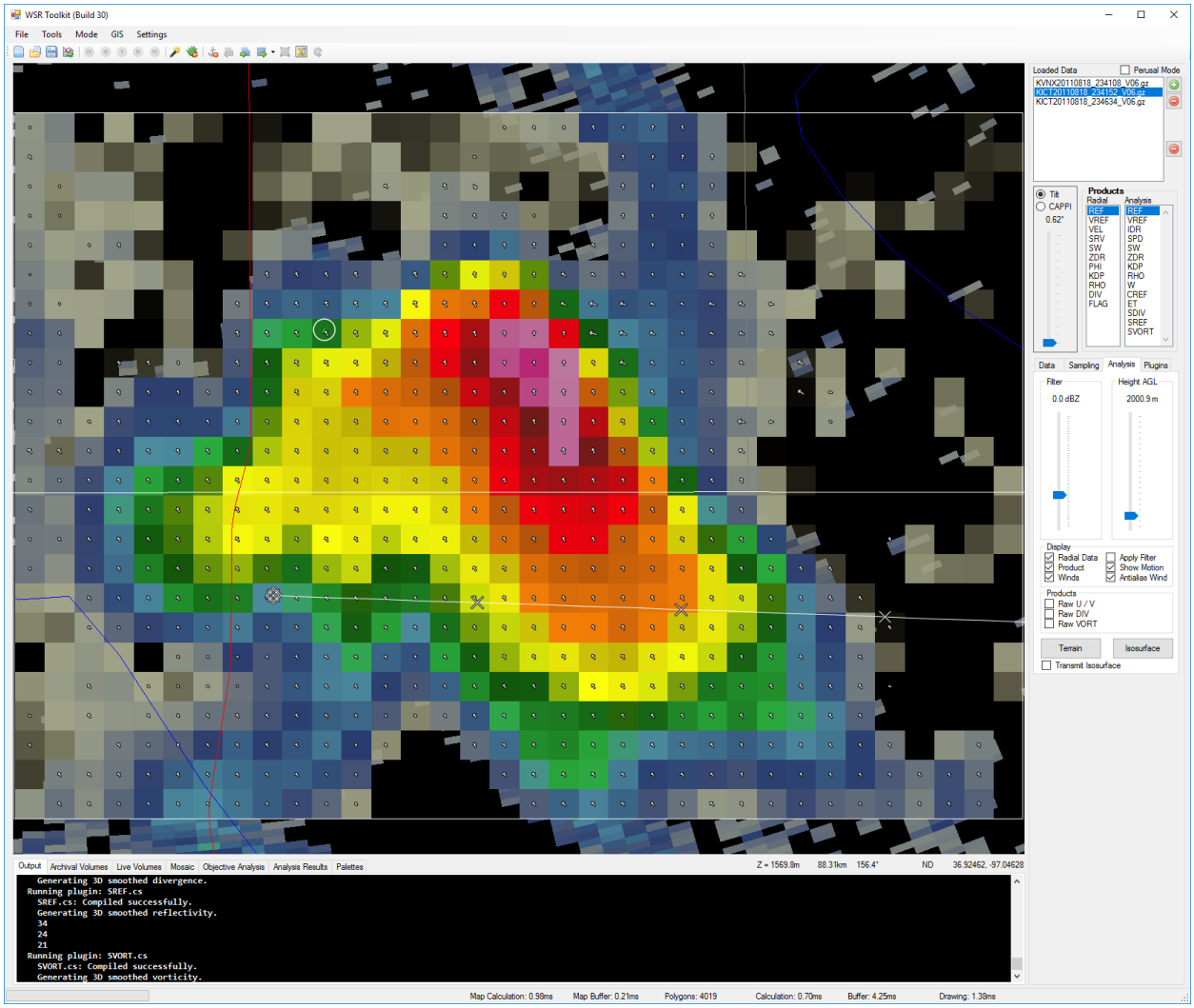

Case 10: Single cell in Kansas on August 18, 2011 at 2341Z. 1.00" hail report.

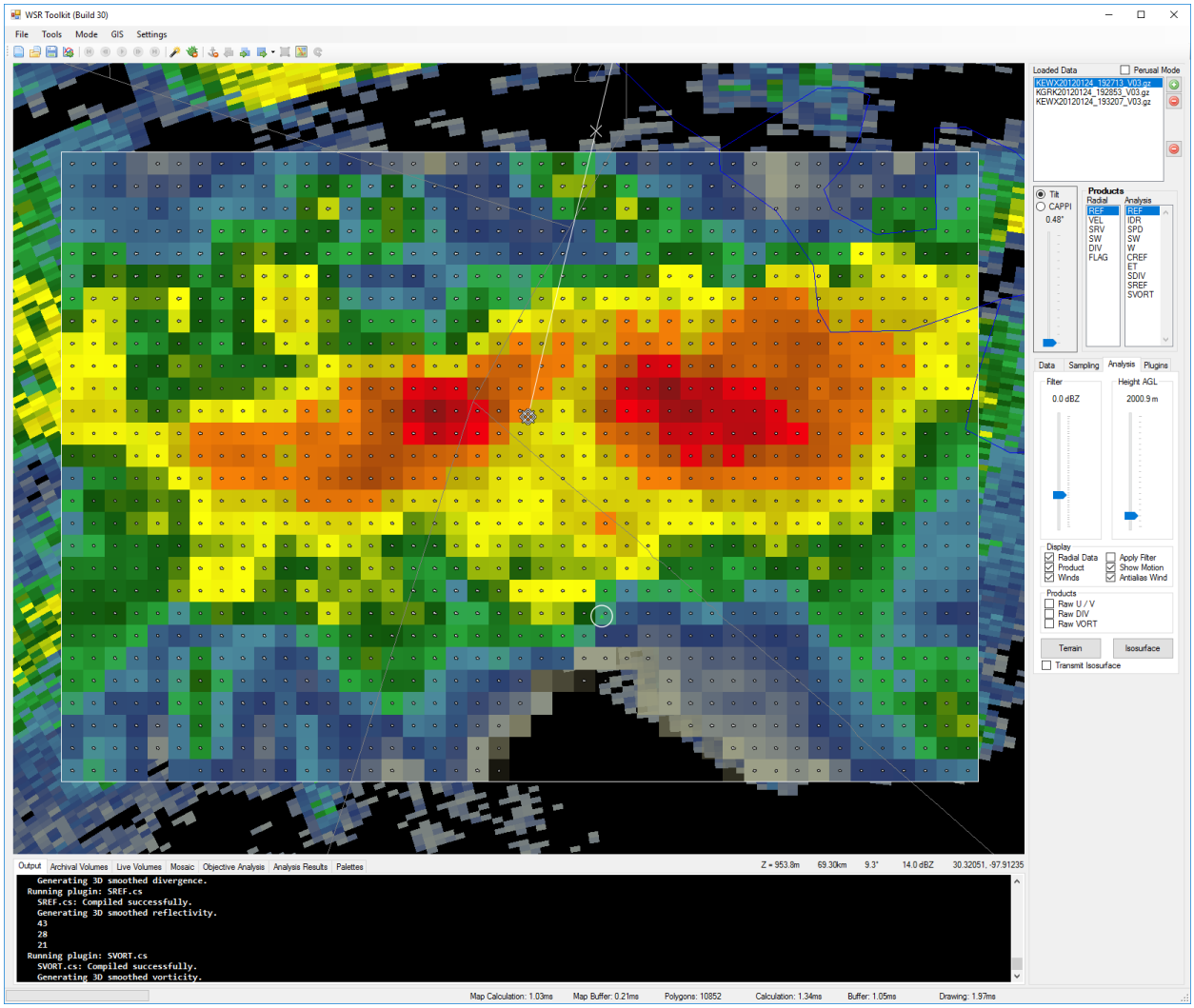

Case 11: Multicell in Texas on January 24, 2012 at 1927Z. 1.00" hail report.

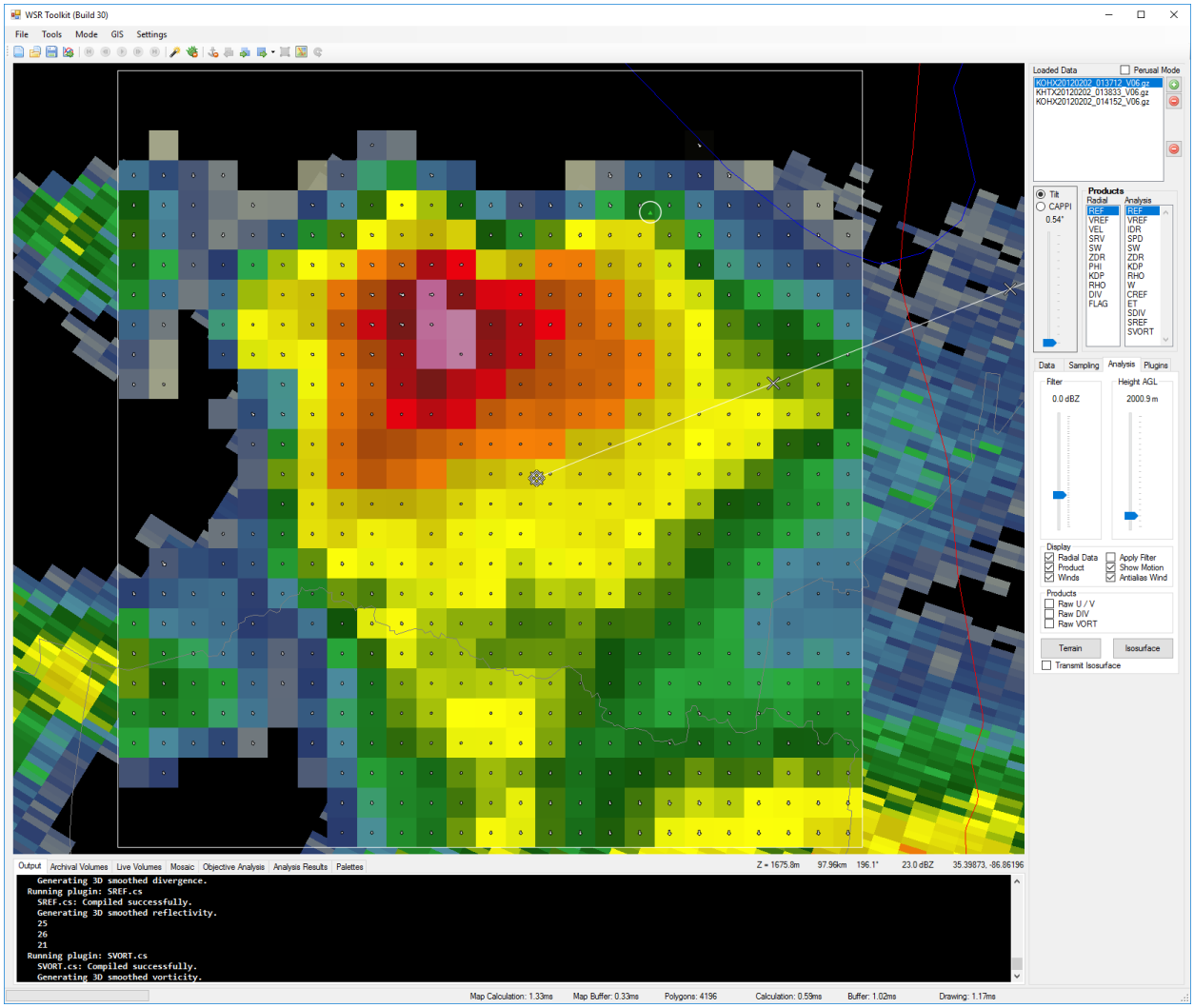

Case 12: Single cell in Tennessee on February 2, 2012 at 0137Z. 0.88" hail report.

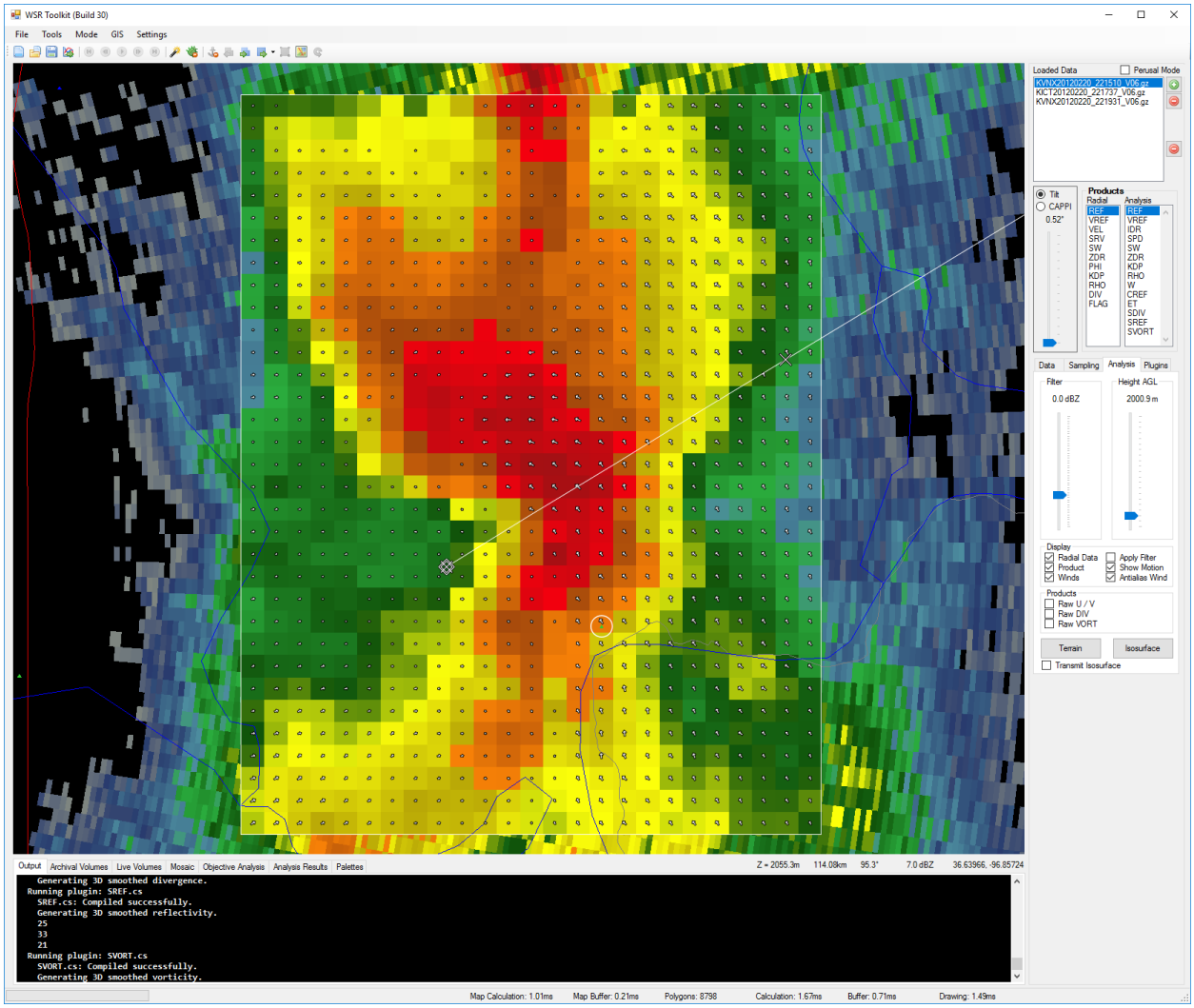

Case 13: Line segment in Kansas on February 20, 2012 at 2215Z. 0.88" hail report.

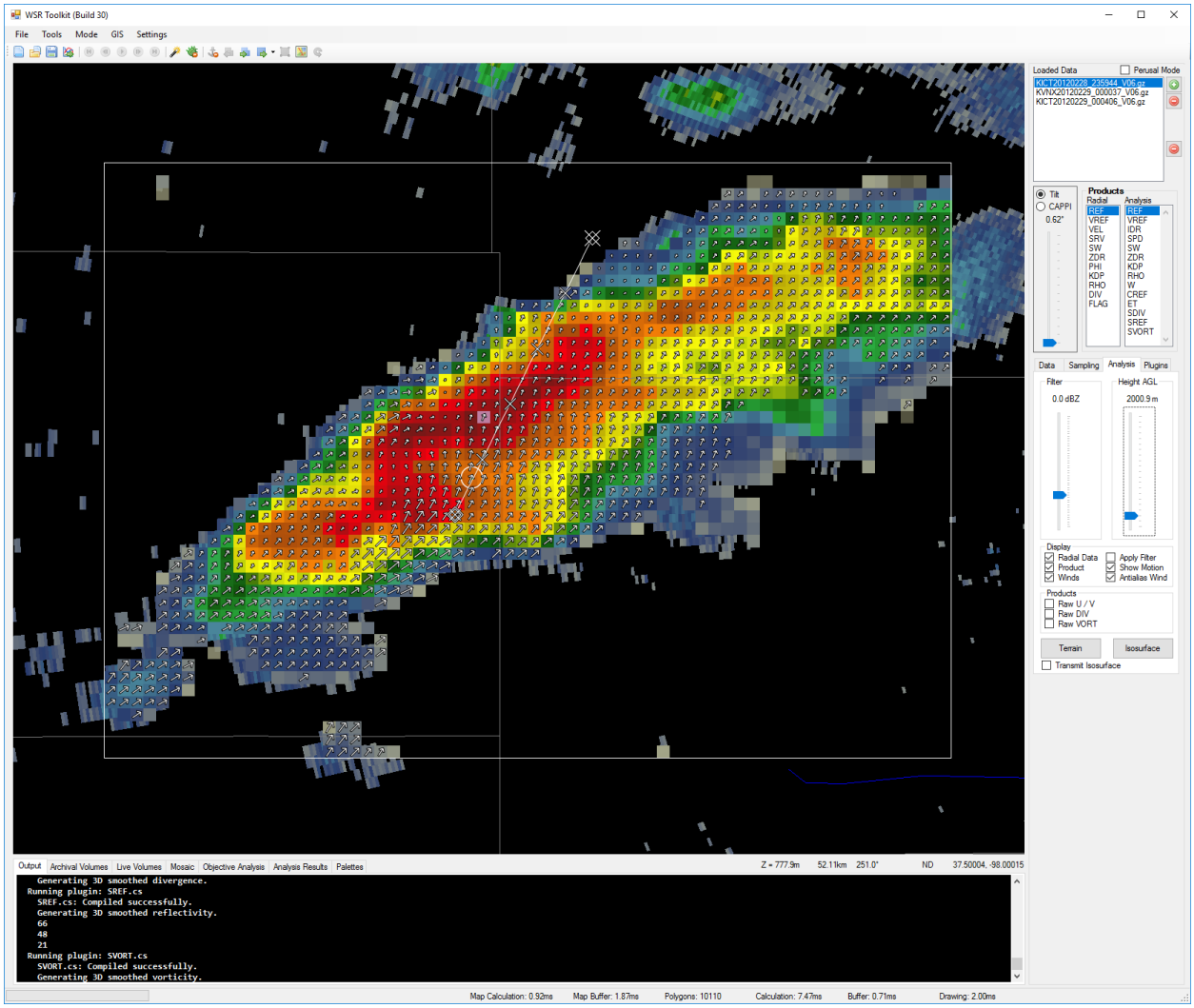

Case 14: Line segment in Kansas on February 28, 2012 at 2359Z. 0.75" hail report.

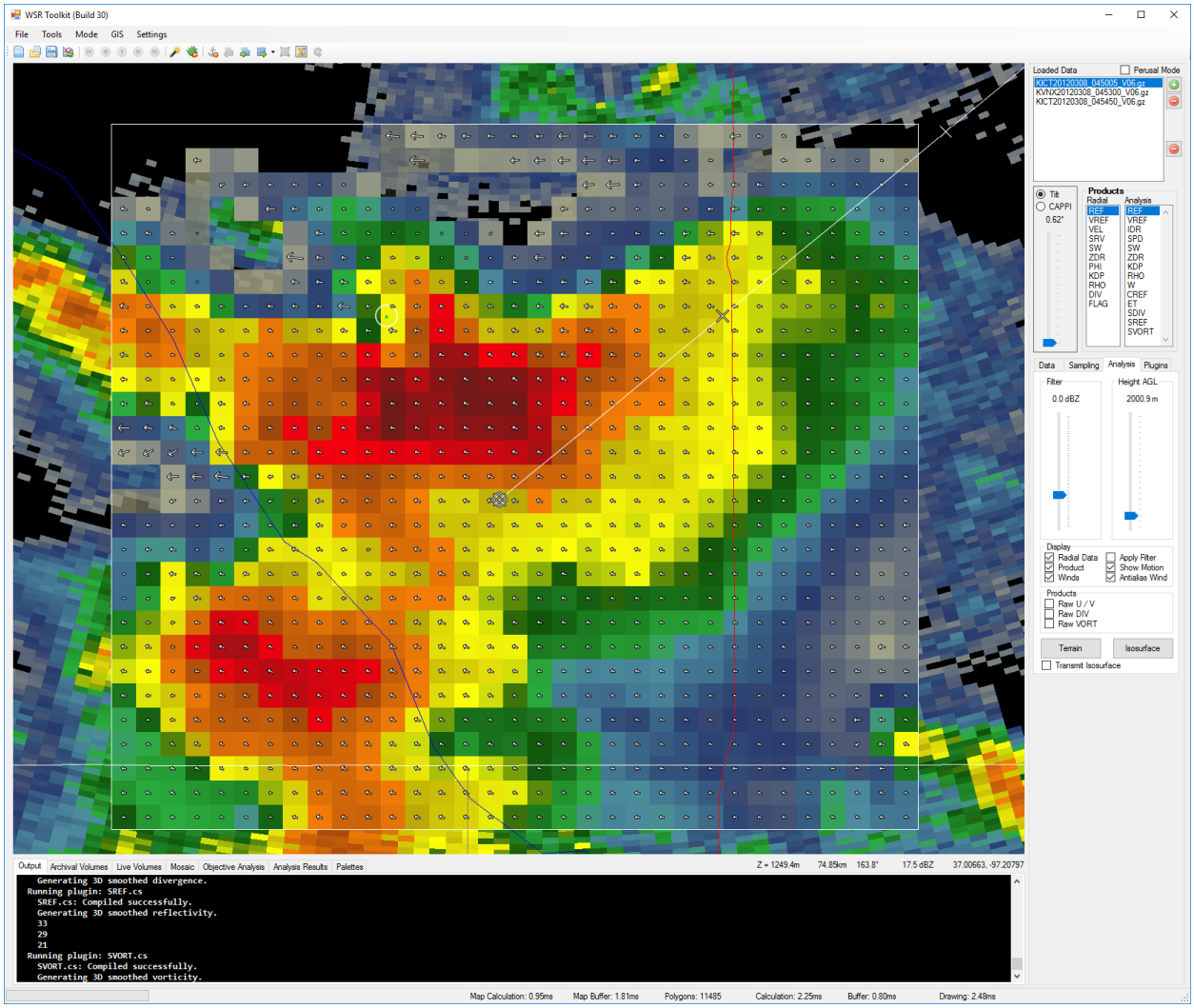

Case 15: Multicell in Kansas on March 8, 2012 at 0450Z. 1.00" hail report.

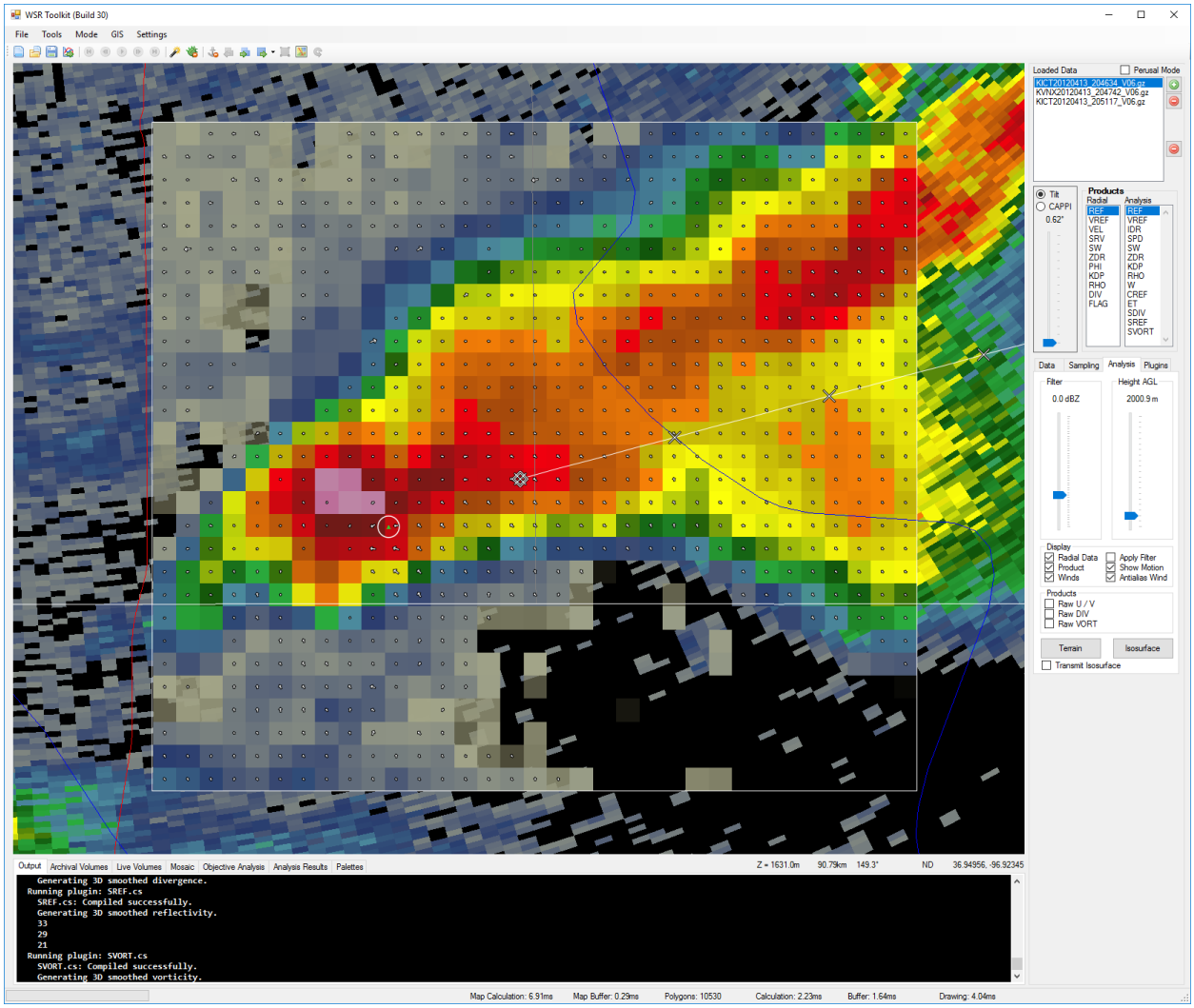

Case 16: Line segment in Kansas on April 13, 2012 at 2046Z. 0.75" hail report.

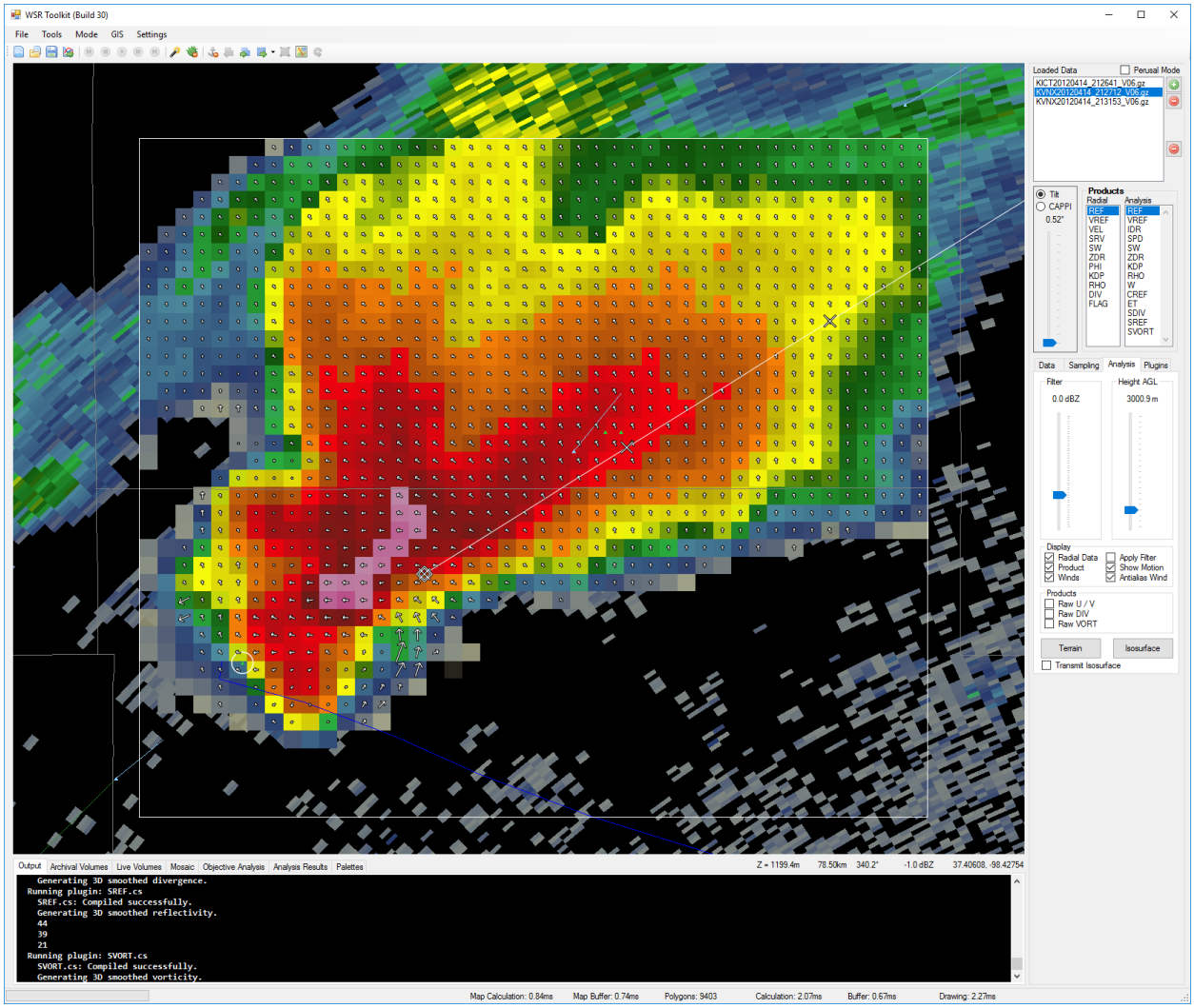

Case 17: Supercell in Kansas on April 14, 2012 at 2126Z. 1.75" hail report.

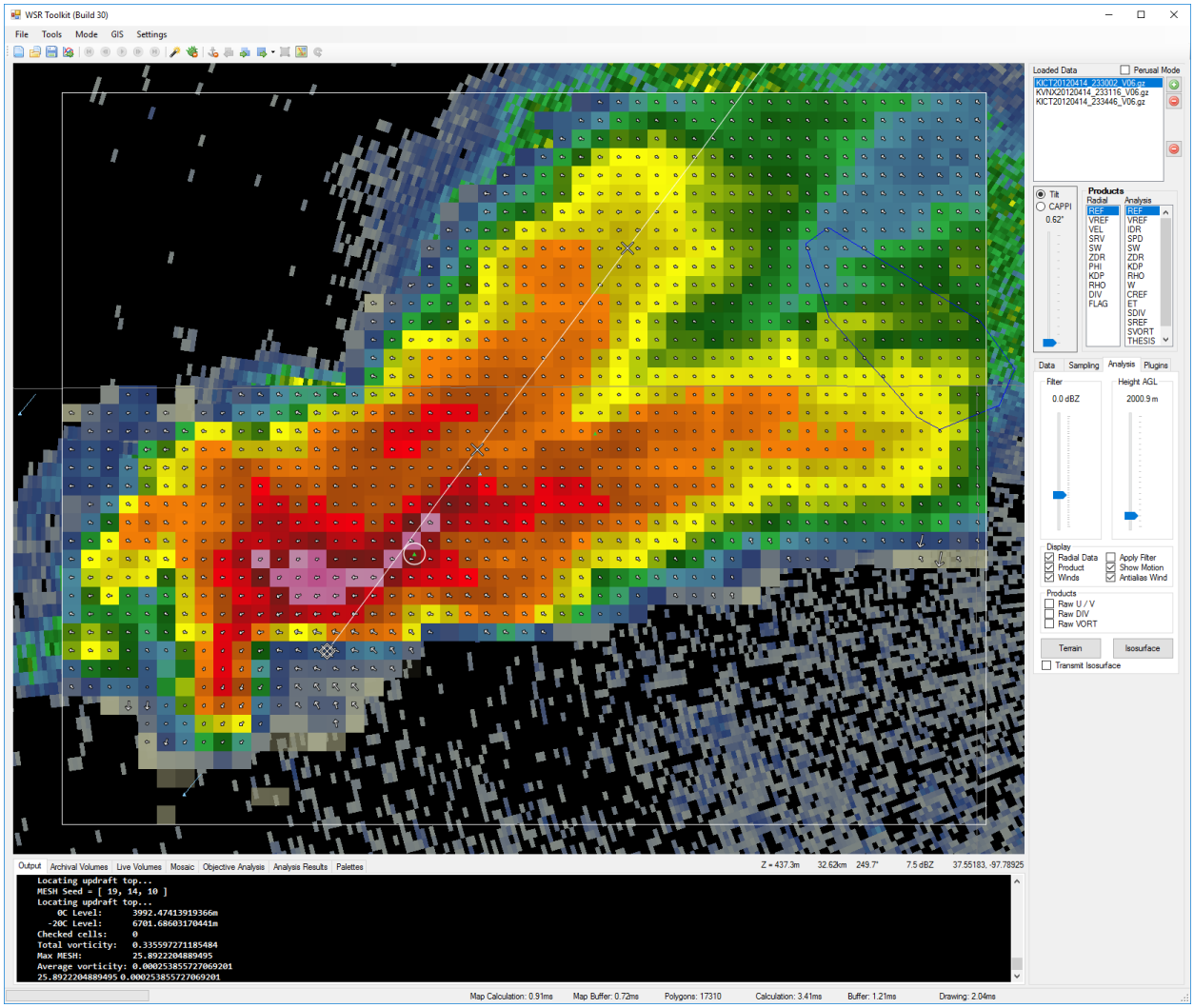

Case 18: Supercell in Kansas on April 14, 2012 at 2330Z. 1.00" hail report.

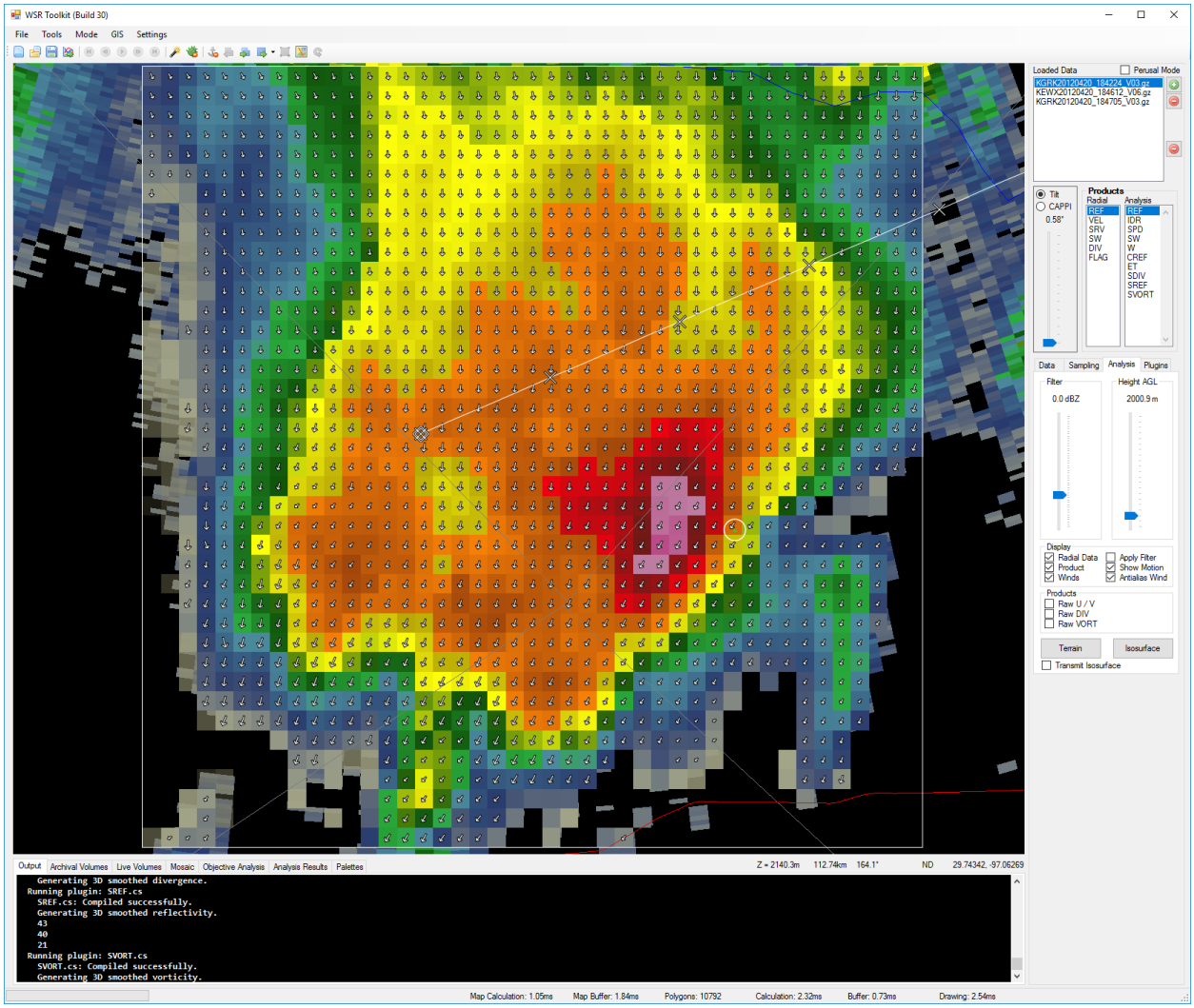

Case 19: Single cell in Texas on April 20, 2012 at 1842Z. 1.00" hail report.

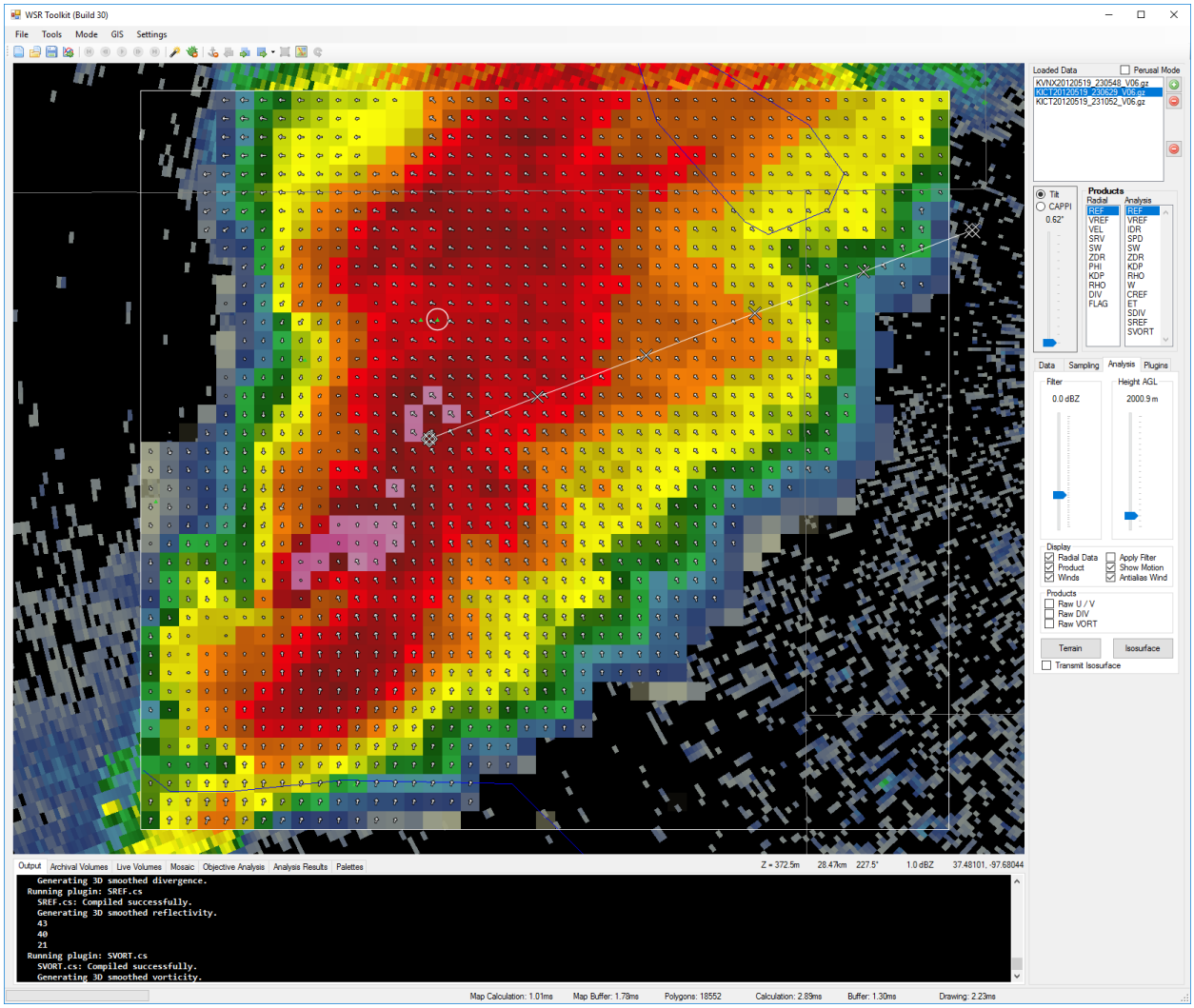

Case 20: Squall line in Kansas on May 19, 2012 at 2305Z. 3.00" hail report.

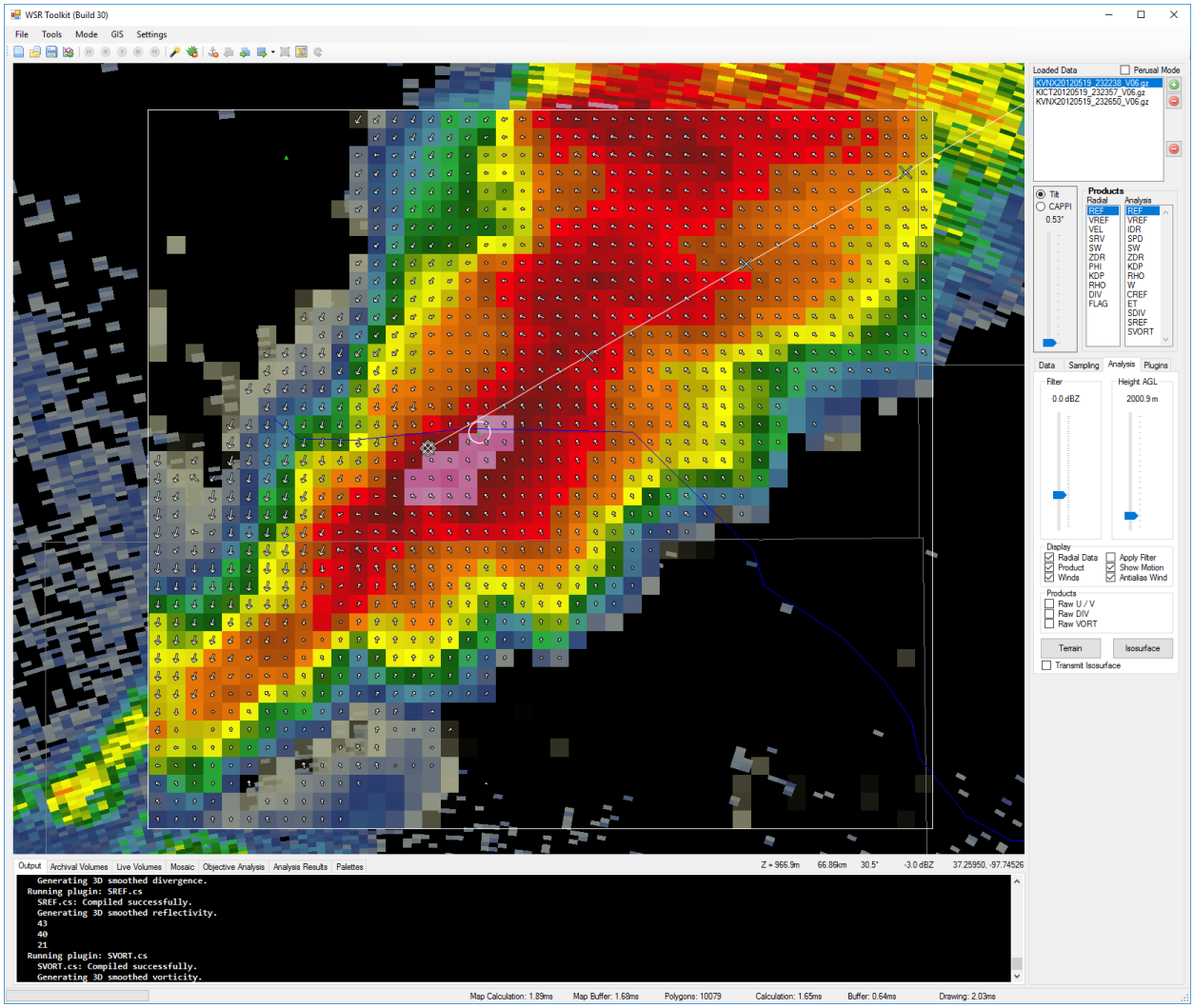

Case 21: Squall line in Kansas on May 19, 2012 at 2322Z. 1.75" hail report.

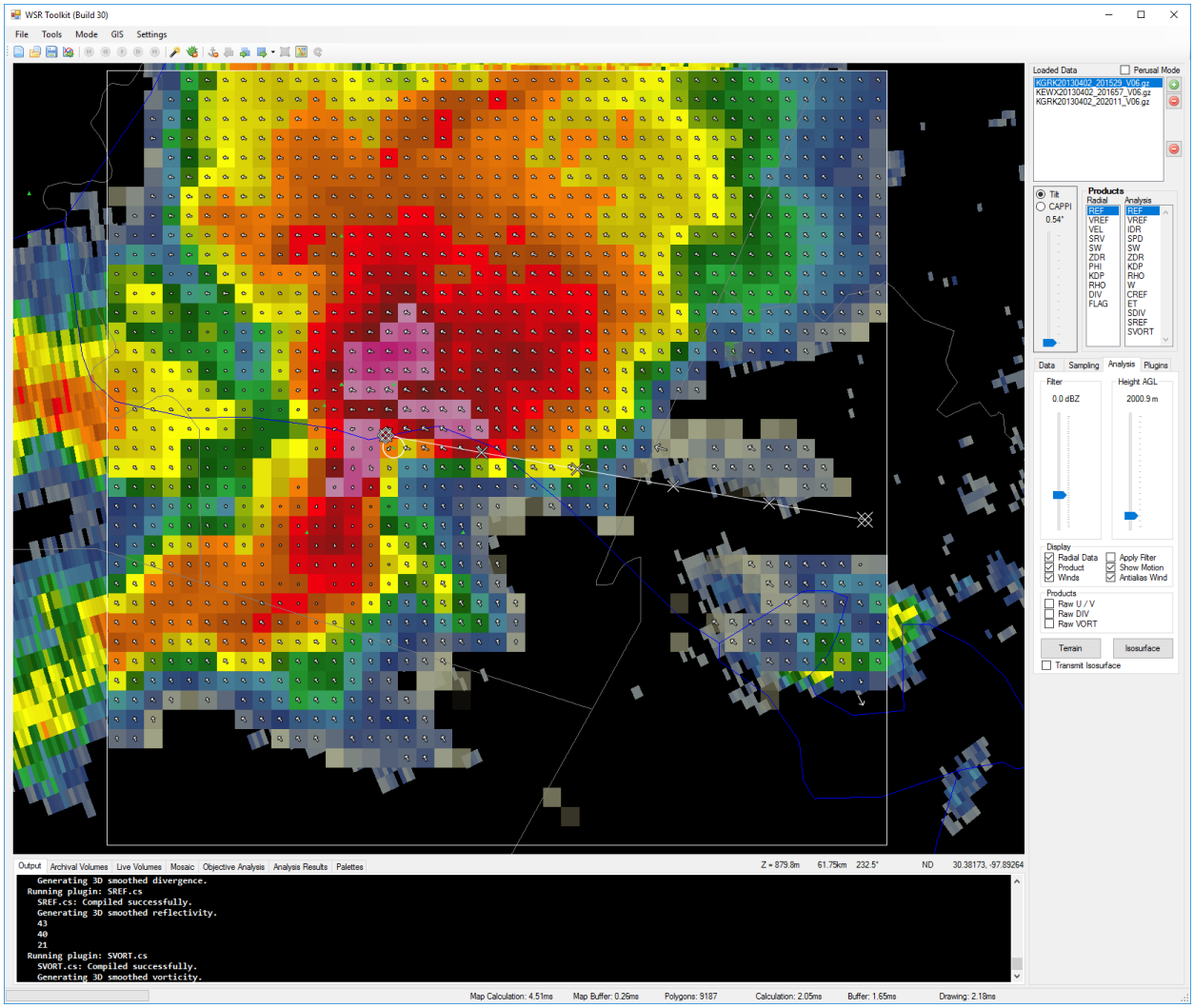

Case 22: Supercell in Texas on April 2, 2013 at 2015Z. 2.00" hail report.

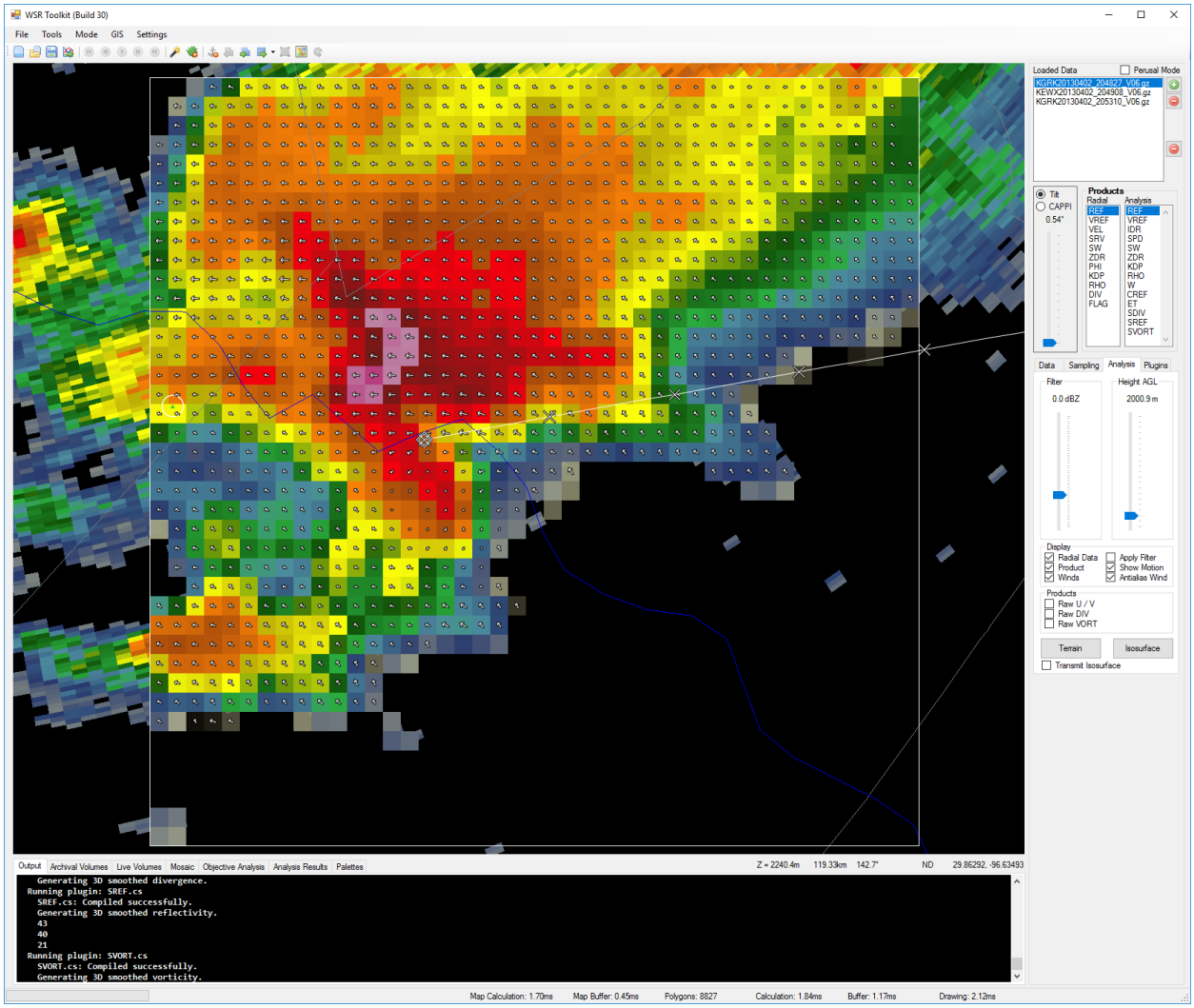

Case 23: Supercell in Texas on April 2, 2013 at 2048Z. 2.00" hail report.

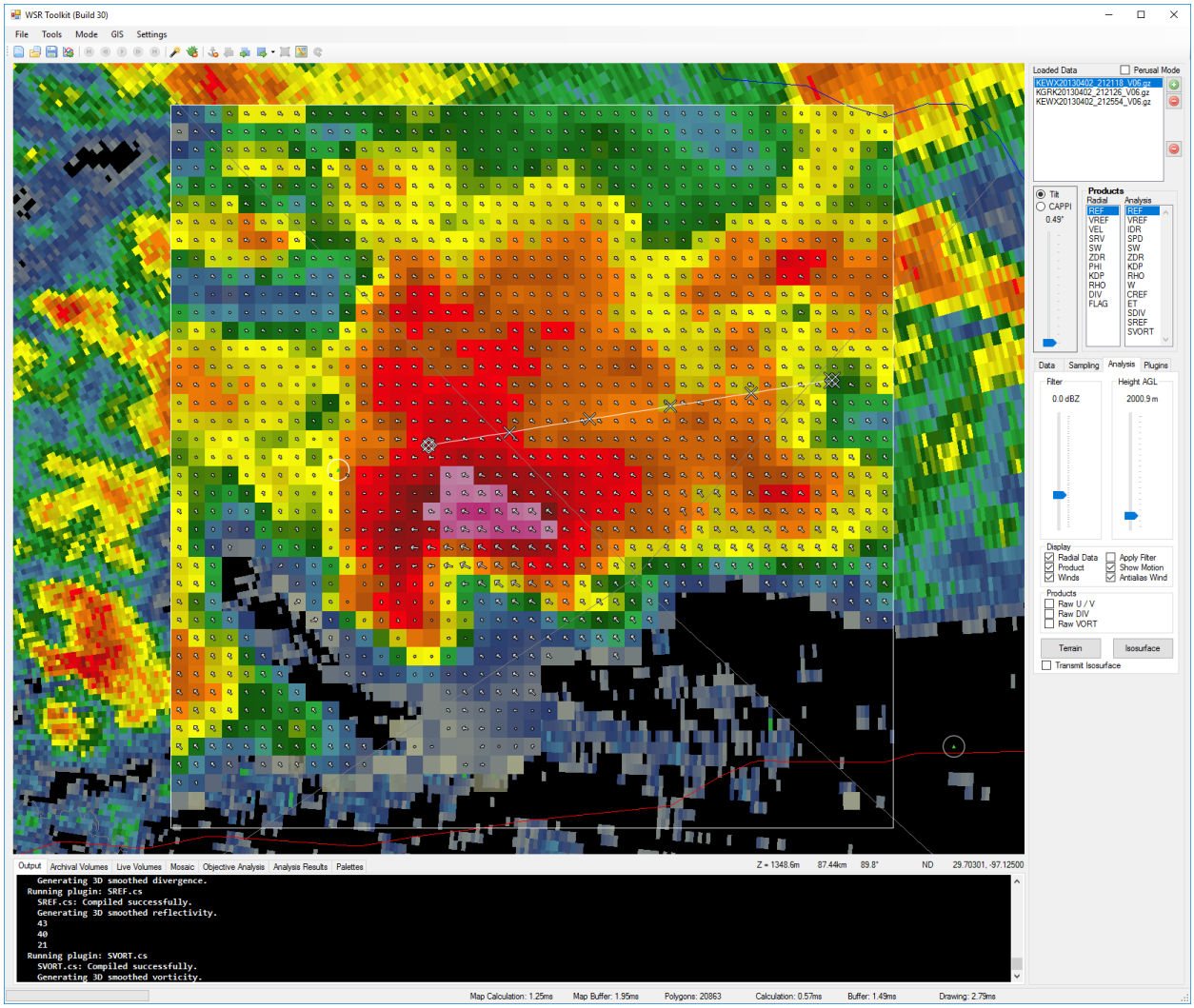

Case 24: Supercell in Texas on April 2, 2013 at 2121Z. 1.75" hail report.

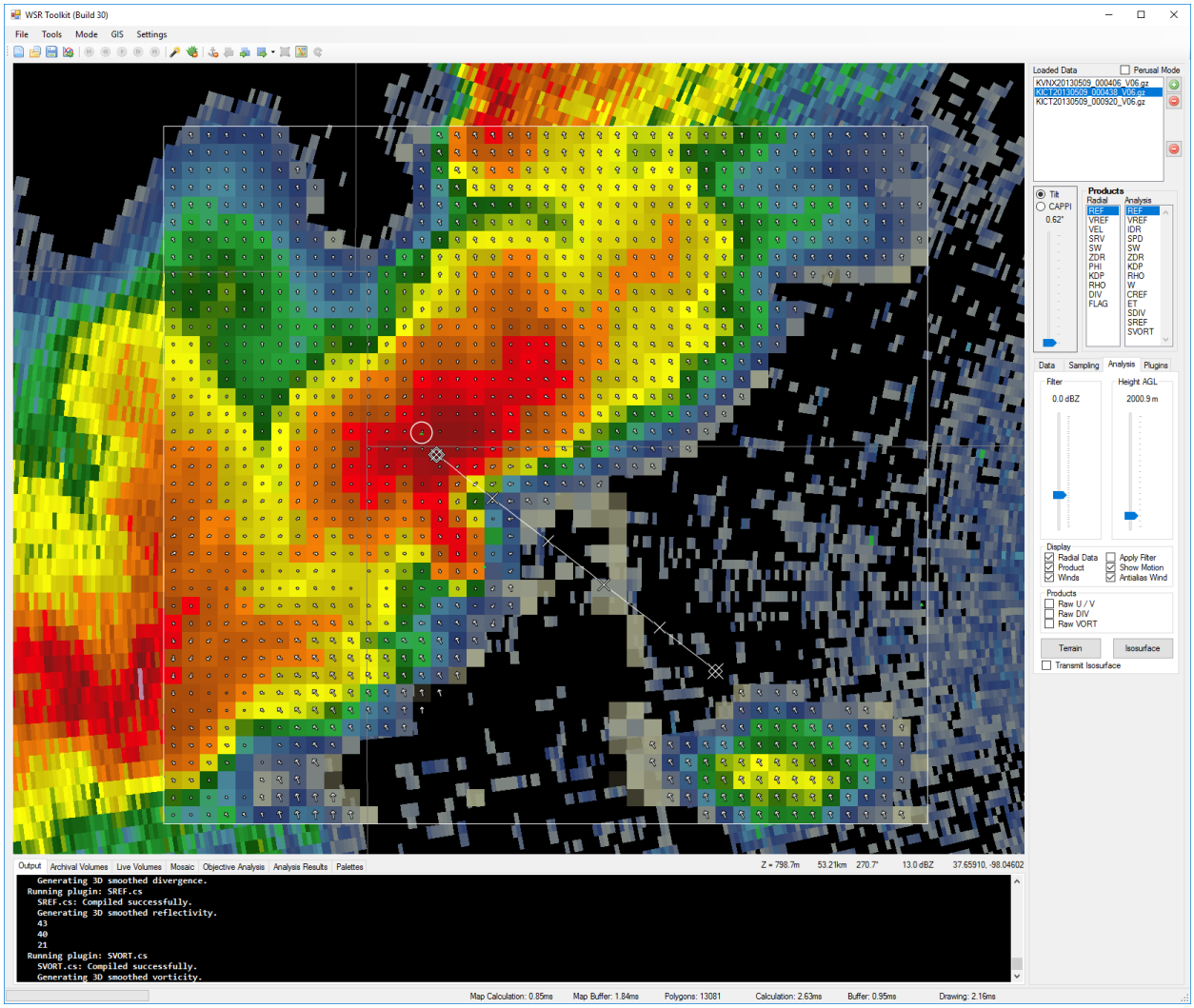

Case 25: Supercell in Kansas on May 9, 2013 at 0004Z. 0.88" hail report.

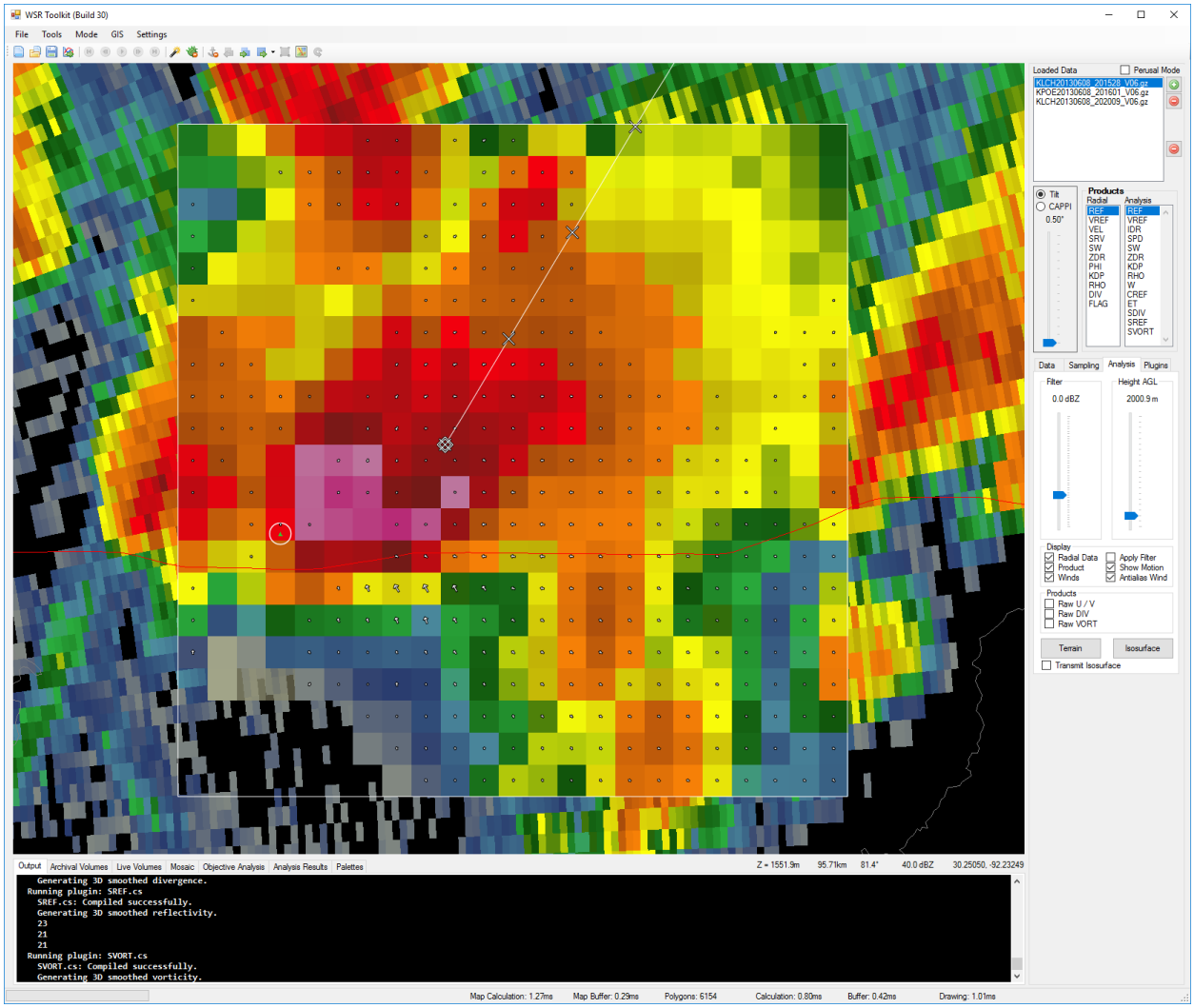

Case 26: Multicell in Louisiana on June 8, 2013 at 2015Z. 1.75" hail report.

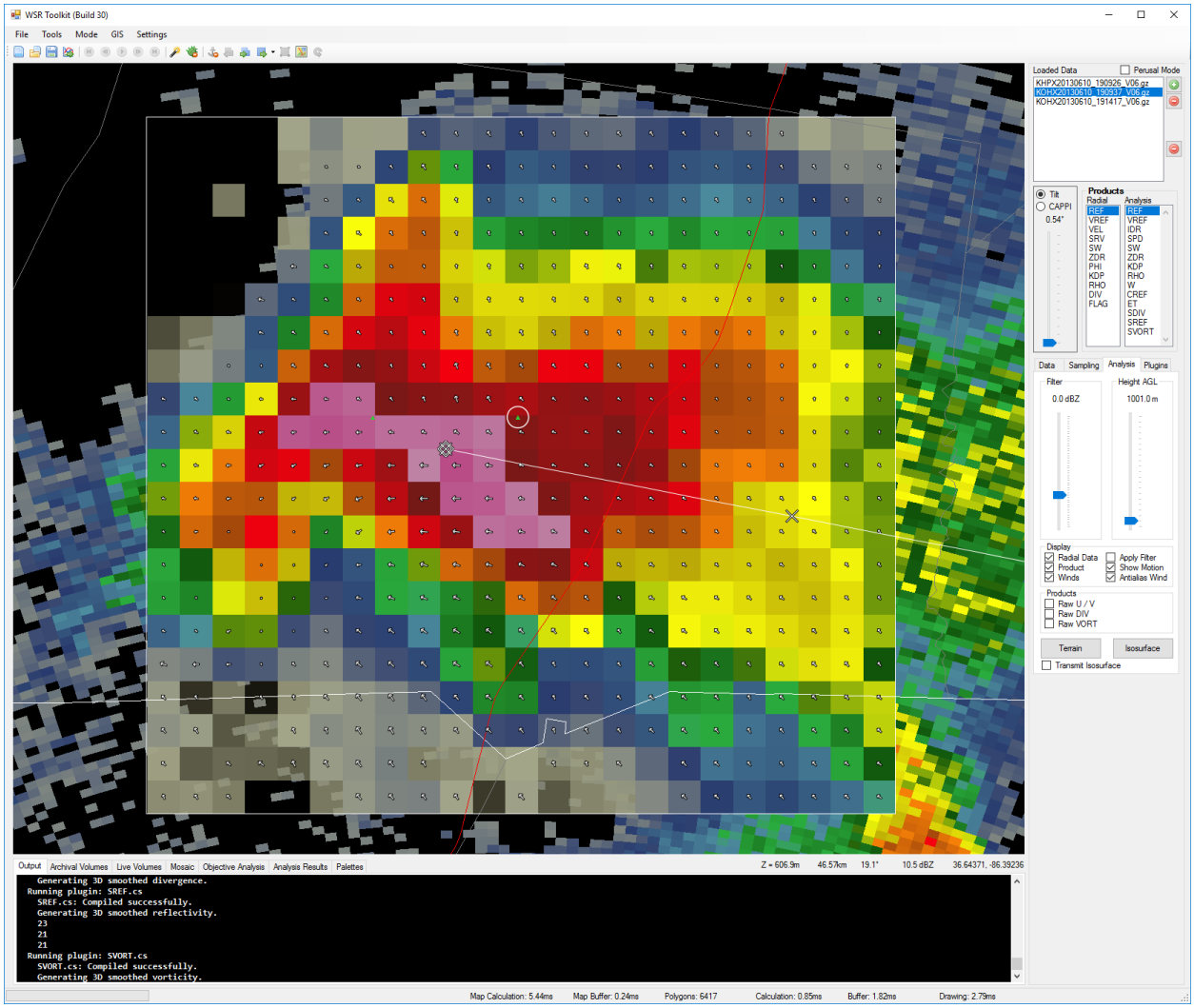

Case 27: Supercell in Kentucky on June 10, 2013 at 1909Z. 2.00" hail report.

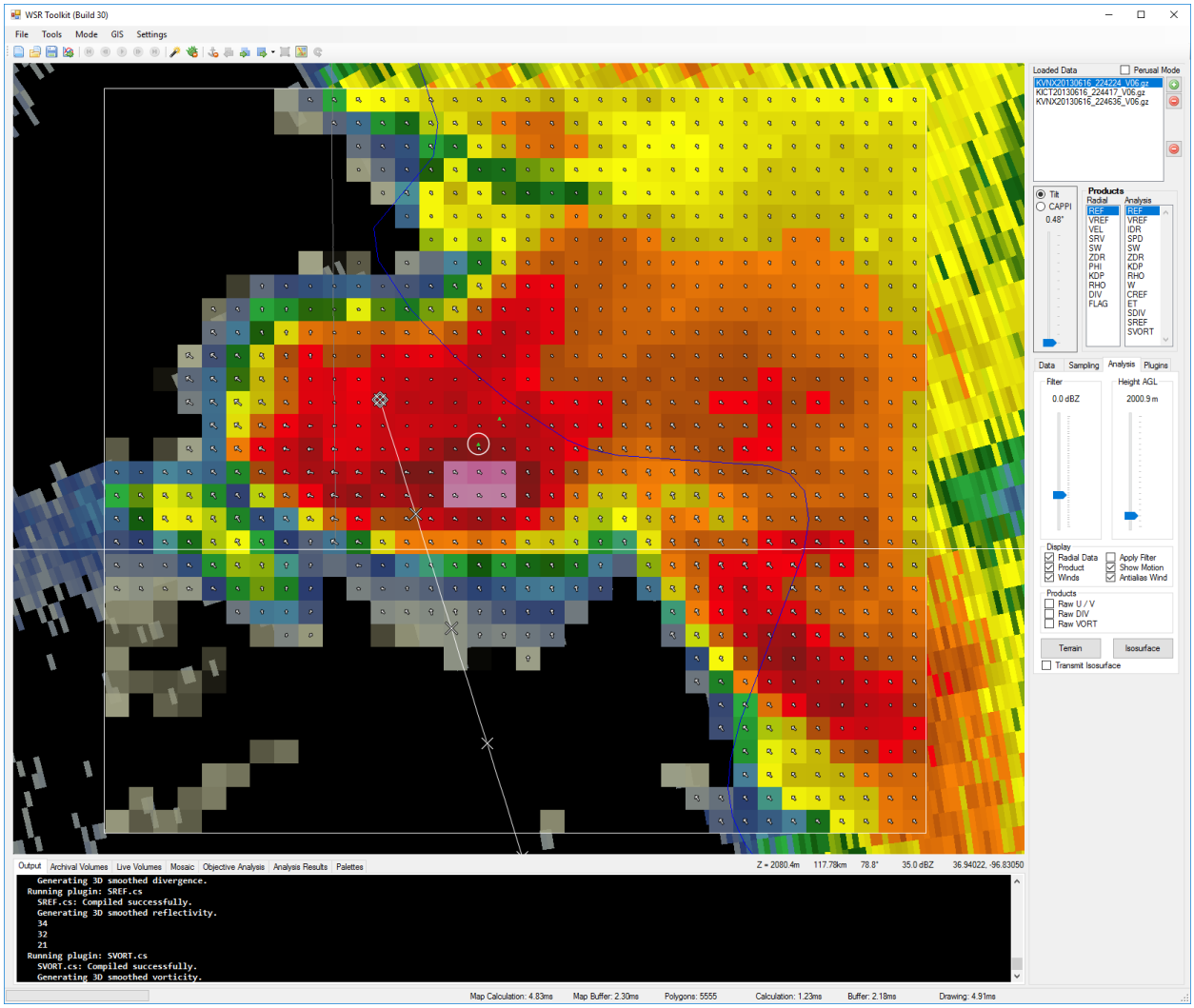

Case 28: Multicell in Kansas on June 16, 2013 at 2242Z. 1.50" hail report.

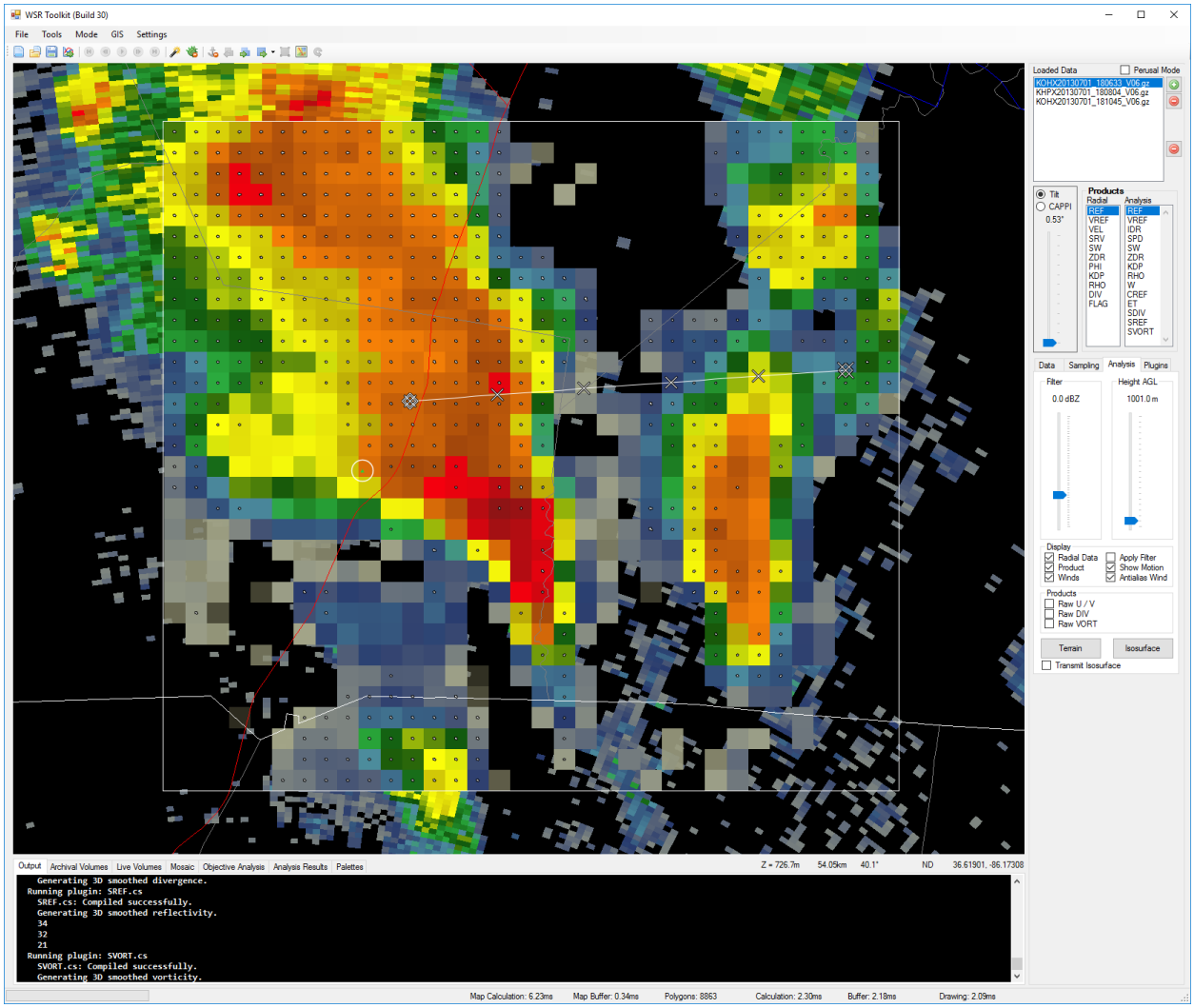

Case 29: Multicell in Kentucky on July 1, 2013 at 1806Z. 1.00" hail report.

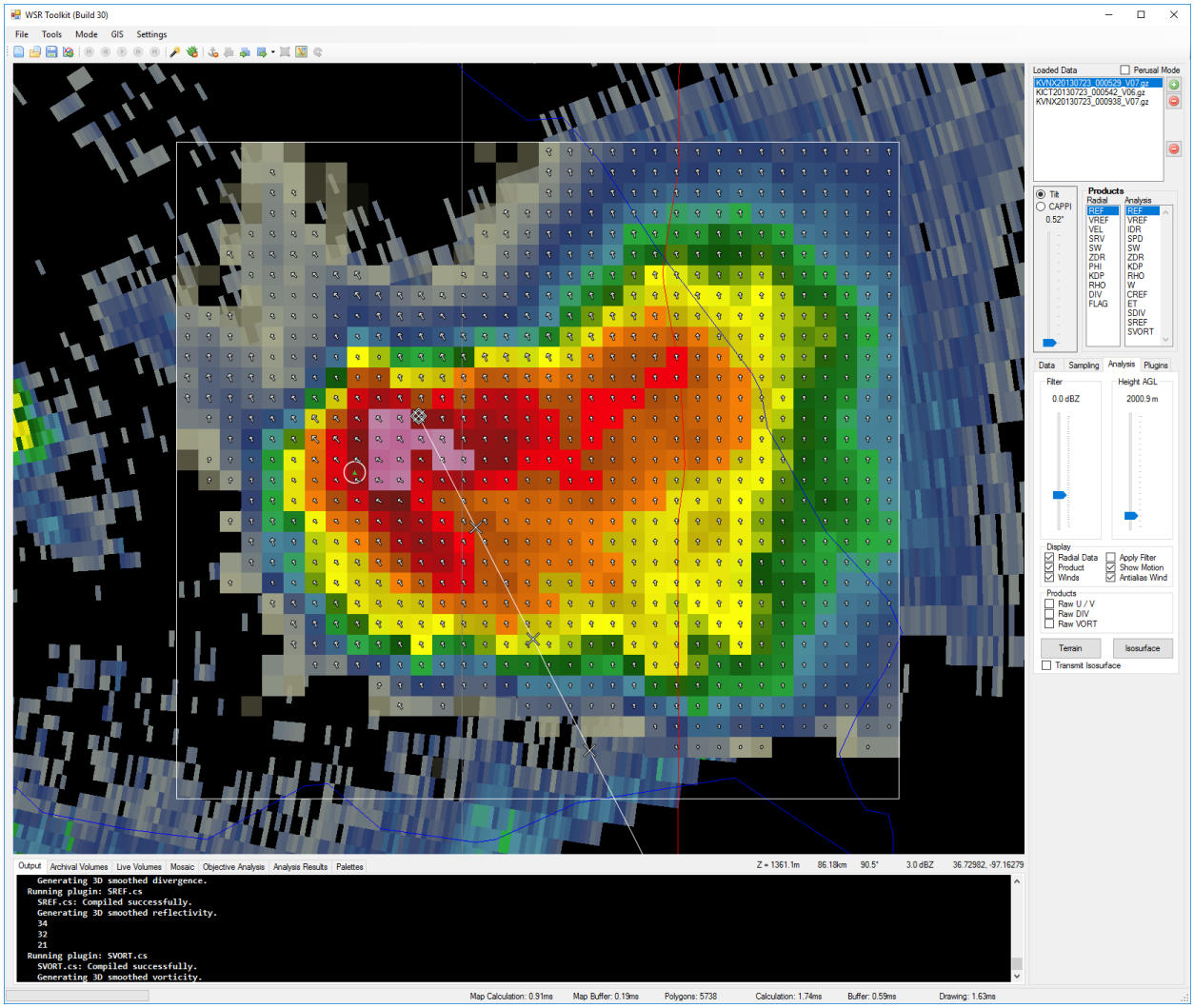

Case 30: Single cell in Kansas on July 23, 2013 at 0005Z. 1.00" hail report.

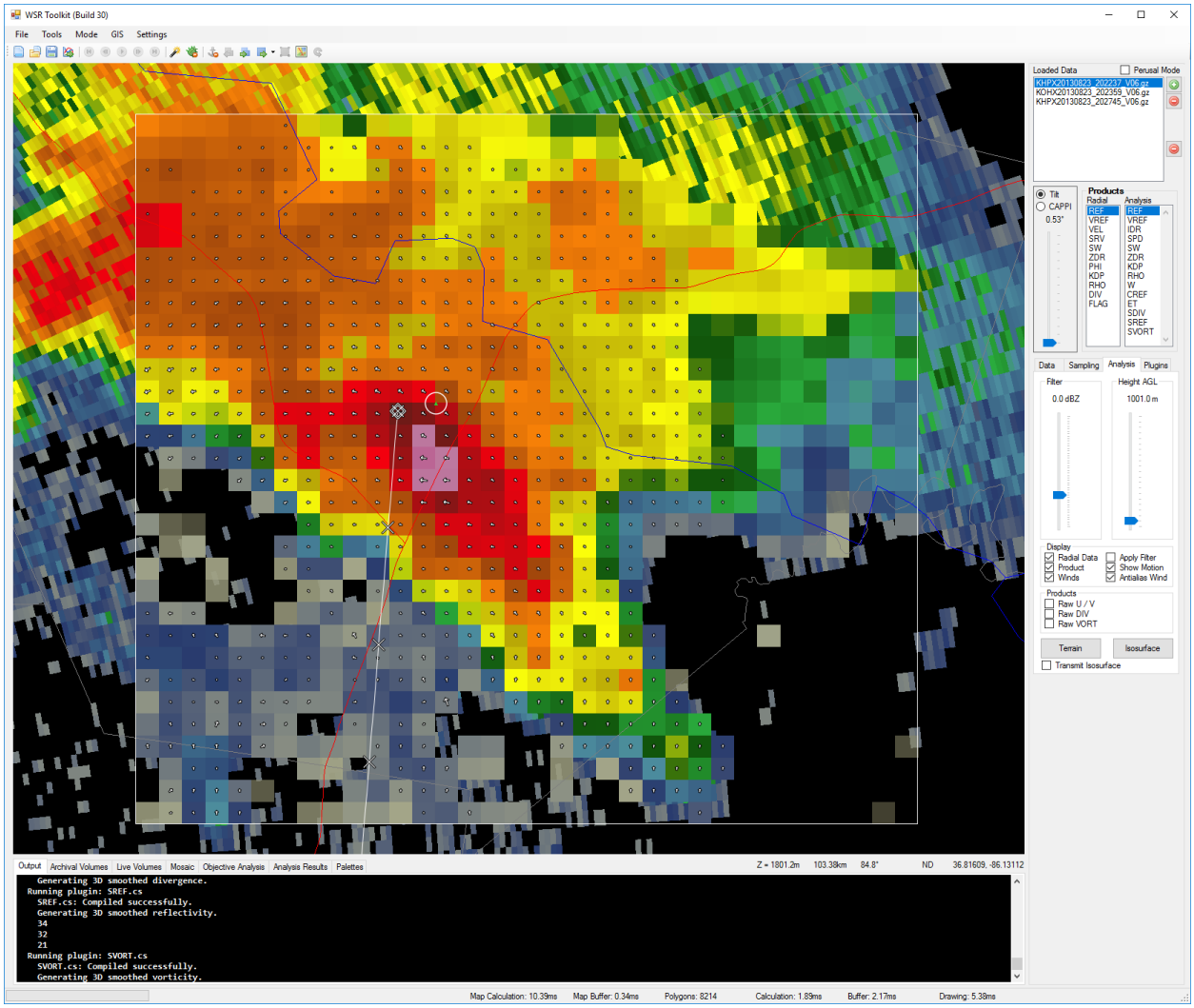

Case 31: Multicell in Kentucky on August 23, 2013 at 2022Z. 1.00" hail report.

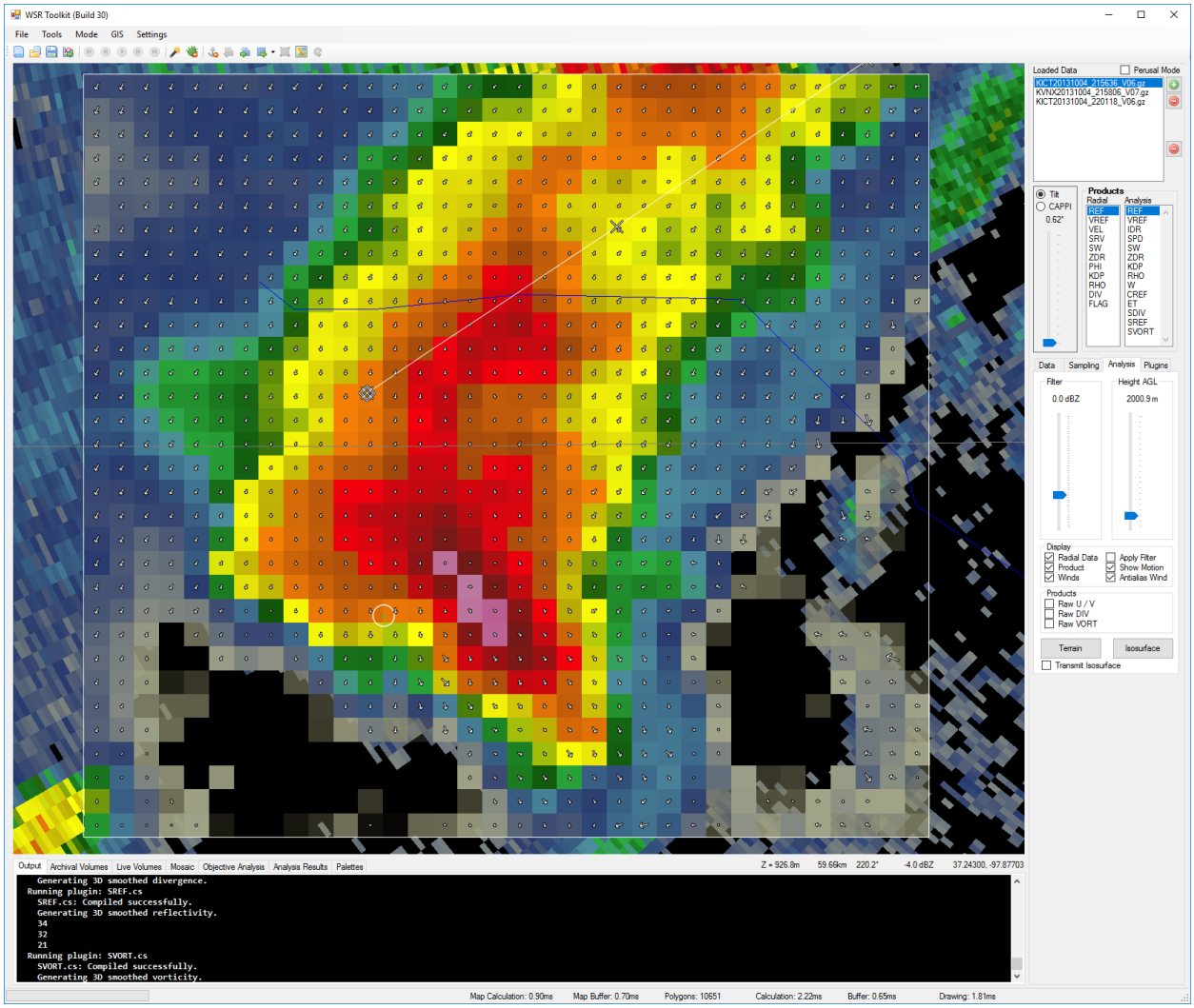

Case 32: Multicell in Kansas on October 4, 2013 at 2156Z. 1.00" hail report.

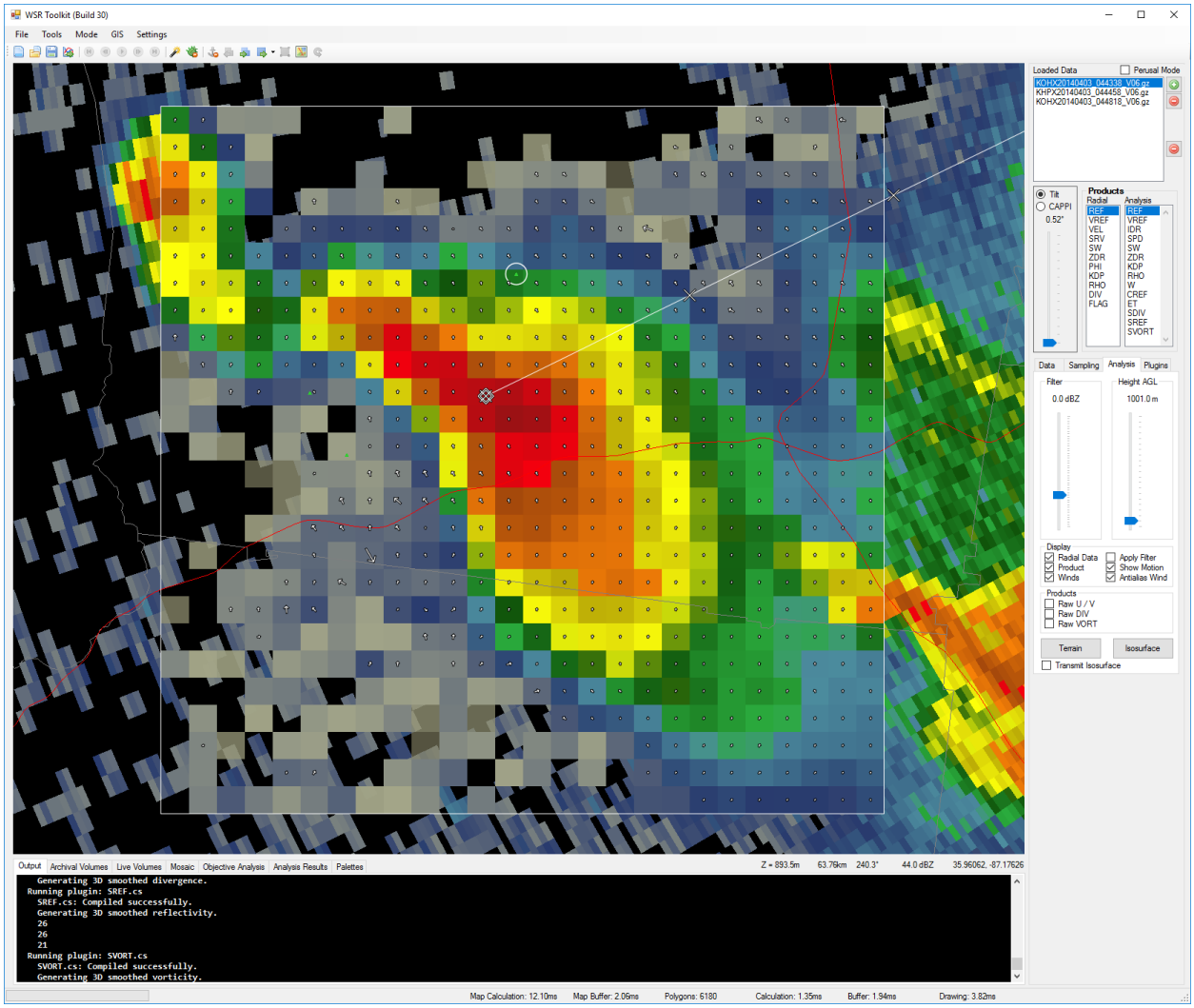

Case 33: Single cell in Kentucky on April 23, 2014 at 0443Z. 1.25" hail report.

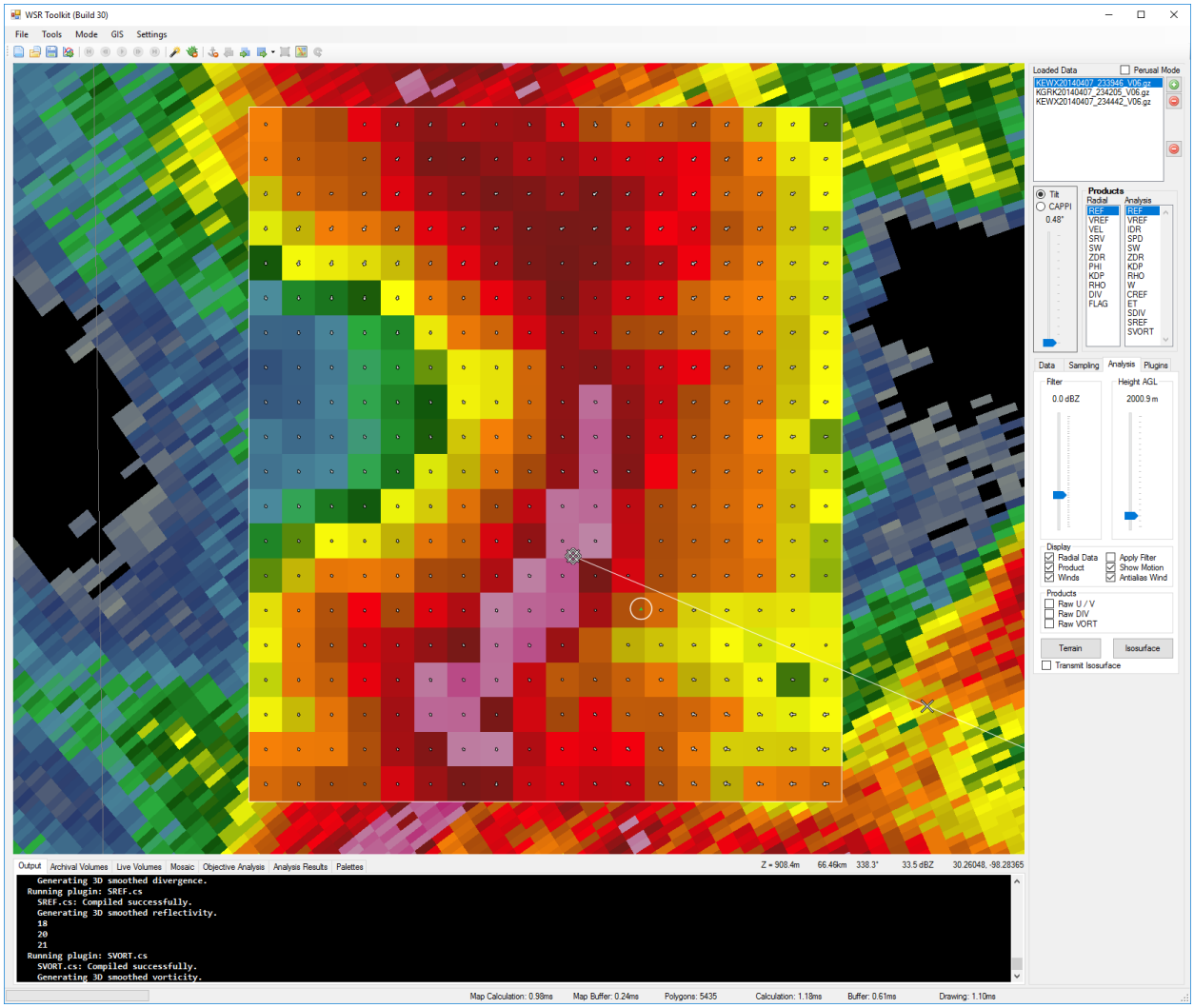

Case 34: Line segment in Texas on April 7, 2014 at 2339Z. 0.75" hail report.

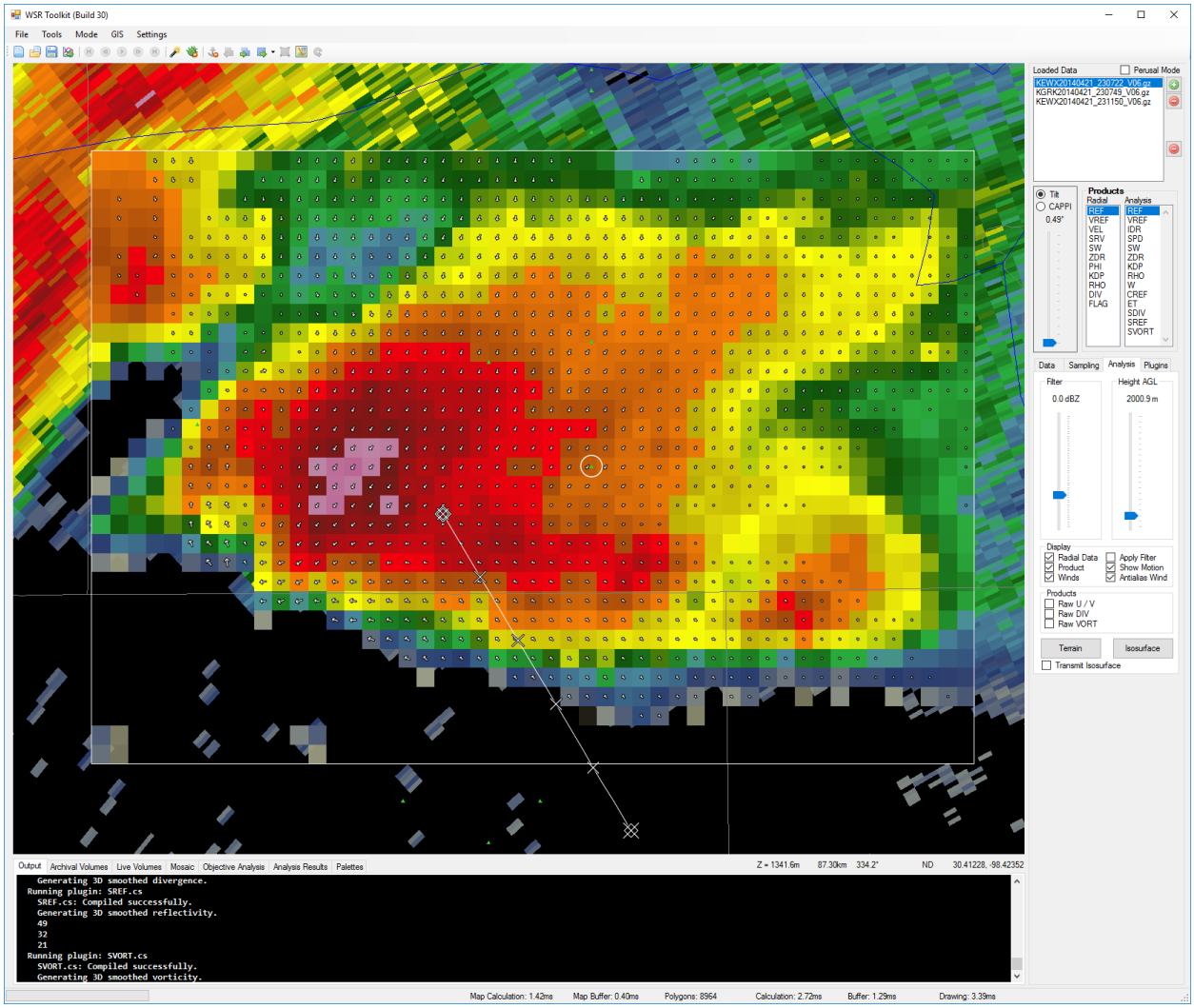

Case 35: Single cell in Texas on April 21, 2014 at 2307Z. 1.75" hail report.

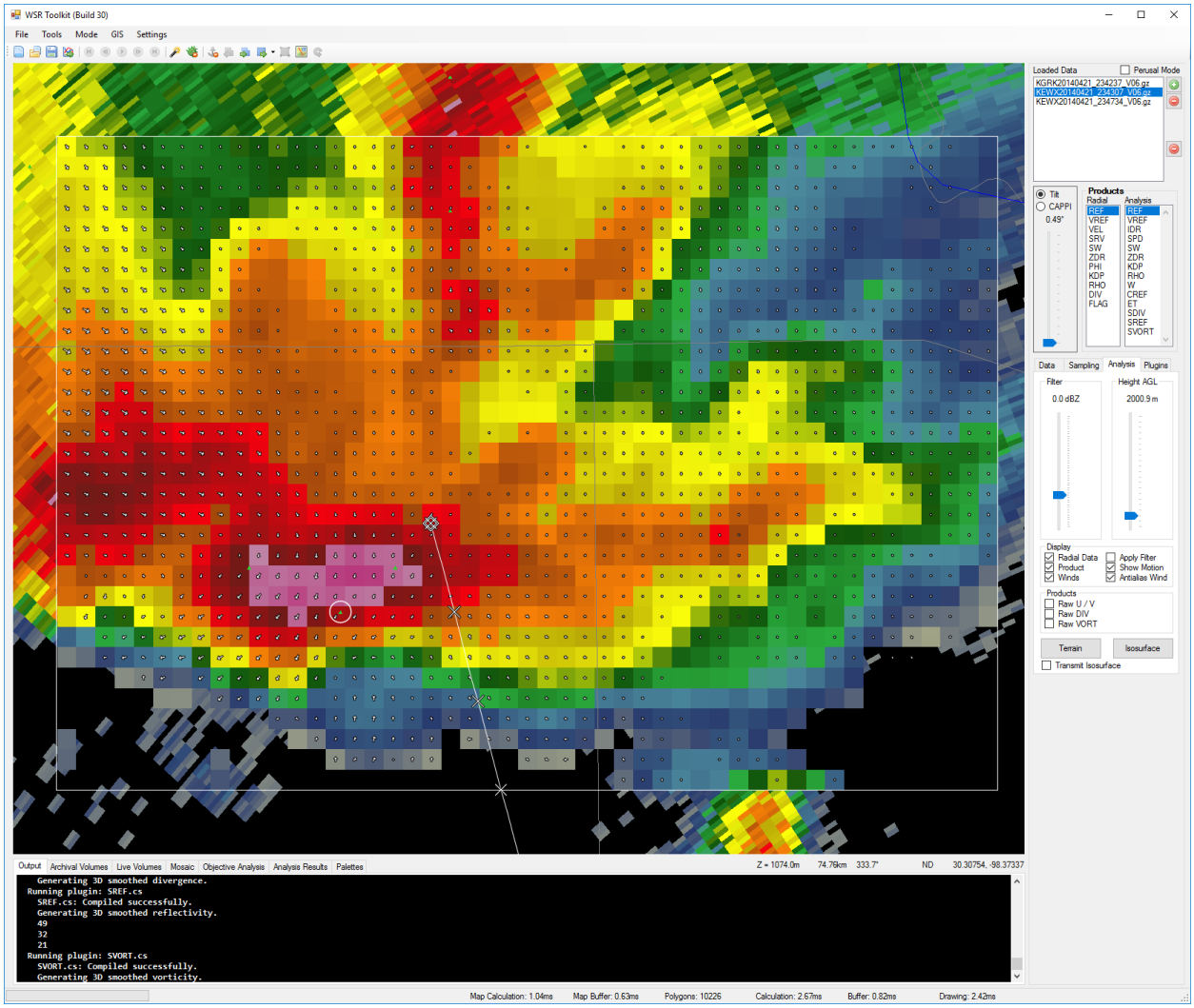

Case 36: Multicell in Texas on April 21, 2014 at 2342Z. 2.00" hail report.

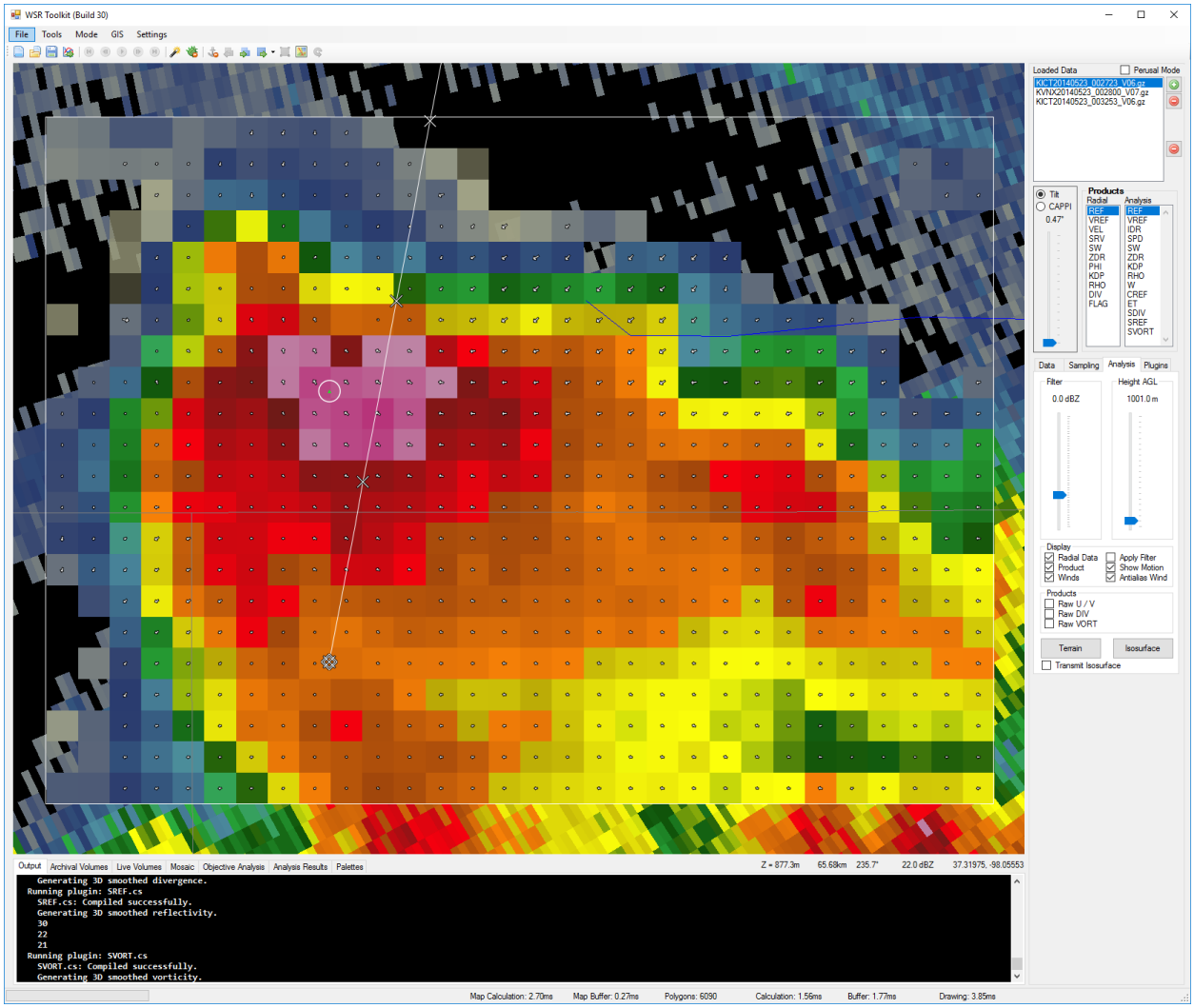

Case 37: Single cell in Kansas on May 23, 2014 at 0027Z. 1.75" hail report.

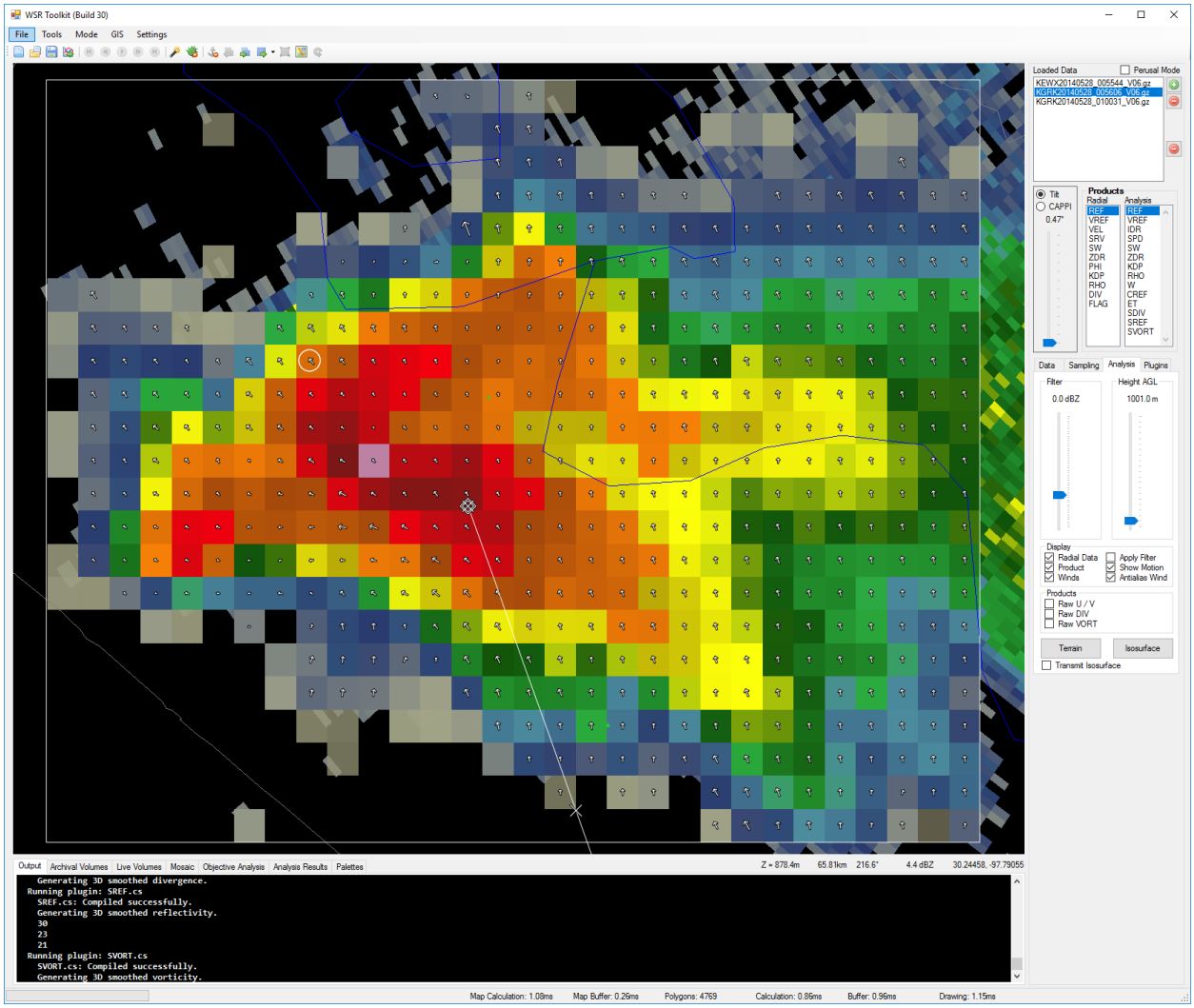

Case 38: Single cell in Texas on May 28, 2014 at 0055Z. 1.00" hail report.

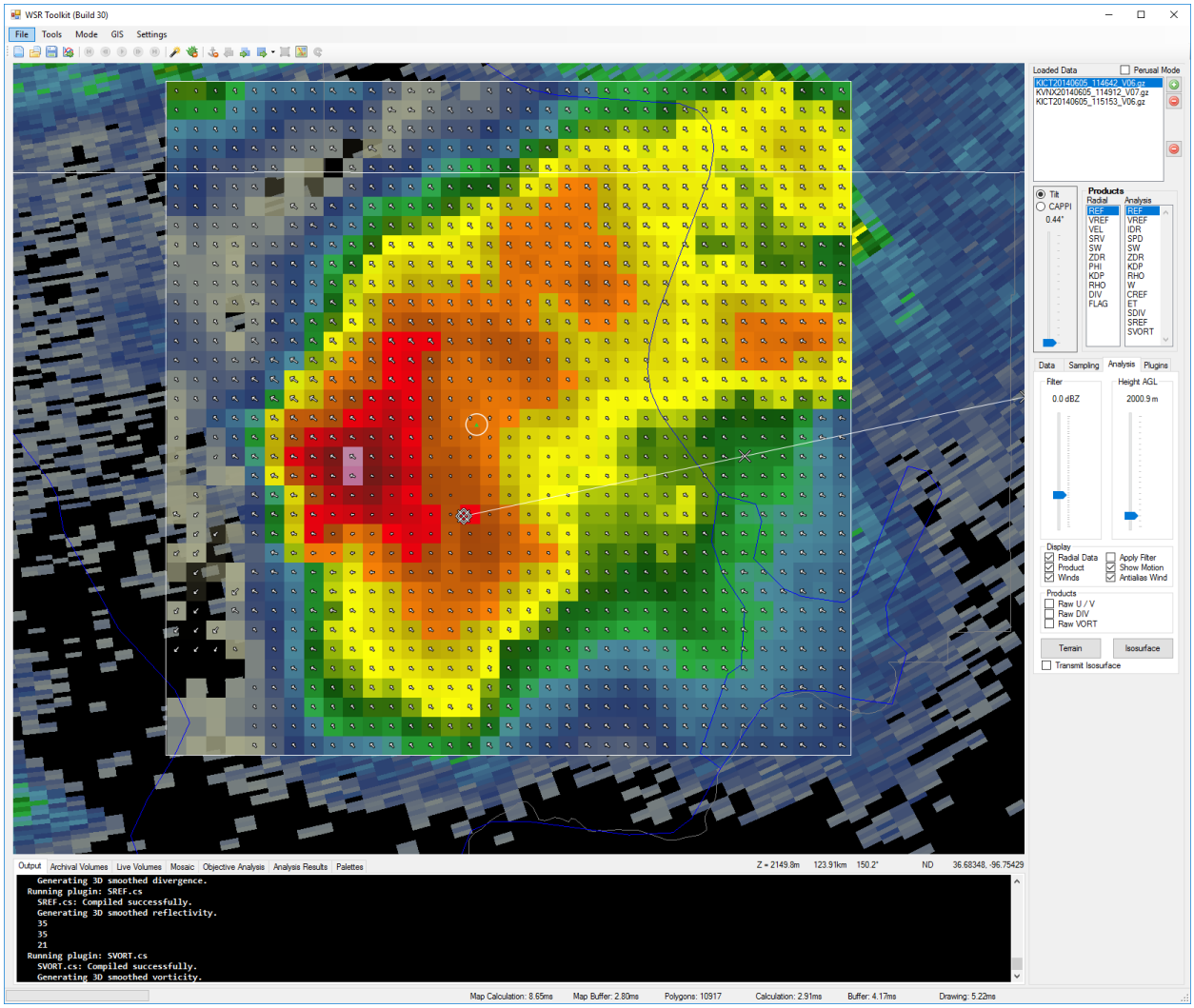

Case 39: Single cell in Kansas on June 5, 2014 at 1146Z. 2.25" hail report.

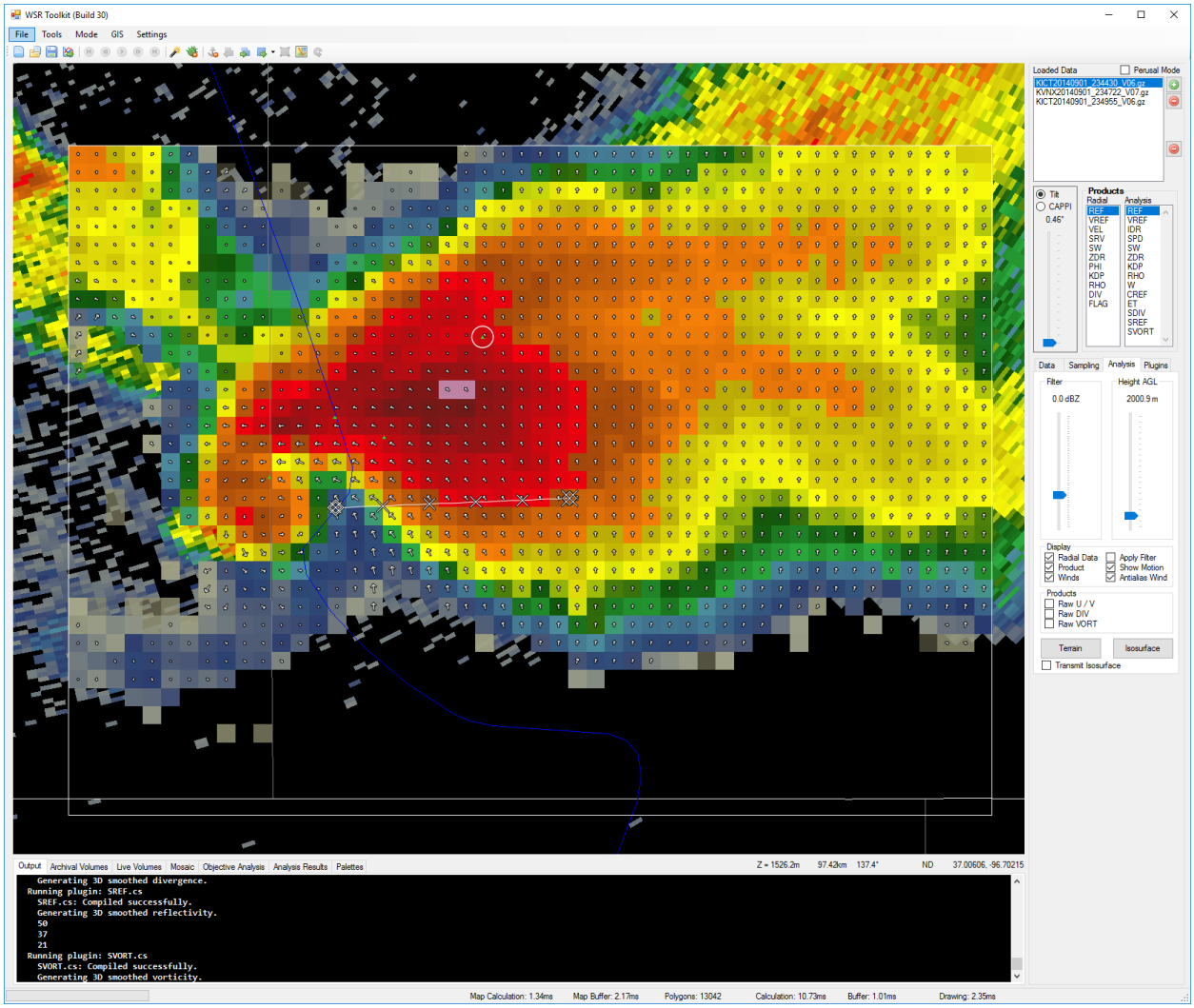

Case 40: Supercell in Kansas on September 1, 2014 at 2344Z. 2.75" hail report.

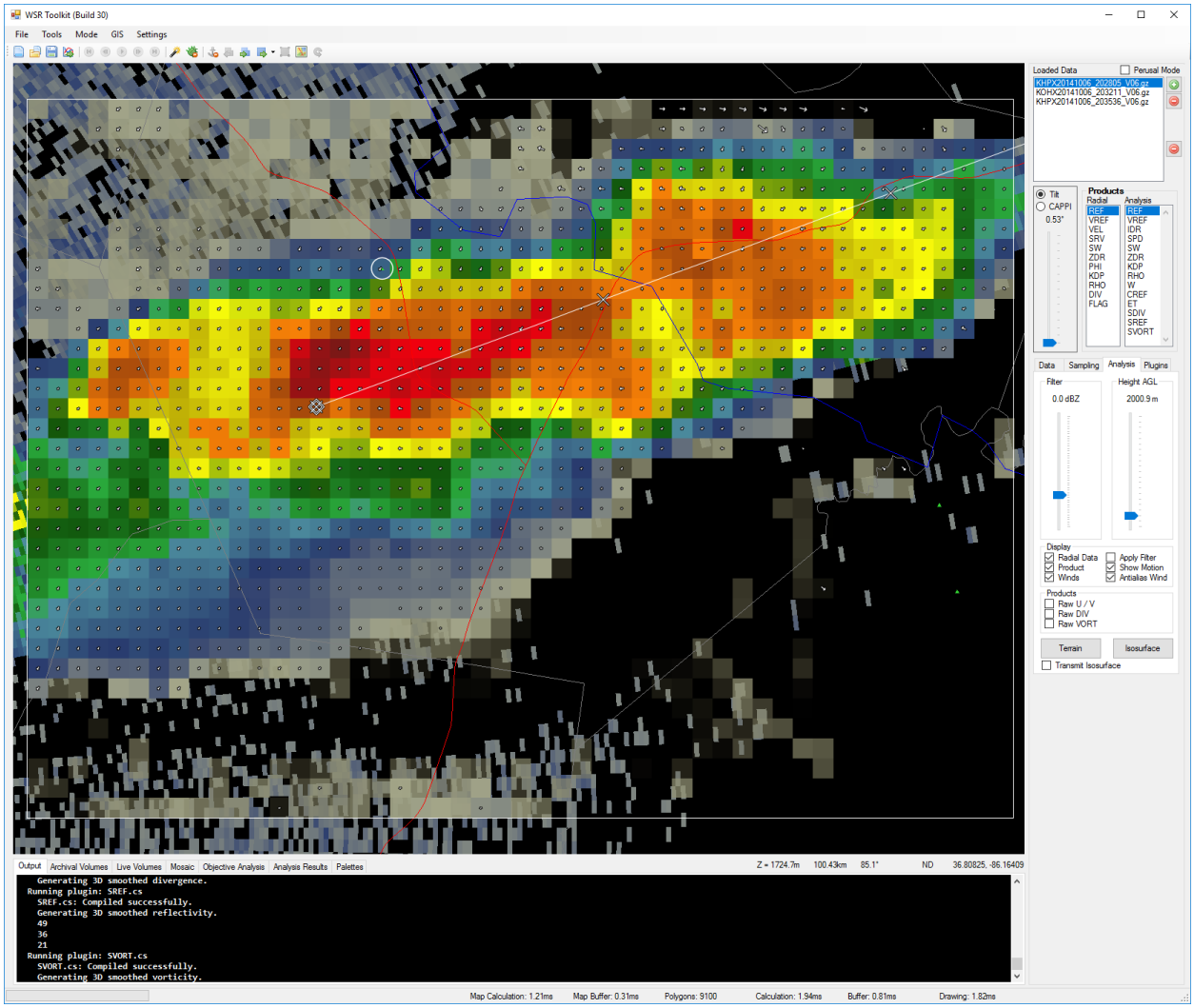

Case 41: Line segment in Kentucky on October 6, 2014 at 2028Z. 1.00" hail report.

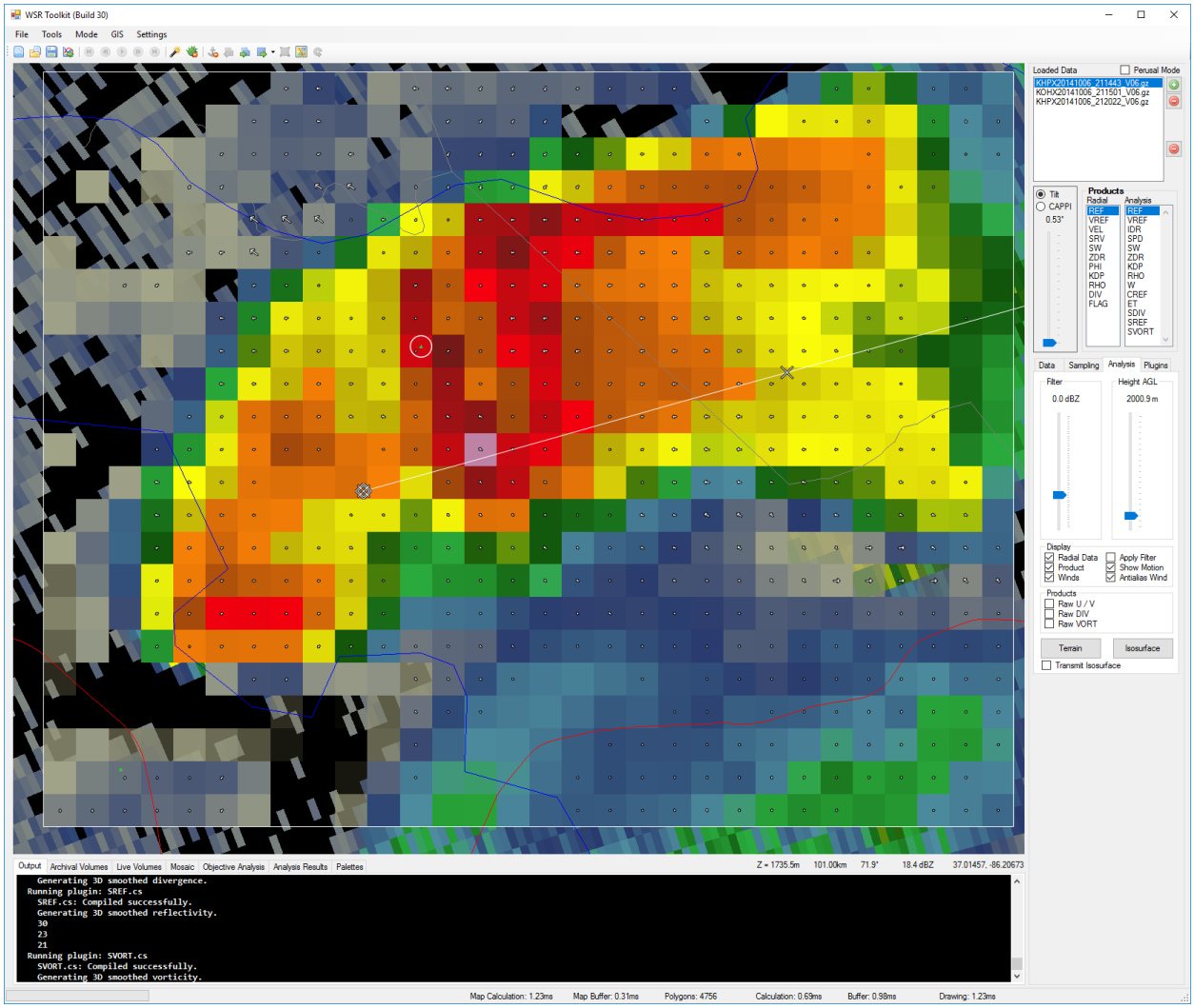

Case 42: Single cell in Kentucky on October 6, 2014 at 2114Z. 1.75" hail report.

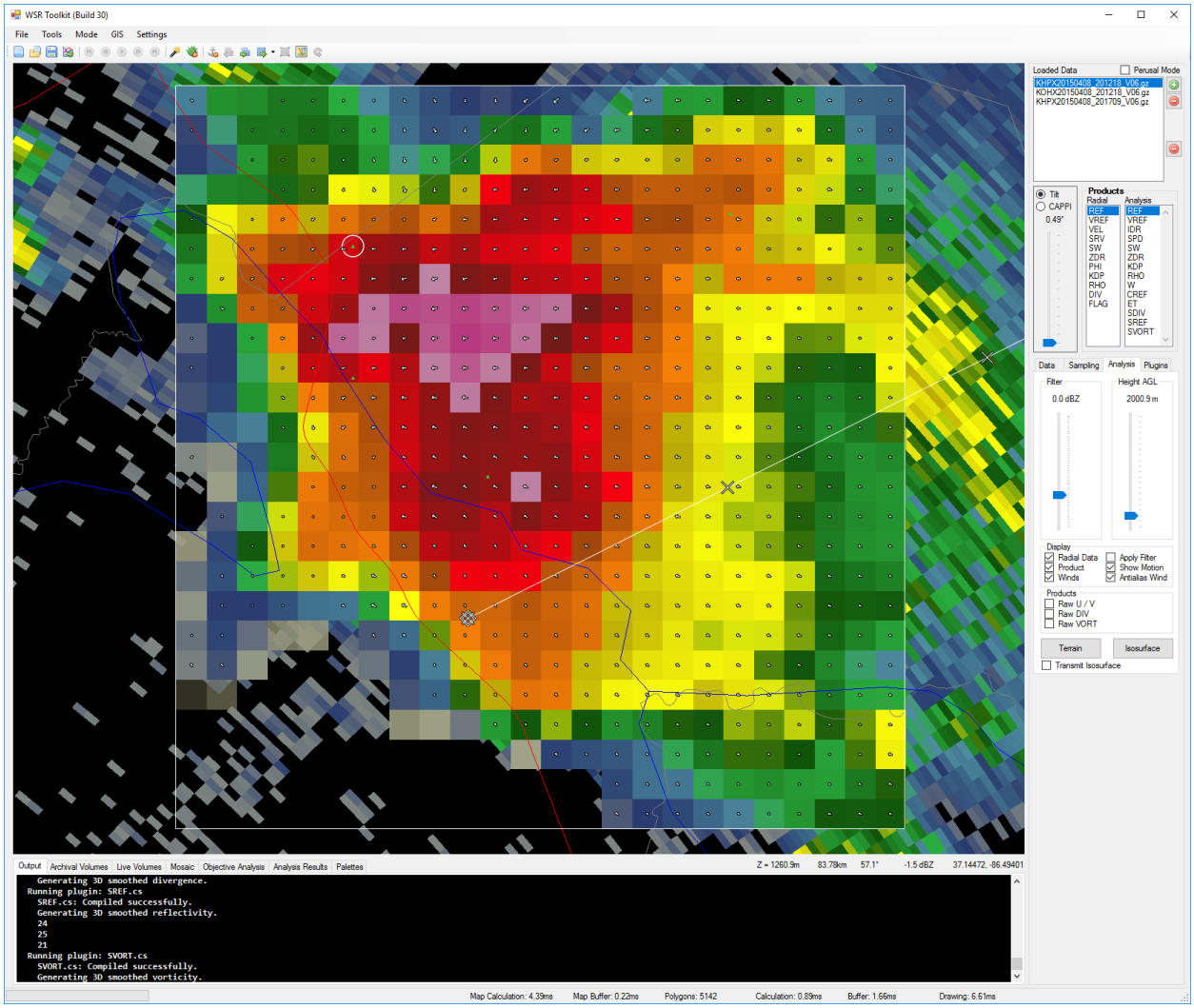

Case 43: Single cell in Kentucky on April 8, 2015 at 2012Z. 2.00" hail report.

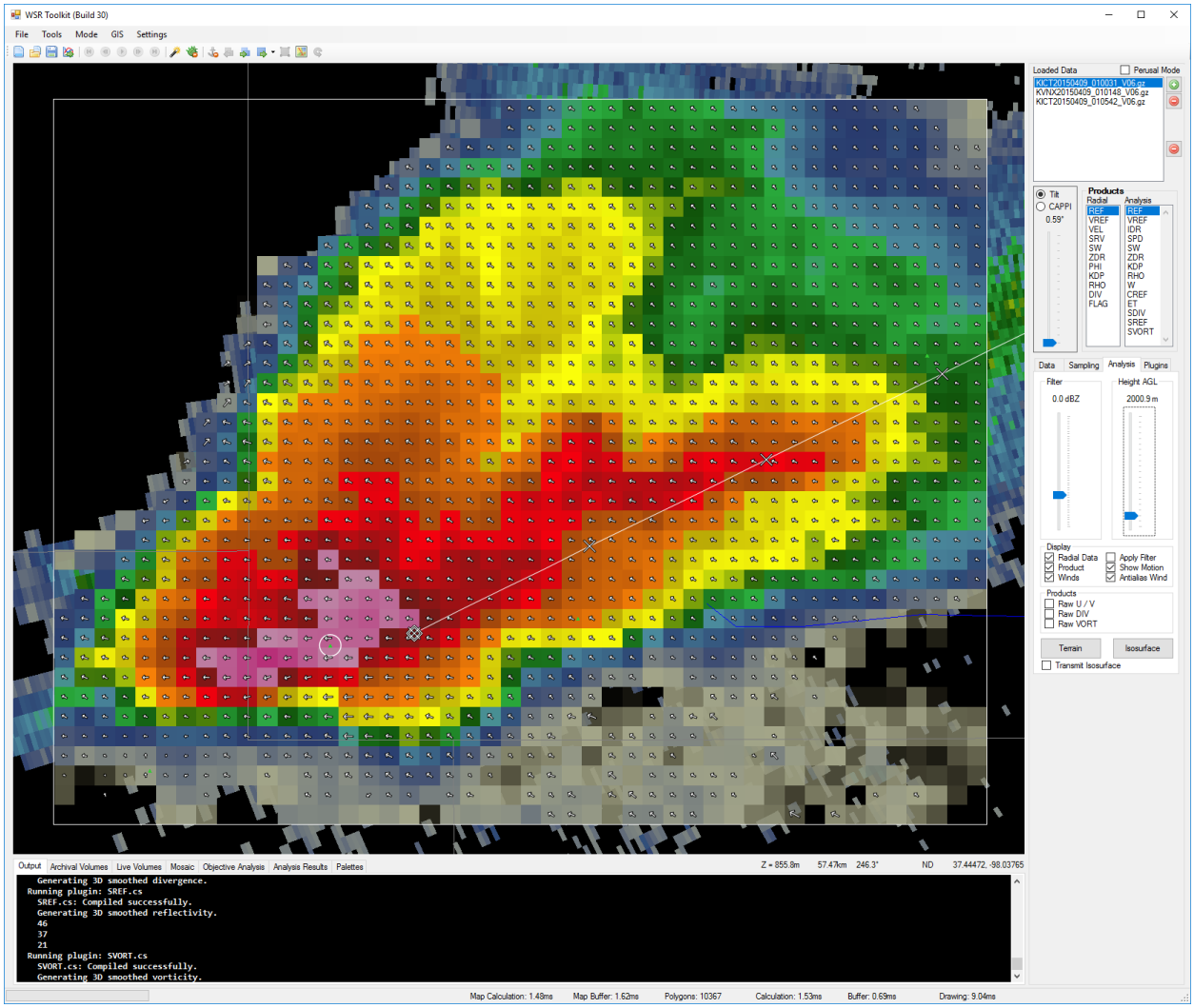

Case 44: Single cell in Kansas on April 9, 2015 at 0100Z. 2.75" hail report.

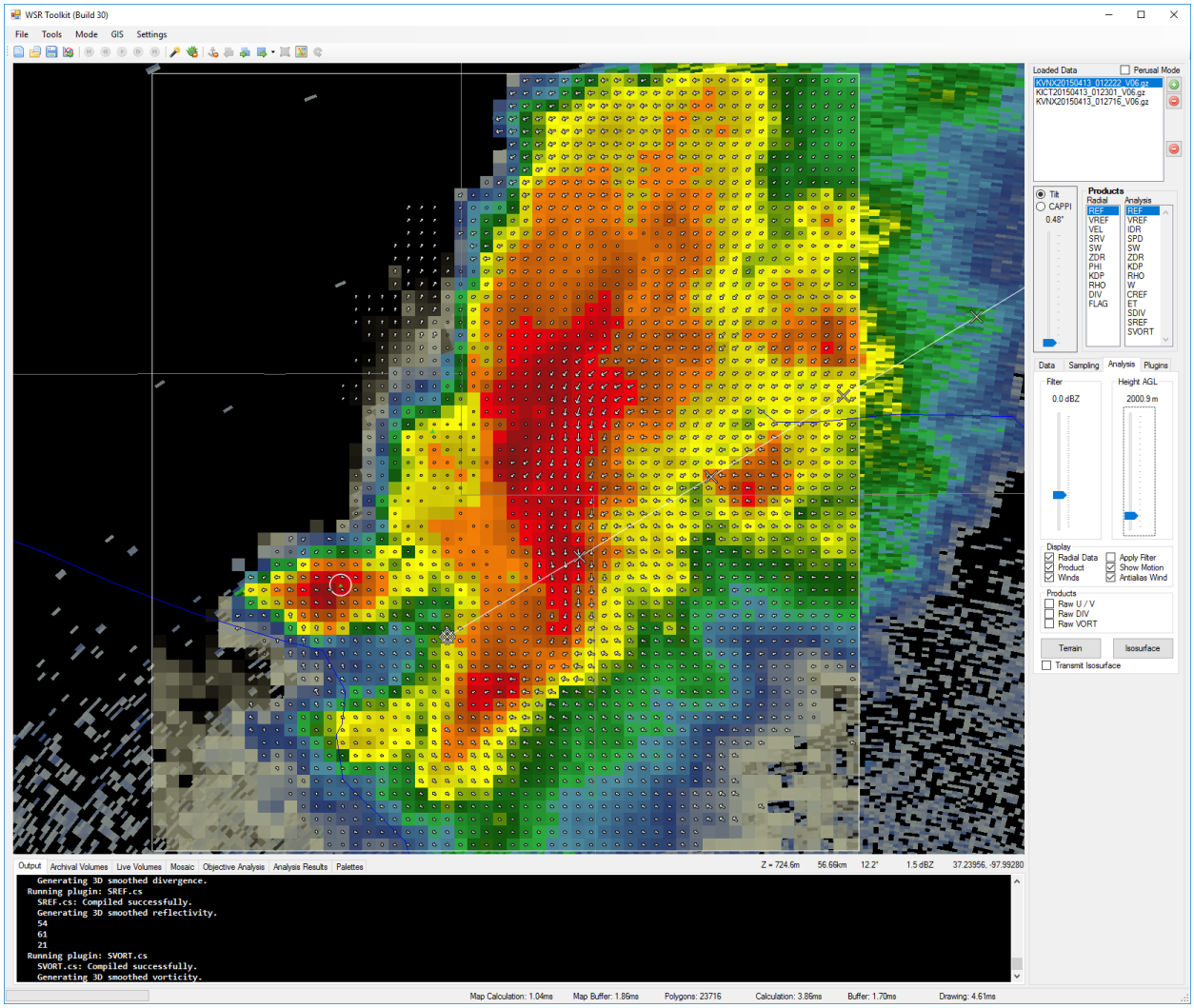

Case 45: Line segment in Kansas on April 13, 2015 at 0122Z. 0.75" hail report.

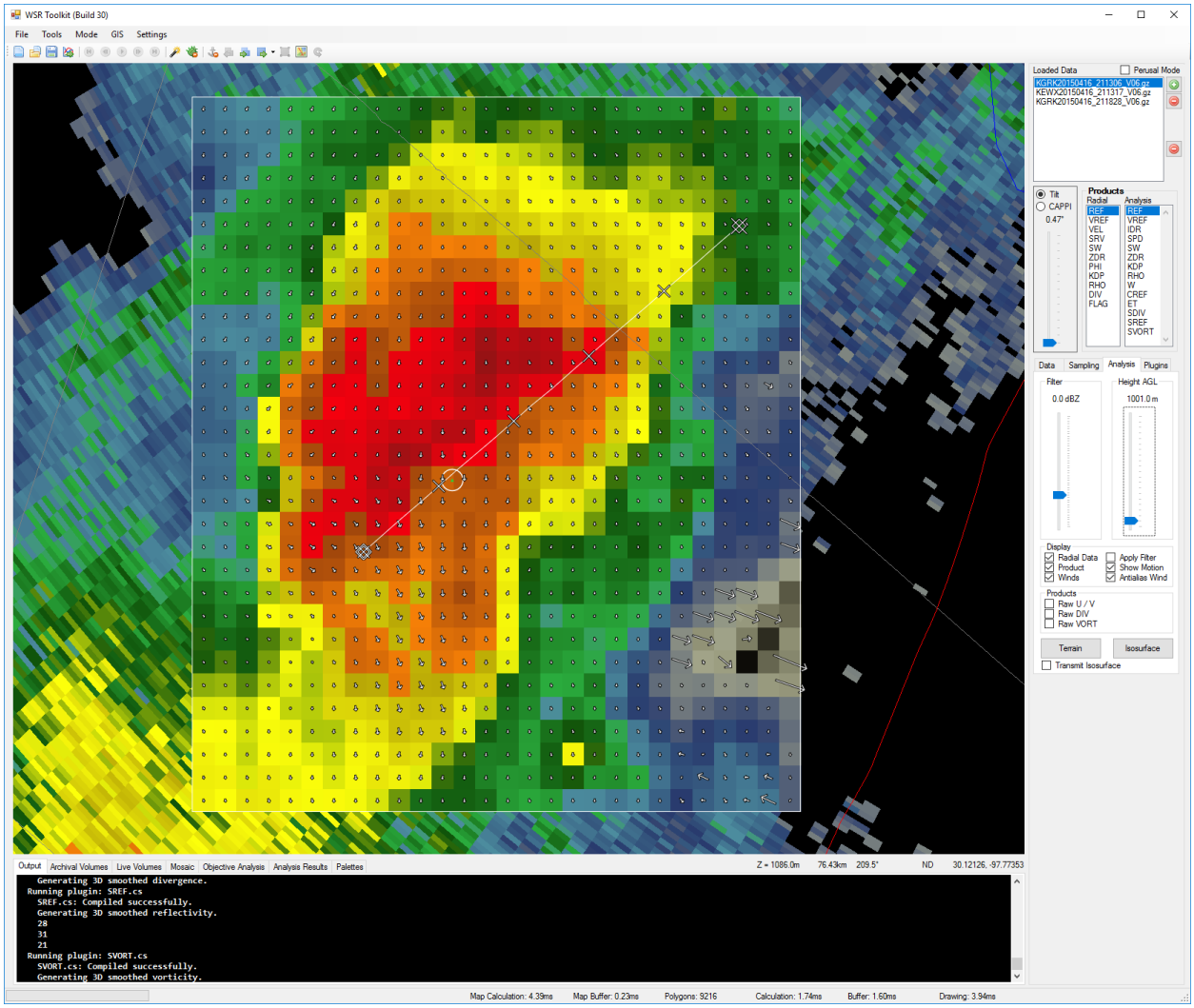

Case 46: Single cell in Texas on April 16, 2015 at 2113Z. 0.88" hail report.

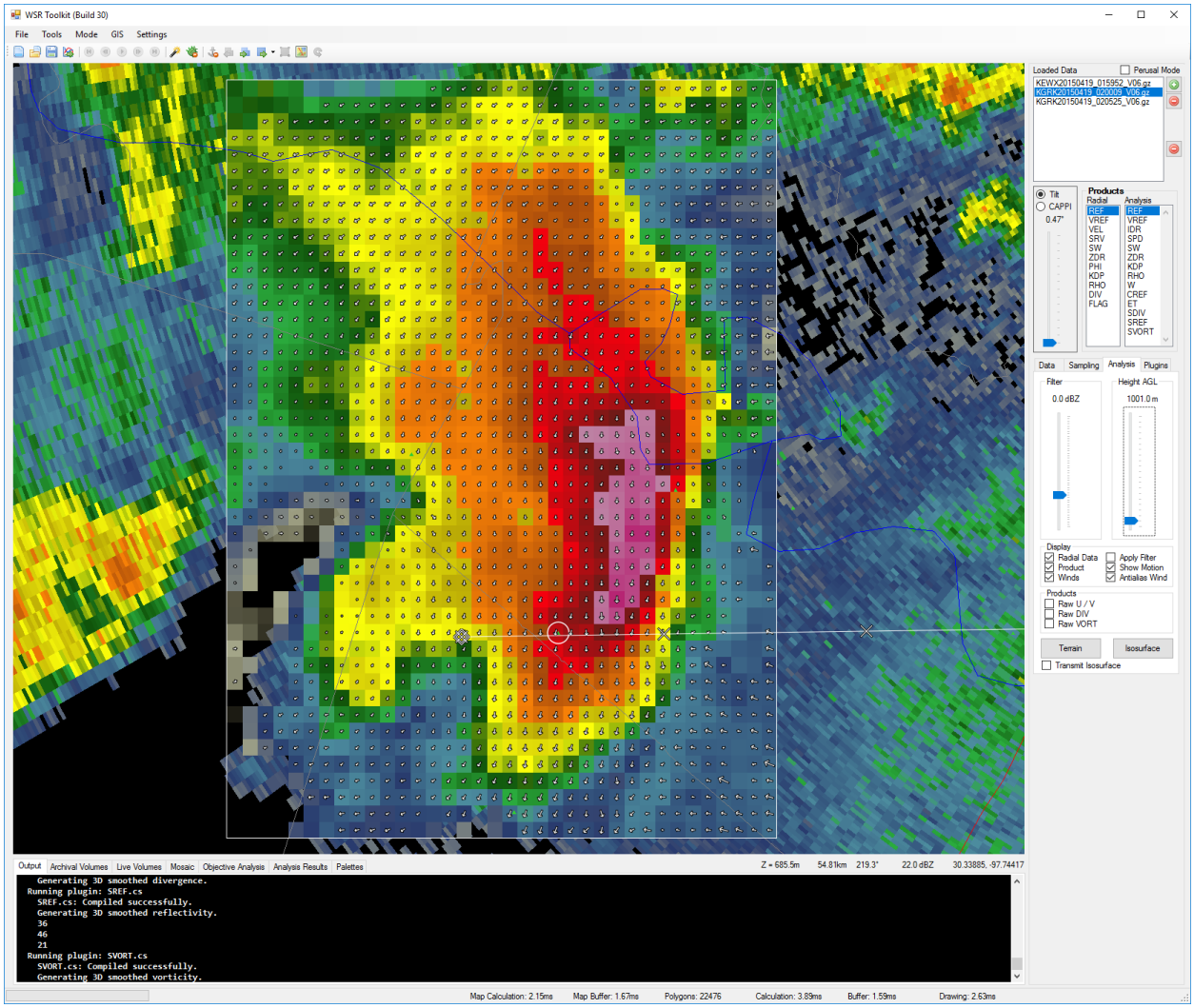

Case 47: Line segment in Texas on April 19, 2015 at 0159Z. 1.75" hail report.

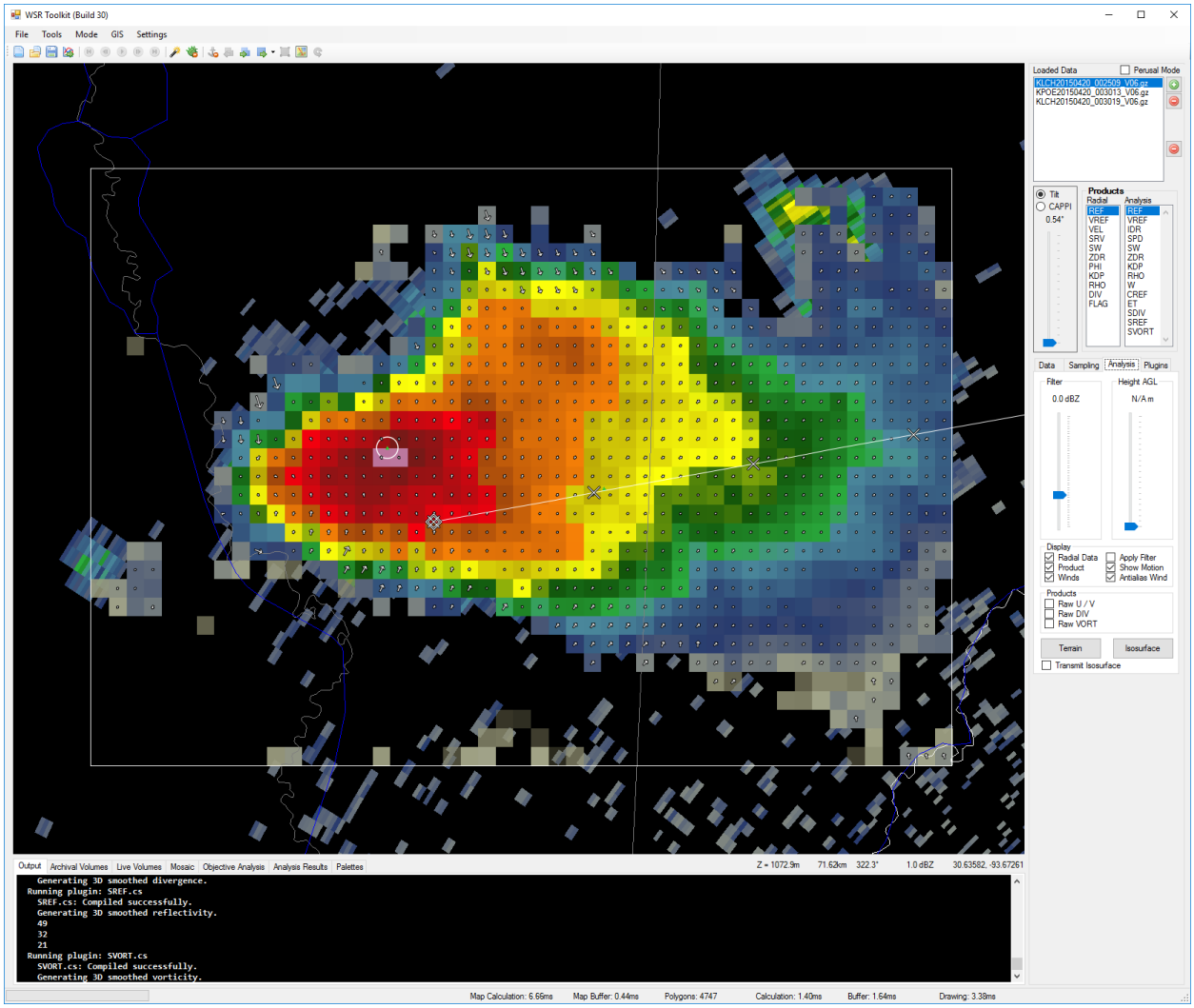

Case 48: Single cell in Texas on April 20, 2015 at 0025Z. 2.00" hail report.

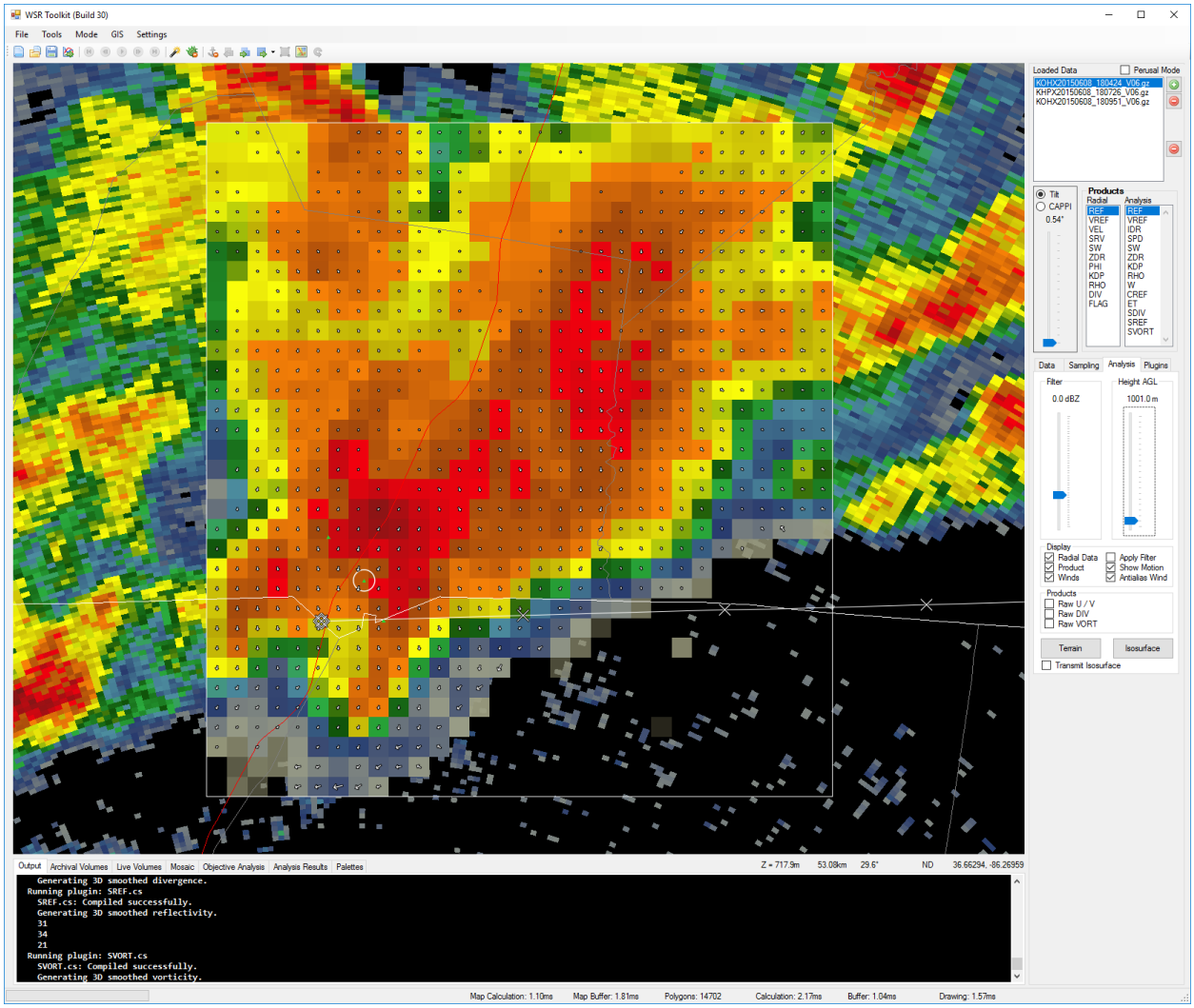

Case 49: Multicell in Kentucky on June 8, 2015 at 1804Z. 1.50" hail report.

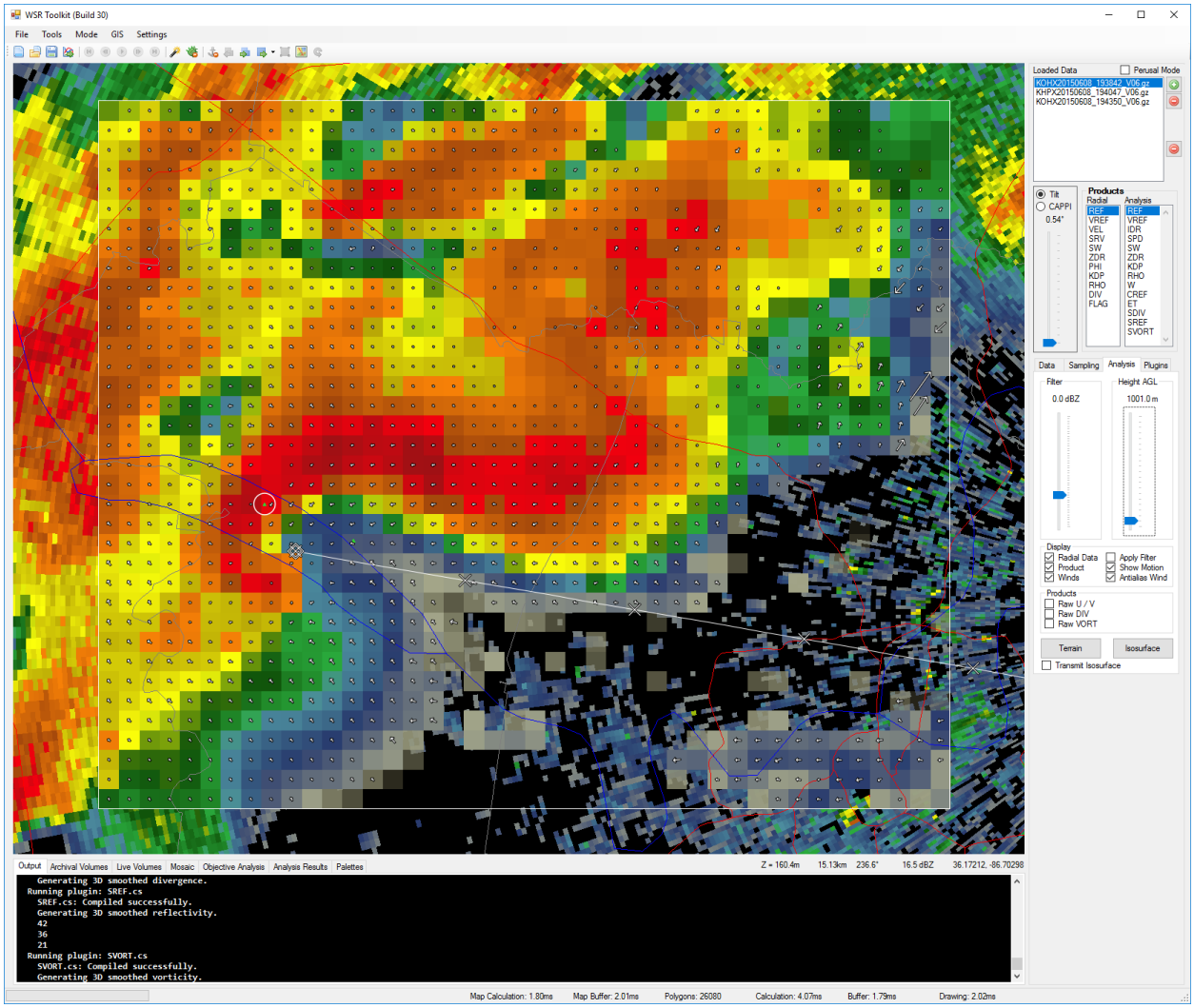

Case 50: Embedded supercell in Kentucky on June 8, 2015 at 1938Z. 1.75" hail report.

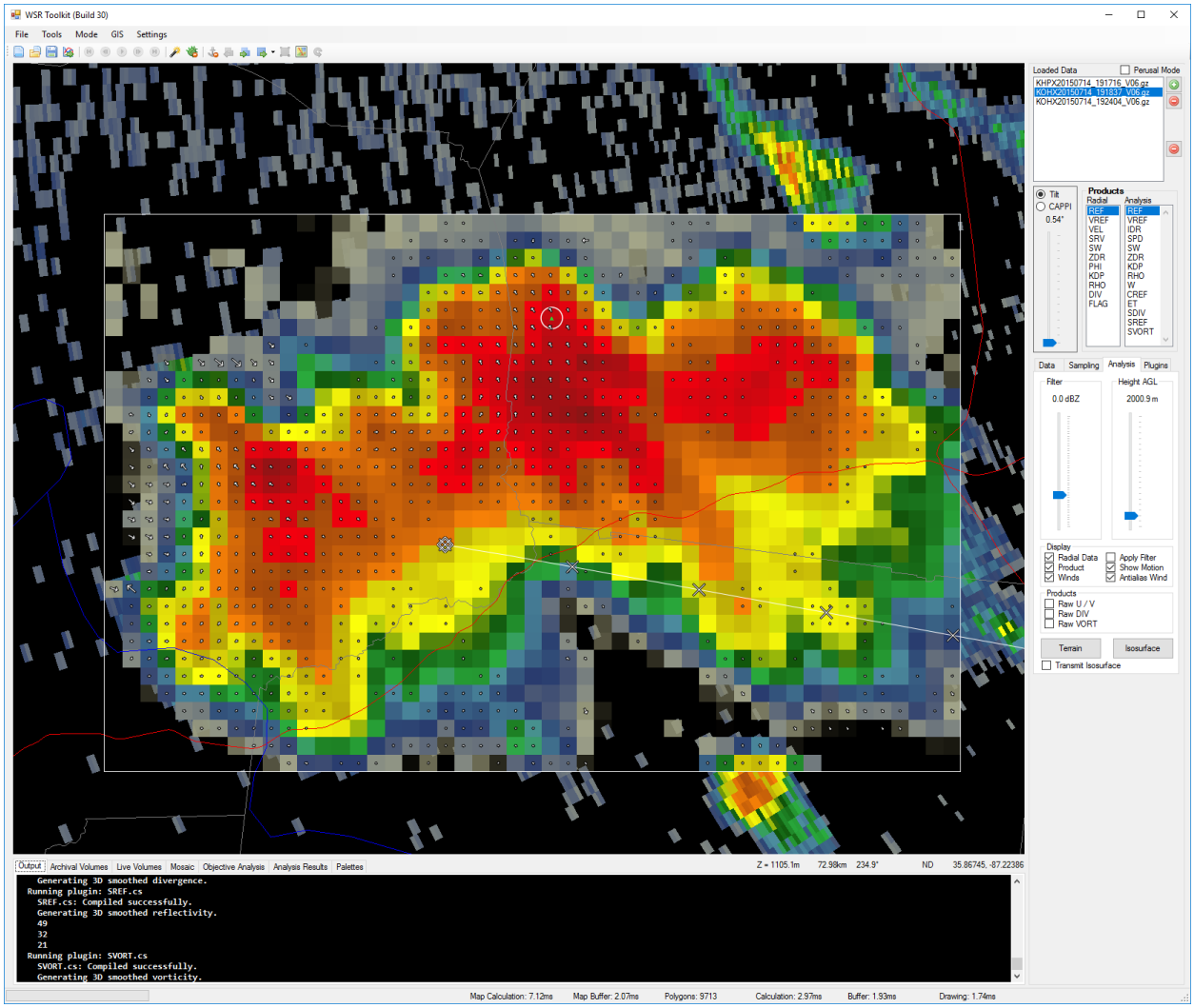

Case 51: Multicell in Kentucky on July 14, 2015 at 1917Z. 1.75" hail report.

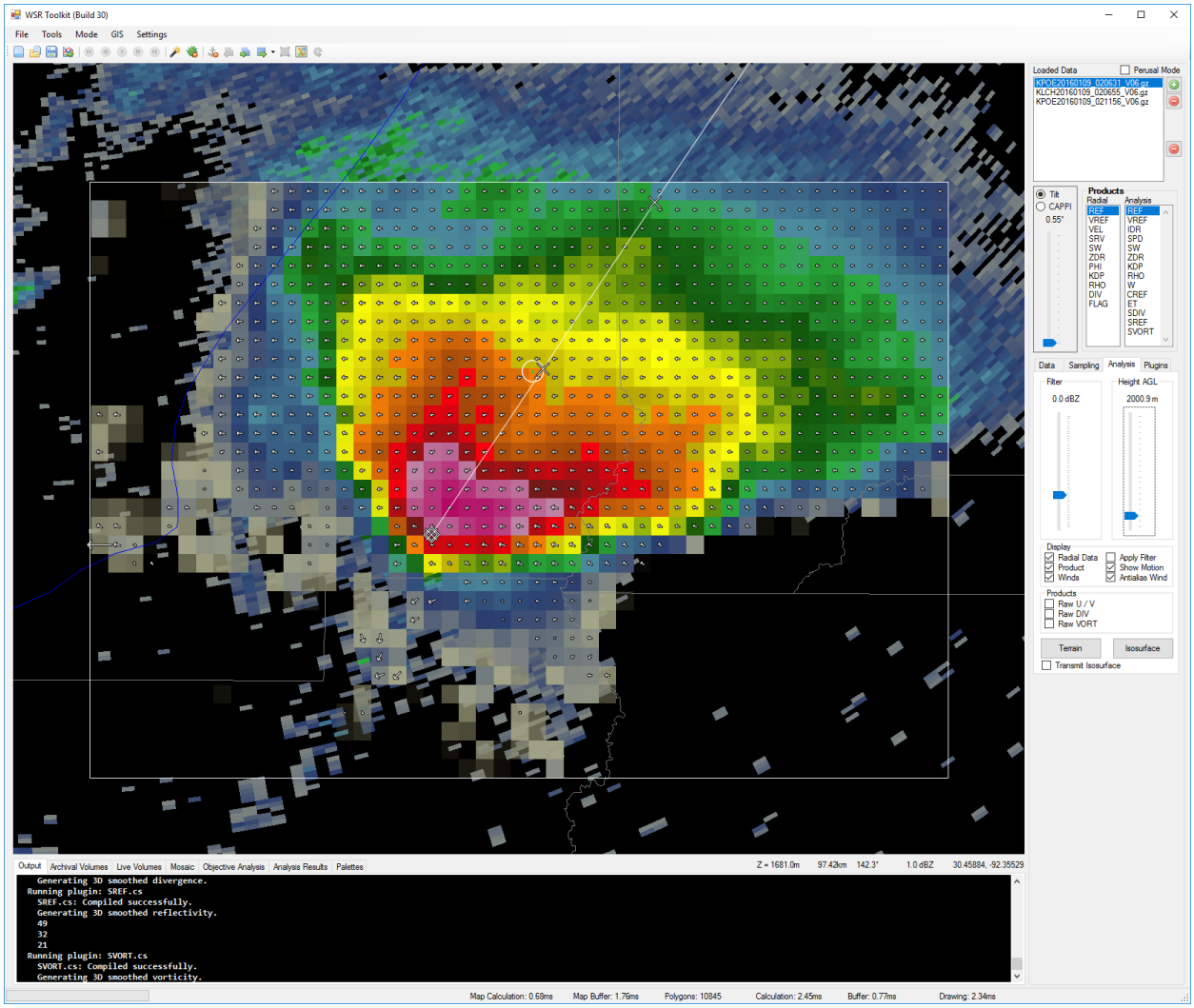

Case 52: Single cell in Louisiana on January 9, 2016 at 0206Z. 1.50" hail report.

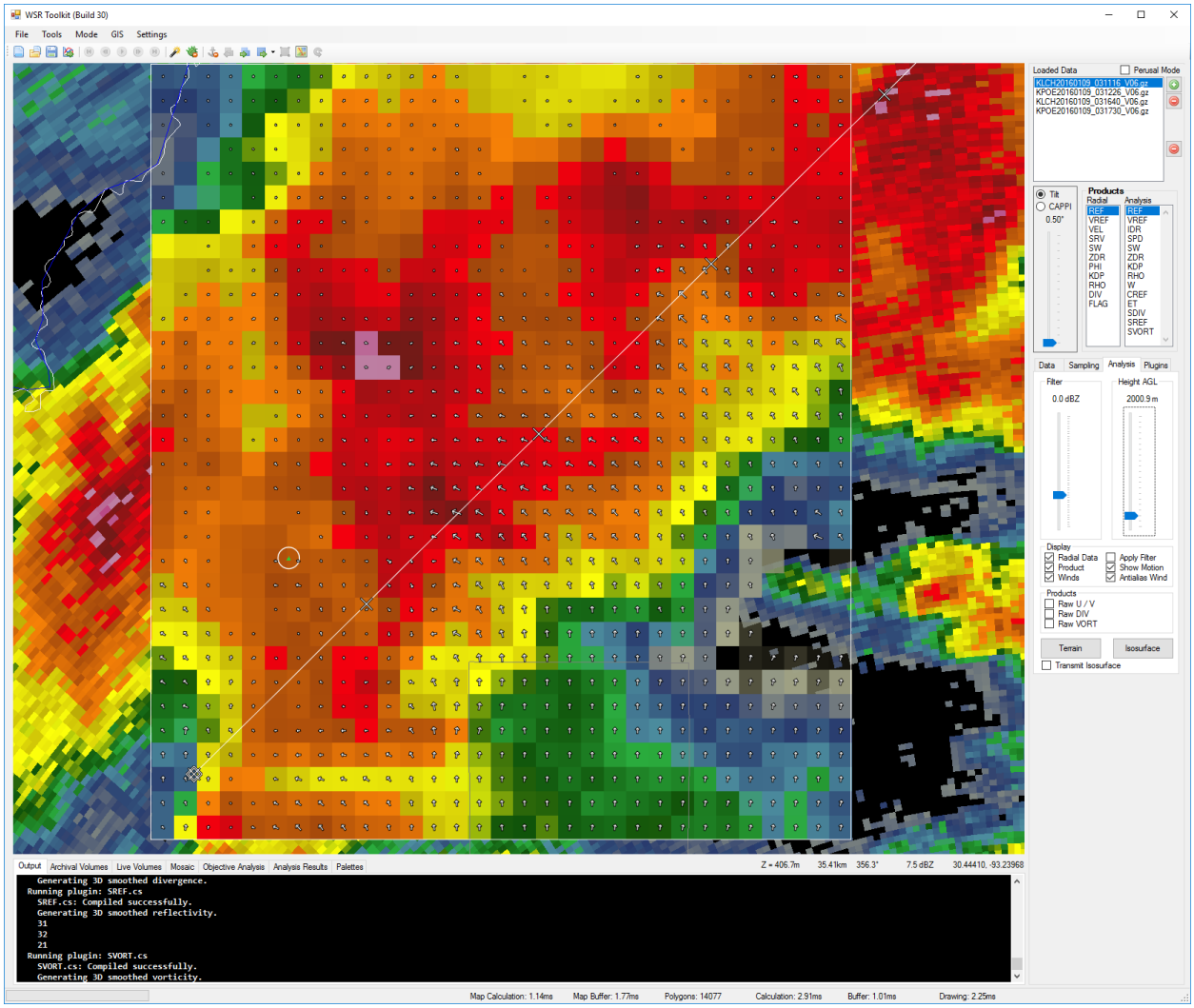

Case 53: Squall line in Louisiana on January 9, 2016 at 0311Z. 1.50" hail report.

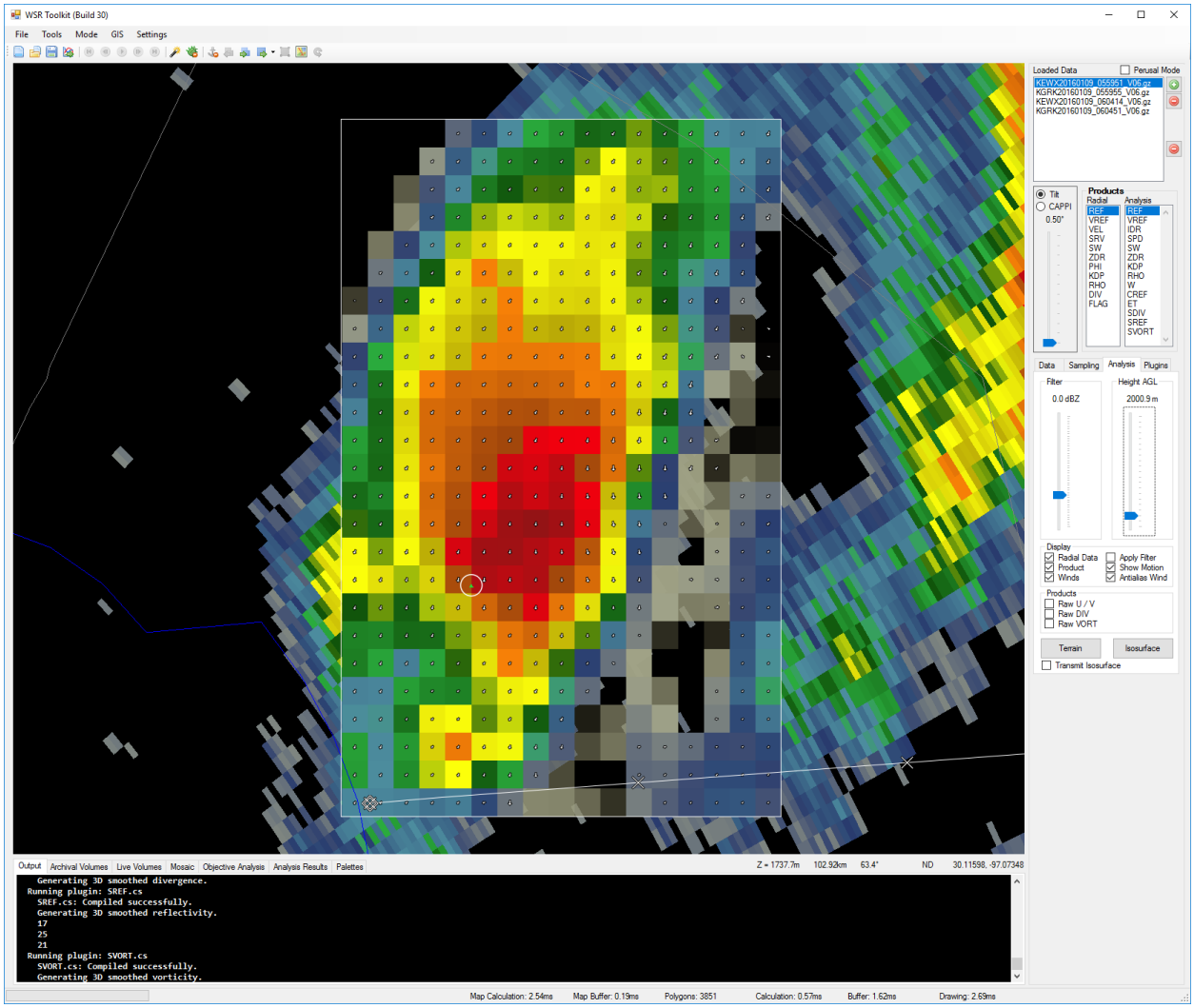

Case 54: Single cell in Texas on January 9, 2016 at 0559Z. 0.75" hail size.

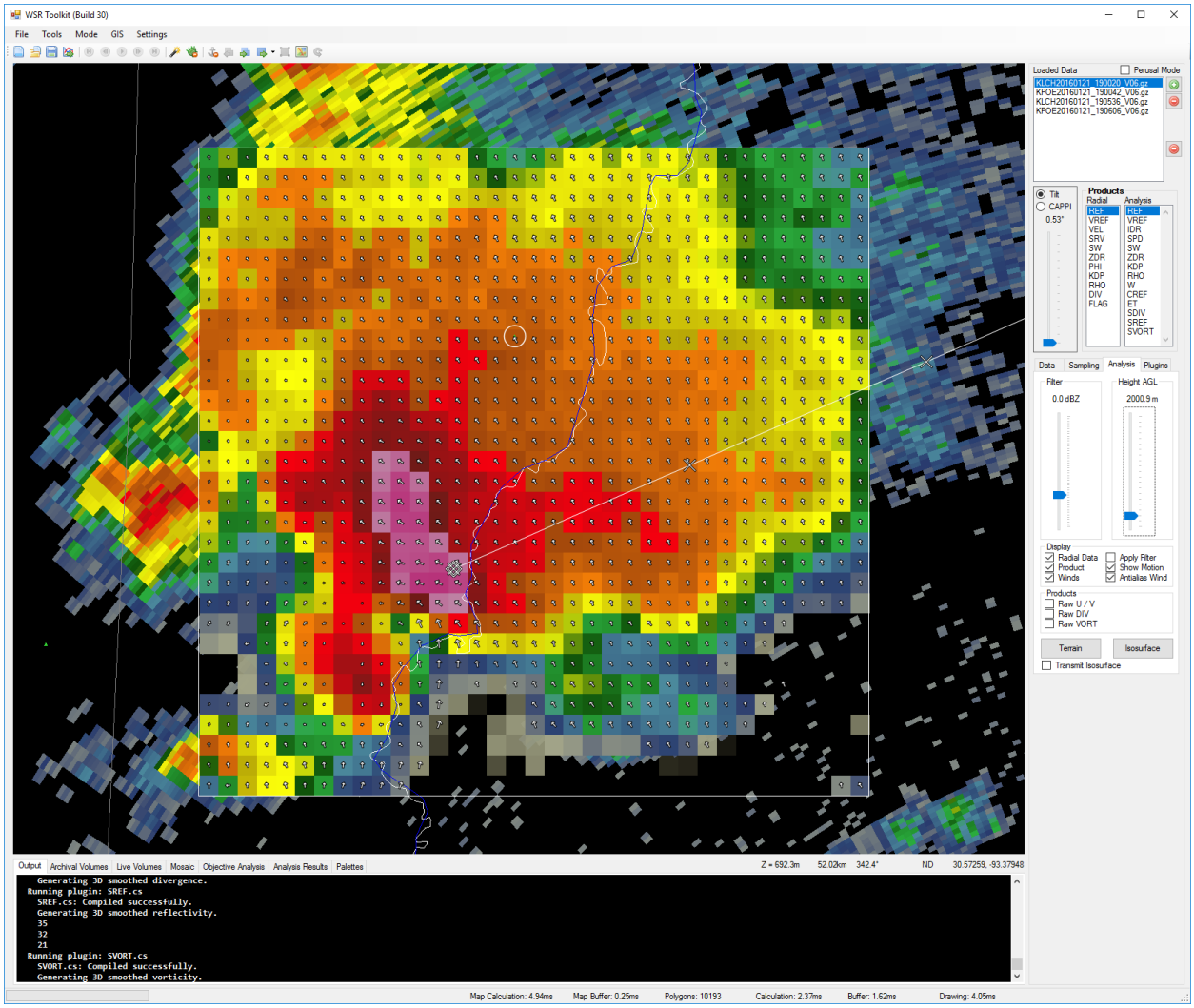

Case 55: Supercell in Louisiana on January 21, 2016 at 1900Z. 1.75" hail report.

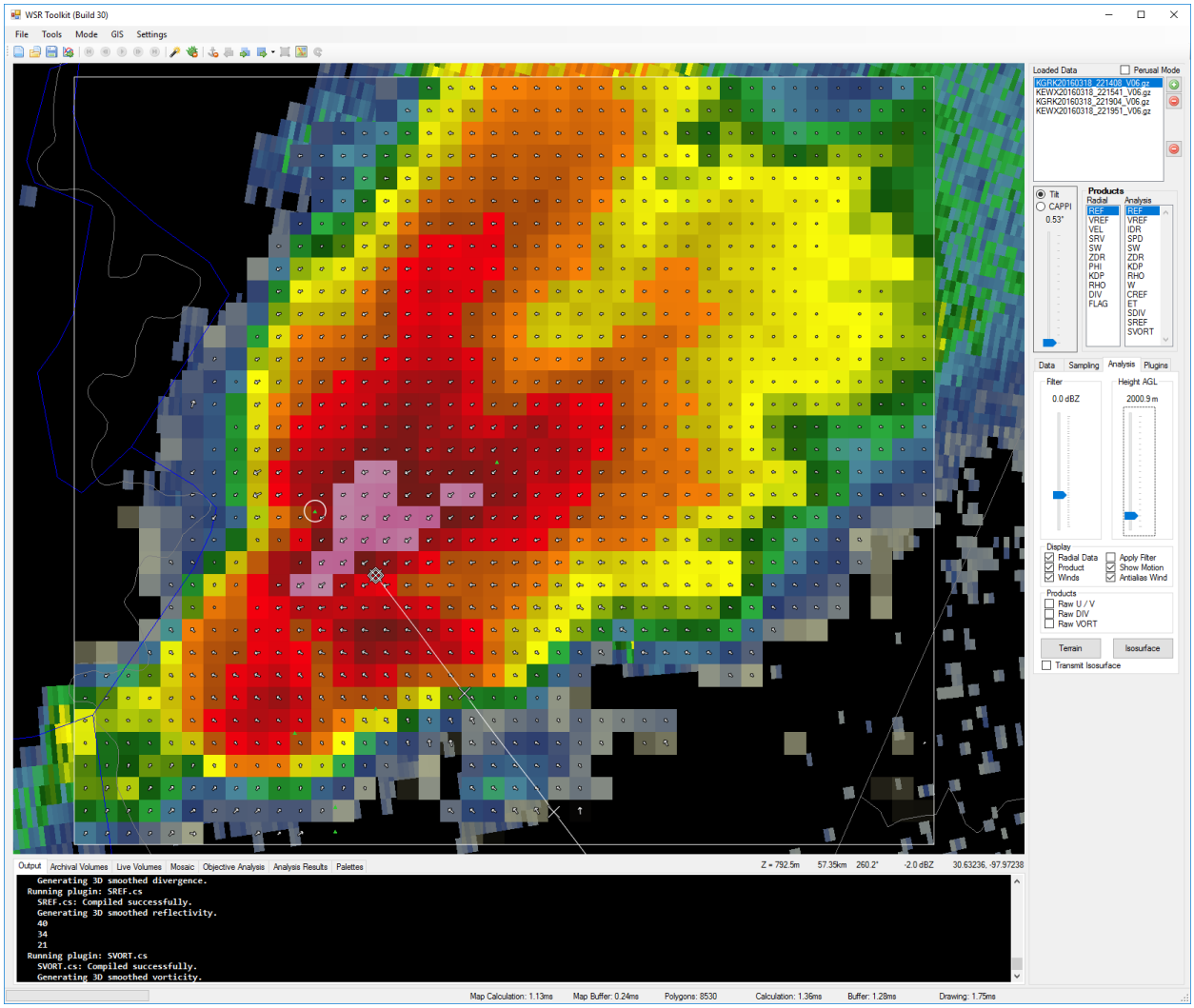

Case 56: Supercell in Texas on March 18, 2016 at 2214Z. 2.25" hail report.

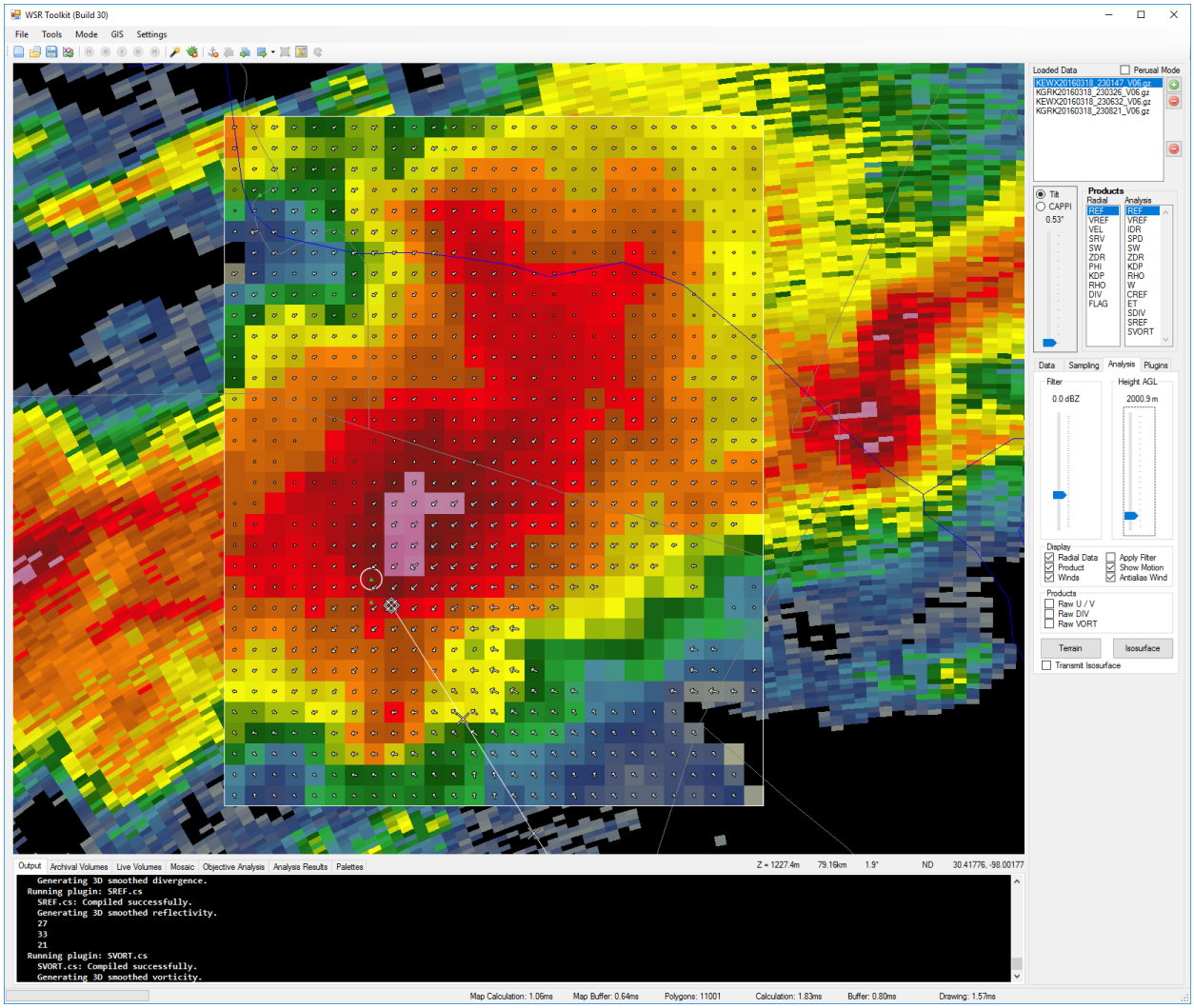

Case 57: Multicell in Texas on March 18, 2016 at 2301Z. 1.50" hail report.

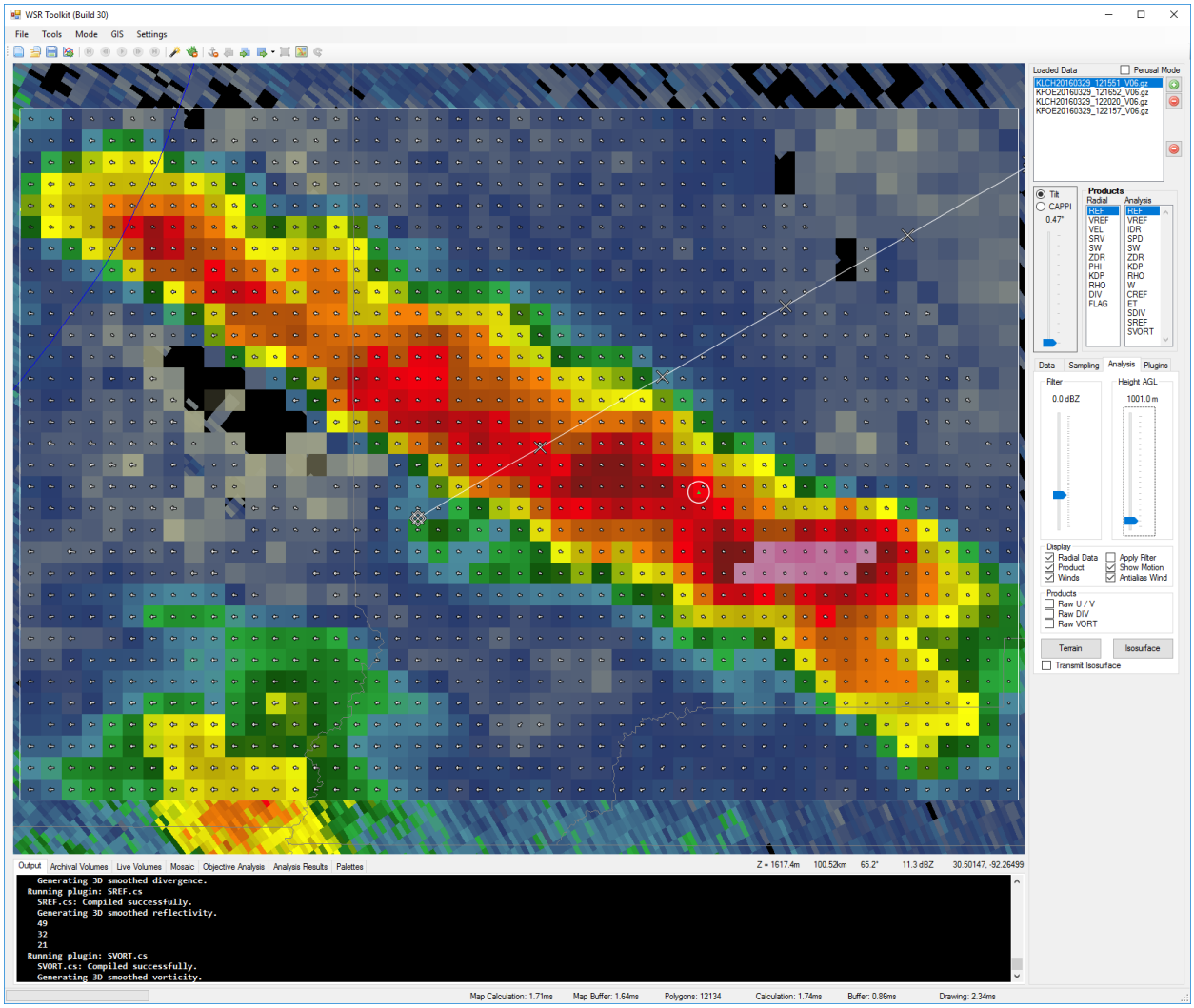

Case 58: Line segment in Lousiana on March 29, 2016 at 1215Z. 0.88" hail report.

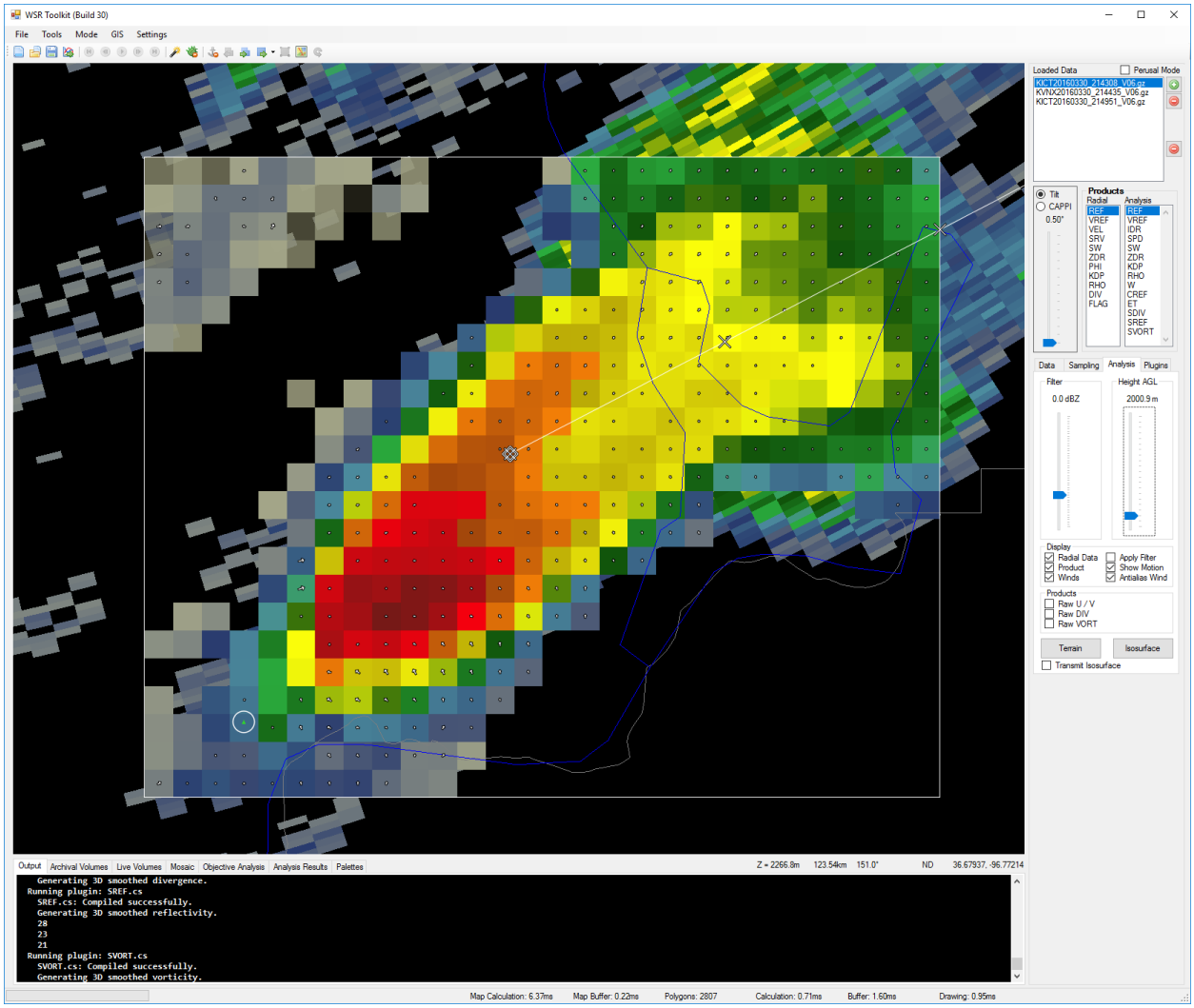

Case 59: Single cell in Kansas on March 30, 2016 at 2143Z. 1.50" hail report.